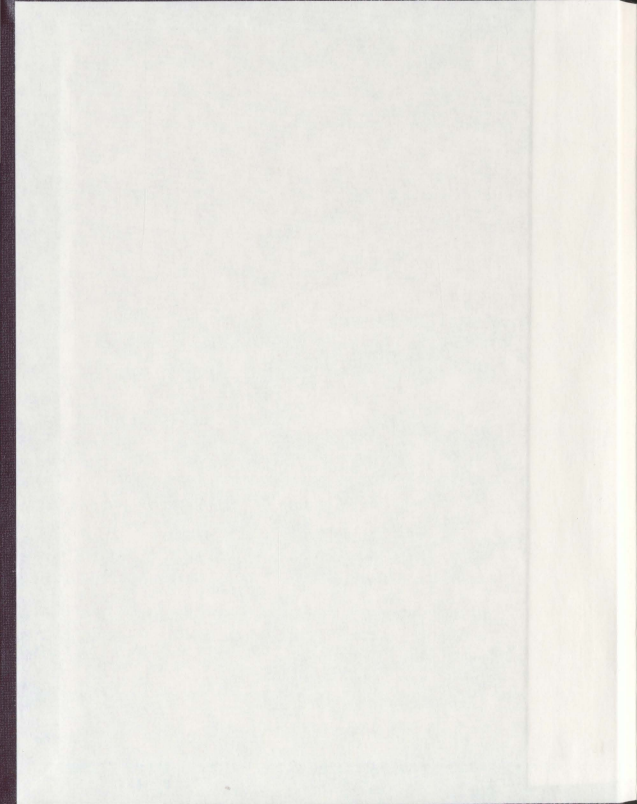


SEISMIC MODELING AND INTERPRETATION OF
POROSITY IN THE UPPER ST. GEORGE GROUP
(ORDOVICIAN) CARBONATES, PORT AU PORT
PENINSULA, WESTERN NEWFOUNDLAND

SEAN COREY HULBURT



**Seismic Modeling and Interpretation of Porosity in the Upper St.
George Group (Ordovician) Carbonates, Port au Port Peninsula,
Western Newfoundland**

By

© Sean Corey Hulbert, B.Sc.

A thesis submitted in partial fulfillment of the requirements

for the degree of Master of Science

Department of Earth Sciences

Memorial University of Newfoundland

St. John's, Newfoundland

June, 2011

Abstract

The geophysical and lithological heterogeneous nature of the Ordovician St. George Group Carbonates complicates the exploration process on the West coast of Newfoundland. Preferential hydrothermal dolomitization, uplift along the St. George Unconformity, and multiphase structural deformation are responsible for reservoir development in the Upper St. George Group. The ability to map porosity in a heterogeneous dolomitized reservoir such as the Upper St. George Group, prior to drilling, on 2-D seismic data is particularly advantageous for cost effective exploration. Porosity alters the acoustic response of seismic data and a synthetic seismogram study is designed to reveal the effect of porosity on waveform. Block porosity models are designed by statistical analysis in reservoir intervals known from well log data in the Upper St. George Group. The block models are representations of petrophysical changes in bulk density and sonic interval transit time caused by increasing porosity. Since the synthetic seismic trace is a product of the two petrophysical parameters, bulk density and sonic interval transit time, attributes displaying changes from porosity can be recorded and used as proxies for finding porosity related attribute changes on 2- D seismic data. Four well data sets on the Port au Port Peninsula (Port au Port -1, Long Range A-09, St. George's Bay A-36, and Long Point M-16) are used in generating models for this study. Synthetic seismograms are designed from block models at 0, 5, 10, and 15% porosity at 20, 40 and 80Hz Ricker wavelets. Multiple Ricker wavelets are implemented to determine which frequency best reveals porosity effects on the synthetics. Complex trace attributes (Instantaneous phase, instantaneous frequency,

and reflection strength) are analyzed on each modeled synthetic seismogram. Ultimately, this process creates a predictive tool for mapping porosity in the vicinity of a well in 2-D seismic sections by matching attributes from models to attributes from the real seismic data.

Keywords: St. George Group, Lower Ordovician, western Newfoundland, hydrothermal dolomite, Aguathuna Formation, Catoche Formation, petrophysical modeling, complex trace attribute analysis, Hilbert Transform, Instantaneous phase, Instantaneous frequency, Reflection strength, Synthetic seismograms, Noise sensitivity analysis

Acknowledgements

The author would like to thank Dr. Charles A. Hurich who agreed to take on a geologist unsure of his path in geophysics and supervise this thesis. Your willingness to always take time to help, to provide criticism, and thoughtful input were greatly appreciated. Dr. Hurich is also thanked for providing funding to travel and explore the field area of this study. It was valuable to put an image, feel, and scale to the data in the lab.....Even though it rained all of the second day.

Funding for this study was provided by an NSERC grant to C.A. Hurich and SGS funding provided by the School of Graduate of Studies, Memorial University of Newfoundland.

Dr. Joe MacQuaker is thanked for his input to this project as well as mentorship in Calgary in the summer of 2010.

The author would also like to acknowledge Landmark Geophysical Software for providing the software used in this study.

To my wife, Jen, who supported the idea of packing up everything and moving to some island in the middle of the very tropical and exotic, North Atlantic: Newfoundland.

Table of Contents

Abstract.....	i
Acknowledgements.....	iii
Table of Contents.....	iv
List of Figures.....	vii
List of Figures (Continued).....	viii
List of Figures (Continued).....	ix
List of Figures (Continued).....	x
List of Figures (Continued).....	xi
List of Figures (Continued).....	xii
List of Figures (Continued).....	xiii
List of Figures (Continued).....	xiv
List of Plates.....	xv
List of Equations.....	xvi
List of Tables.....	xvii
Chapter 1: Introduction.....	1
1.1 Purpose of Study.....	1
1.2 Location and Methodology.....	2
1.3 Regional Setting.....	5
Chapter 2: Geologic Framework.....	7
2.1 Previous Work.....	7
2.2 Lithostratigraphy of the Catoche Formation.....	8
2.3 Lithostratigraphy of the Agnathuna Formation.....	16
2.4 St. George Unconformity and Table Point Formation.....	21
2.5 Structural Framework.....	32
2.6 Diagenesis, Dolomitization, and Porosity Development.....	40
2.6.1 Reservoir targets.....	46
2.7 Facies Interpretation.....	50
Chapter 3: Synthetic Seismogram Analysis.....	55

3.1 Preliminary Statistical Assessment	58
3.2 Lithologic Segregation in Well Data.....	67
3.3 Well Data Porosity Filter Analysis	71
3.4 Frequency Analysis	72
3.5 Block Porosity Models	77
3.6 Synthetic seismogram analysis.....	85
3.6.1 Qualitative and Quantitative analysis of Synthetic Seismograms	89
3.6.2 Synthetic Seismogram Analysis of well A-09.....	90
3.6.3 Synthetic Seismogram Analysis of well A-36.....	104
3.6.4 Synthetic Seismogram analysis of well M-16.....	116
3.6.5 Synthetic Seismogram analysis of well PAP-1	125
3.7 Discussion of Synthetic Seismogram Analysis	134
Chapter 4: 2-D Seismic Line Complex Trace Attribute Analysis	141
4.1 Introduction to 2-D Seismic Attribute study.....	141
4.2 Simulated, Variable Porosity 2-D seismic line generation	142
4.3 Synthetic 2-D Seismic Model Complex Trace Attribute Analysis and Correlation	148
4.3.1. 2-D seismic model quality assessment.....	149
4.3.2 Instantaneous Phase analysis of the modeled 2-D seismic models.....	153
4.3.3 Instantaneous Frequency analysis of the modeled 2-D seismic models.....	157
4.3.4 Reflection Strength analysis of the modeled 2-D seismic models	161
4.3.5 Discussion of Complex Trace Attributes in the 2-D seismic models.....	165
4.4 Noise sensitivity analysis of 2-D seismic model complex trace attributes.....	167
4.4.1 Noise Sensitivity of the thin Table Point Formation seismic model.....	168
4.4.2 Noise Sensitivity of the thick Table Point Formation seismic model.....	182
4.5 Discussion of noise sensitivity analysis of 2-D seismic model complex trace attributes.....	196
Chapter 5: Conclusions and future recommendations	197
5.1 Conclusions	197
5.2 Suggestions for Future Work.....	204

References.....	206
Appendix A: Petrophysical X-Y Cross Plots.....	214
Appendix B: Neutron Porosity Matrix Correction Curve.....	221
Appendix C: Frequency distribution analyses.....	222
Appendix D: Block Porosity Models.....	240
Appendix E: Lithologic Cross plots.....	244

List of Figures

Figure 1.2.1 Location map of Newfoundland and the Port au Port Peninsula.....	3
Figure 1.3.1. Generalized chronostratigraphic column of western Newfoundland.....	6
Figure 2.2.1: Lithostratigraphy of the Upper St. George Group and Table Head Group. .. Error! Bookmark not defined.	
Figure 2.4.1: Schematic diagram showing the progress events leading up to development of the St. George Unconformity.....	23
Figure 2.4.2: Schematic diagram displaying various karst features located along the St. George Unconformity.....	27
Figure 2.4.3 A) Generalized stratigraphy section of the early Paleozoic autochthonous sedimentary strata in western Newfoundland. B) Localized stratigraphy of the Table Head Group and overlying Middle Ordovician siliclastics.....	31
Figure 2.5.1 Schematic diagram displaying progression of deformation from the migration of forebulge, Taconic, Salinic, and Acadian Orogenies.....	35
Figure 2.5.2. Structural and lithologic map displaying locations of wells, structural features, and surface lithology. Port au Port Peninsula, Western Newfoundland.....	36
Figure 2.5.3 Cross section line trajectory and targets of the PAP-1 and A-09 wells.....	37
Figure 2.5.4 Interpreted structural and stratigraphic section well trajectory M-16 ..	38
Figure 2.5.5. Interpreted stratigraphic and structural cross section well trajectory for A-36.....	39
Figure 2.6.1. Chronologic diagram of paragenetic events occurring in diagenetic environments.....	42
Figure 2.7.1. Generalized chronostratigraphic column of western Newfoundland.....	51

List of Figures (Continued)

Figure 2.7.2 Lithostratigraphy of the Upper St. George Group and Table Head Group	52
Figure 3.1.1: Lithostratigraphy of the Upper St. George Group and Table Head Group.)	61
Figure 3.1.2: Standard X-Y Plot of Bulk Density (RHOB) vs. Corrected Neutron Porosity in well A-09. 62	
Figure 3.1.3: Standard X-Y plot of Sonic Slowness (Δt) vs. Corrected Neutron Porosity (NPOR) in well A-09.....	65
Figure 3.1.4: Standard X-Y plot of Acoustic Impedance (AI) vs. Corrected Neutron Porosity (NPOR) in well A-09.....	66
Figure 3.2.1. Matrix correction plot from (Schlumberger, 2009).	69
Figure 3.2.2: Example of a selected and bulk lithology X-Y cross plot of Bulk Density	70
Figure 3.4.1: Graph displaying frequency distribution of Bulk Density (RHOB) at 5% Neutron Porosity (NPOR).	74
Figure 3.4.2: Graph displaying frequency distribution of Sonic Slowness (Δt) $\mu\text{s/m}$ at 5% Neutron Porosity (NPOR).	75
Table 3.4.1: Table displaying all frequency distribution analyses for the four wells in this study.....	76
Figure 3.5.1 Correlation of A-36, A-09, PAP-1, and M-16.....	78
Figure 3.5.2. Diagram displaying comparison of the original and calibration block model interval transit time (Δt) and bulk density curves (ρ).	80
Figure 3.5.3 Synthetic seismogram comparison between original and calibration block models at 20, 40, and 80 Hz.	81

List of Figures (Continued)

Figure 3.5.4. Block modeled well curve diagram for bulk density in well A-09 with Neutron Porosity correlation curve.....	83
Figure 3.5.5. Block model well curve diagram for sonic interval transit time (ΔT) in well A-09 with Neutron Porosity correlation curve.....	84
Figure 3.6.2.1. Instantaneous Phase analysis of well A-09 (synthetic seismic traces in yellow), Ricker wavelet 20Hz.....	92
Figure 3.6.2.2. Instantaneous Phase analysis of well A-09 (synthetic seismograms in yellow), Ricker wavelet 40Hz.....	93
Figure 3.6.2.3. Empirical measurement of instantaneous phase on the peak amplitude, A-09 40 Hz Ricker wavelet.....	94
Figure 3.6.2.4. Instantaneous Phase analysis of well A-09 (synthetic seismograms in yellow), Ricker wavelet 80Hz.....	95
Figure 3.6.2.5 Instantaneous Frequency analysis of well A-09, (synthetic seismograms in white), Ricker wavelet 20Hz.....	96
Figure 3.6.2.6 Instantaneous Frequency analysis of well A-09, (synthetic seismograms in white), Ricker wavelet 40Hz.....	97
Figure 3.6.2.7. Empirical measurement of instantaneous frequency on the peak amplitude, A-09 40 Hz Ricker, Original to 15% porosity modelsl.....	98
Figure 3.6.2.8 Instantaneous Frequency analysis of well A-09, (synthetic seismograms in white), Ricker wavelet 80Hz.....	99
Figure 3.6.2.9. Reflection Strength analysis of well A-09, Ricker filter 20Hz.....	100
Figure 3.6.2.10. Reflection Strength analysis of well A-09, Ricker wavelet 40Hz.....	101

List of Figures (Continued)

Figure 3.6.2.11. Empirical measurement of reflection strength on the peak amplitude, A-09 40 Hz	102
Figure 3.6.2.12. Reflection Strength analysis of well A-09, Ricker filter 80Hz.	103
Figure 3.6.3.1. Instantaneous Phase analysis of well A-36, Ricker wavelet 20Hz.	105
Figure 3.6.3.2. Instantaneous Phase analysis of well A-36, Ricker wavelet 40Hz.	106
Figure 3.6.3.3. Instantaneous Phase analysis of well A-09, Ricker wavelet 80Hz.	107
Figure 3.6.3.4 Instantaneous Frequency analysis of well A-36, Ricker wavelet 20Hz	108
Figure 3.6.3.5 Instantaneous Frequency analysis of well A-36, Ricker wavelet 40Hz.	109
Figure 3.6.3.6. Empirical measurement of instantaneous frequency, A-36 40 Hz Ricker.	110
Figure 3.6.3.7. Instantaneous Frequency analysis of well A-36, Ricker wavelet 80Hz	111
Figure 3.6.3.7. Reflection Strength analysis of well A-36, Ricker wavelet 20Hz ,	112
Figure 3.6.3.8. Reflection Strength analysis of well A-36, Ricker wavelet 40Hz.	113
Figure 3.6.3.9. Empirical measurement of instantaneous frequency, A-36 40 Hz. Ricker t.	114
Figure 3.6.3.10. Reflection Strength analysis of well A-36, Ricker wavelet 80Hz	115
Figure 3.6.4.1 Instantaneous Phase analysis of well M-16, Ricker wavelet 20Hz.	117
Figure 3.6.4.2 Instantaneous Phase analysis of well M-16, Ricker wavelet 40Hz.	118

List of Figures (Continued)

Figure 3.6.4.3. Instantaneous Frequency analysis of well M-16, 20Hz Ricker filter..	119
Figure 3.6.4.4 Instantaneous Frequency analysis of well M-16, 40Hz Ricker filter..	120
Figure 3.6.4.5. Empirical measurement of instantaneous frequency on the peak crest or trough amplitude within the reservoir intervals, M-16 40 Hz Ricker..	121
Figure 3.6.4.6 Reflection Strength analysis of well M-16, 20Hz Ricker filter. I.	122
Figure 3.6.4.7. Reflection Strength analysis of well M-16, 40Hz Ricker filter..	123
Figure 3.6.6.8. Empirical measurement of reflection strength on the peak crest or trough amplitude in the reservoir intervals, M-16 40 Hz Ricker.	124
Figure 3.6.5.1. Instantaneous Phase analysis of well PAP-1, Ricker wavelet 20Hz.	126
Figure 3.6.5.2. Instantaneous Phase analysis of well PAP-1, Ricker wavelet 40Hz.	127
Figure 3.6.5.3. Instantaneous Frequency analysis of well PAP-1, Ricker wavelet 20Hz..	128
Figure 3.6.5.4 Instantaneous Frequency analysis of well PAP-1, Ricker wavelet 40Hz..	129
Figure 3.6.5.5. Empirical measurement of instantaneous frequency on the peak crest or trough amplitude within the reservoir intervals, PAP-1 40 Hz Ricker..	130
Figure 3.6.5.6 Reflection strength analysis of well PAP-1, Ricker wavelet 20Hz..	131
Figure 3.6.5.7 Reflection strength analysis of well PAP-1, Ricker wavelet 40Hz..	132
Figure 3.6.5.8. Empirical measurement of reflection strength on the peak crest or trough amplitude within the reservoir intervals, PAP-1 40 Hz Ricker..	133

List of Figures (Continued)

Figure 4.2.1. 2-D gray scale model representing a thin succession of the Table Point Formation.....	146
Figure 4.2.2. 2-D gray scale model representing a thick succession of the Table Point Formation.....	147
Figure 4.3.1.1. 2-D synthetic seismic model, thick Table Point Formation.....	150
Figure 4.3.1.2. 2-D synthetic seismic model, thick Table Point Formation.....	151
Figure 4.3.1.3. 2-D synthetic seismic model, thin Table Point Formation.....	152
Figure 4.3.2.1. Instantaneous Phase Analysis on the thin model.....	155
Figure 4.3.2.2. Instantaneous Phase analysis of thick model.....	156
Figure 4.3.3.1. Instantaneous Frequency Analysis on the 2-D thin model.....	159
Figure 4.3.3.2. Instantaneous frequency analysis on 2-D thick model.....	160
Figure 4.3.4.1. Reflection Strength analysis on the 2-D thin model.....	163
Figure 4.3.4.2. Reflection Strength analysis on the 2-D thick model.....	164
Figure 4.4.1.1. Reflection strength analysis of the thin model with a 2:1 signal to noise ratio.....	170
Figure 4.4.1.2. Reflection strength analysis of the thin model with a 1:1 signal to noise ratio.....	171
Figure 4.4.1.3. Reflection strength analysis of the thin model with a 0.7:1 signal to noise ratio.....	172
Figure 4.4.1.4. Reflection strength analysis of the thin with a 0.5:1 signal to noise ratio.....	173
Figure 4.4.1.6. Instantaneous phase analysis of the thin model with a 1:1 signal to noise ratio.....	175

List of Figures (Continued)

Figure 4.4.1.7. Instantaneous phase analysis of the thin model with a 0.7:1 signal to noise ratio.....	176
Figure 4.4.1.8. Instantaneous phase analysis of the thin model with a 0.5:1 signal to noise ratio.....	177
Figure 4.4.1.9. Instantaneous frequency analysis of the thin model with a 2:1 signal to noise ratio.....	178
Figure 4.4.1.10. Instantaneous frequency analysis of the thin model with a 1:1 signal to noise ratio.	179
Figure 4.4.1.11. Instantaneous frequency analysis of the thin model with a 0.7:1 signal to noise ratio.....	180
Figure 4.4.1.12. Instantaneous frequency analysis of the thin model with a 0.5:1 signal to noise ratio.	181
Figure 4.4.2.1. Reflection strength analysis of the thick model with a 2:1 signal to noise ratio.....	184
Figure 4.4.2.2. Reflection strength analysis of the thick model with a 1:1 signal to noise ratio.....	185
Figure 4.4.2.3. Reflection strength analysis of the thick model with a 0.7:1 signal to noise ratio.	186
Figure 4.4.2.4. Reflection strength analysis of the thick model with a 0.5:1 signal to noise ratio.....	187
Figure 4.4.2.5. Instantaneous phase analysis of the thick model with a 2:1 signal to noise ratio.....	188
Figure 4.4.2.6. Instantaneous phase analysis of the thick model with a 1:1 signal to noise ratio.	189
Figure 4.4.2.7. Instantaneous phase analysis of the thick model with a 0.7:1 signal to noise ratio.	190
Figure 4.4.2.8. Instantaneous phase analysis of the thick model with a 0.5:1 signal to noise ratio.	191
Figure 4.4.2.9. Instantaneous frequency analysis of the thick model with a 2:1 signal to noise ratio.	192

List of Figures (Continued)

Figure 4.4.2.10. Instantaneous frequency analysis of the **thick** model with a 1:1 signal to noise ratio.193

Figure 4.4.2.11. Instantaneous frequency analysis of the **thick** model with a 0.7:1 signal to noise ratio. .194

Figure 4.4.2.12. Instantaneous frequency analysis of the **thick** model with a 0.5:1 signal to noise ratio. .195

List of Plates

Plate 2.2.1.....	14
Plate 2.2.2.....	15
Plate 2.3.1.....	20
Plate 3.6.1.....	87

List of Equations

Equation 3.6.1	86
----------------------	----

List of Tables

Table 4.2.1. Table displaying the average interval transit time (sonic slowness) ($\mu\text{s}/\text{m}$) and converted average acoustic velocities (m/s) of the four wells in this study.....	145
--	-----

Chapter 1: Introduction

1.1 Purpose of Study

The Cambrian-Ordovician eastern North American carbonate reservoirs, in particular the St. George Group (Ordovician) of western Newfoundland and its coeval strata, have been targets of many economic and academic geological studies (e.g. Haywick 1984; Lane 1990; Cooper, Weissenberger et al. 2001; Stockmal, Slingsby et al. 2004; Knight 2007). In particular hydrothermal dolomite play concepts, in marginal marine facies of the Appalachians, have been the basis of many recent prospective mineral and hydrocarbon exploration studies (e.g Kerans 1989; Lavoie 2005; Smith 2006).

The hydrothermal dolomite reservoir units in the Aguathuna and Catoche Formations of the St. George Group are laterally heterogeneous and contain inter-formation vertical fluid flow barriers. Heterogeneity in this Cambrian-Ordovician shelf carbonate succession is typically attributed to multiphase dolomitization and tectonic deformation associated with the Taconian, Salinian, and Acadian orogenies (Cooper, et al. 2001). The paragenetic succession of dolomitization and cementation has been intricately documented (e.g. Haywick 1984; Lane 1990; Azmy 2008). While many studies address key geophysical, mineralogical, structural, stratigraphic, and geochemical framework of the St. George Group carbonates of western Newfoundland, none have completed integrated geophysical and geologic modeling studies on reservoir

heterogeneity. Specifically, no other researchers have examined for a correlation between seismic waveform attributes and porosity.

The aim of this thesis is to further characterize the St. George Group carbonate reservoirs, integrating geophysical and petrophysical data, by providing a geophysical technique to recognize heterogeneous porosity. With this in place it will be possible to delineate reservoirs in areas with little well and seismic control by providing petrophysical methodologies to extend borehole data away from the immediate bore hole region into the surrounding rock. To meet these aims the acoustic response to changing porosity conditions will be modeled in 1-D synthetic seismograms and synthetically generated 2-D seismic data by the use of complex trace attributes. 1-D synthetic seismograms will be generated using petrophysical information from wireline well logs. Synthetic 2-D seismic lines are generated using a finite difference modeling program built from petrophysical data. The deliverable of this thesis will be a geophysical catalogue featuring correlations of complex trace attributes between 1-D synthetic seismograms, from the well bore, to 2-D seismic line attributes.

1.2 Location and Methodology

The autochthonous St. George Group (Ordovician) shelf succession of western Newfoundland extend nearly 400 km from the Port au Port Peninsula to northwestern Newfoundland (Figure 1.2.1). The lithostratigraphy, structural geology, geochemical, and paleontological studies of the Upper St. George Group has previously been documented (e.g. Haywick 1984; Waldron 1993; Cooper, Weissenberger et al. 2001; Knight 2007;

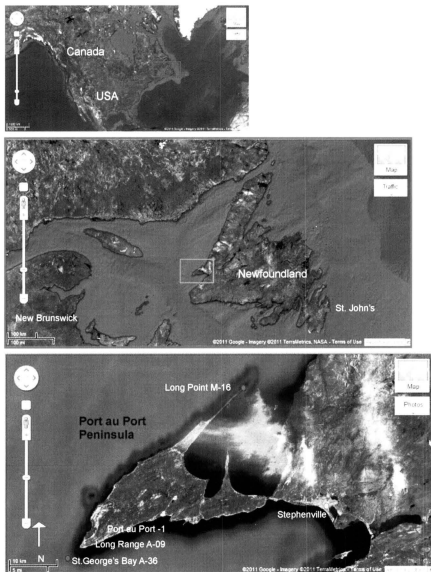


Figure 1.2.1 Location map of Newfoundland and the Port au Port Peninsula, Along with well locations.

Azmy 2008). For this study, four wireline log data suites from the Port Au Port Peninsula area were acquired from the Canadian Newfoundland Offshore Petroleum Board (CNLOPB) and the Newfoundland and Labrador Department of Natural Resources (NL DNR) (Figure 1.3.1). Well data suites from: St. Georges Bay A-36, Port Au Port 1 PAP-1, Long Range A-09, and Long Range M-16 wells (Figure 1.2.1) sampled the complete succession through the St. George Group Carbonate Group. An average of 250 m of sediment through the St. George Group is examined for petrophysical relationships in each well. The well data is initially filtered and processed in Microsoft Excel for applicable range and linear regression modeling. Multiple statistical analyses for petrophysical relationships to porosity are conducted on the well data suites. Well curves are assigned structural and stratigraphic picks in Landmark Geophysical Openworks software application Stratworks. Landmark Geophysical Openworks application Syntool is used in the generation of all synthetic seismograms and altering of well curves for block porosity modeling. Well stratigraphic and structural correlation models are also run in Stratworks. Empirical synthetic seismogram waveform geometries are measured in Syntool while complex trace attribute analyses are evaluated in Landmark Geophysical Openworks application SeisWorks. Complex trace attribute analyses are evaluated in SeisWorks 2-D software on 2-D seismograms.

1.3 Regional Setting

Western Newfoundland lies in the northeastern region of the Canadian Appalachians. Specifically it is located in the Humber zone which is the most westerly province of the four tectono-stratigraphic zones defined by (Williams, 1979) in Newfoundland. Stratigraphically the St. George Group (Ordovician), located on the Port au Port Peninsula, is confined to the Humber zone. The Humber zone is interpreted to be the Cambrian-Ordovician continental margin of the Iapetus Ocean. Sedimentation in the Humber zone was initiated in the early Cambrian following rifting of Grenvillian aged basement (circa 1 Ga) (Williams, 1984). The facies in this succession transition upwards, initially from a rift facies-clastics association in the early Cambrian, to siliclastic shelf deposits of the Labrador Group and then to predominantly carbonate deposits by Middle to Upper Cambrian times of the Port Au Port Group (Figure 1.3.1). Sedimentation of the carbonates continued with little interruption through to the early Ordovician (Knight et al., 2007). During the middle Ordovician, however, a facies shift to deeper marine conditions occurred. This is marked by the deposition of carbonates, and shales (Table Head Group) before finally evolving into a flysch succession that records the collapse of the stable continental margin (Stenzel, 1990). Subsidence of the platform occurred prior to emplacement of allochthonous strata (Humber Arm Super Group) from the east and transported westward (Calon, 2002; Burden, 2004). In the Port au Port area, these allochthonous strata are overlain by the neoallochthonous upper Middle Ordovician Long Point Group, following with the Silurian- Devonian Clam Bank Formation and the Carboniferous Codroy Group (Williams, 1979).

Chapter 2: Geologic Framework

2.1 Previous Work

The stratigraphy of the carbonate shelf successions in western Newfoundland has been studied by many authors since the middle 1860's (The first study is Logan 1863). The name St. George Group name has been used since its initial usage by (Schubert and Dunbar 1934). Since then, however, the stratigraphy has been redefined many times. (e.g. Kindle 1965; Collins 1975; Knight 1977; Haywick 1984; Waldron 1991; Cooper et al. 2001; Knight 2007). In this study the most recent reassessment of stratigraphic nomenclature and structural framework is used (e.g. Cooper et al.2001; Lavoie 2006; Knight et al. 2007; Azmy et al. 2008). The St. George Group platform carbonates and specifically the Aguathuna and Catoche formations, have also been the subject of extensive lithologic, diagenetic, geochemical investigations as well as palinspastic reconstructions. For instance (Cooper et al. 2001) conducted an extensive basin reconstruction analysis in the Humber Zone and divided the carbonate succession into six tectono-stratigraphic mega-sequences. Studies (e.g. Cumming 1968; Collins 1975; Knight 1977; Levesque 1978; Lane 1990; Knight, et al. 1991) to better understand mineralization in the Lower Ordovician strata, linked to the presence of regional unconformities, has generated much research in the Daniel's Harbour area. The complex phases of cementation and dolomitization, typical of Ordovician reservoirs in the Appalachian carbonate platform, have been carefully documented (e.g. Haywick 1984; Lane 1990; Azmy et al. 2008). The subsequent deformational history and palinspastic reconstruction of the Ordovician carbonate shelf and basin is discussed in detail in

(Waldron 1991; Waldron 1993; Cooper, Weissenberger et al. 2001; Calon 2002; Burden 2004; Davies 2006; Smith 2006; Waldron 2008). Overall these existing, multidisciplinary studies on the St. George Group platform carbonates provide the necessary facies descriptions and architectural constraints for modeling to form the basis of this study. In the following sections of this chapter, the primary reservoir units of interest, the Aguathuna and Catoche formations, will be discussed in complete detail. However, it is important to note the reservoir units will be discussed in the context of regional and Port au Port area scale to illustrate key spatial variances of the geology.

2.2 Lithostratigraphy of the Catoche Formation

The Catoche Formation (Figure 2.2.1) composes the middle subtidal interval of the Arenigian passive margin megasequence (PMMS) (Figure 1.3.1) and lies conformably upon the Barbace Cove Member of the Boat Harbour Formation (Knight et al. 2007). The average exposed thickness has been recorded as 160 m from (Knight et al. 2007). The Catoche Formation, at Port au Choix, (200 km further north from the area of study) contains two unnamed members consisting of a lower limestone (120 m) and an upper dolostone that is 40 m thick. The upper dolostone member, extensively documented in (Baker, 1993), has been determined to be a body of replacement dolomite that can be widely mapped on the Port au Port Peninsula and adjacent thrust stacks (Cooper et al. 2001). The upper member dolostone from Port au Choix is the time equivalent of the middle member (40 m) of white dolostone on the Port au Port peninsula. This is due to increased dolomitization of the lower member limestone, now only 80 m

thick as opposed to 120 m on the Port au Port. The remaining 40 m of the Catoche Formation is an upper member categorized as the Costa Bay Member (Figure 2.2.1).

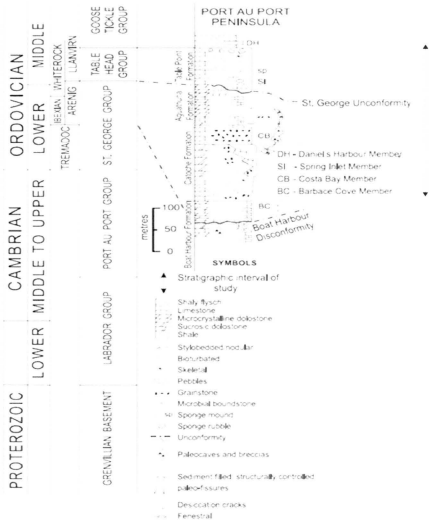


Figure 2.2.1: Lithostratigraphy of the Upper St. George Group and Table Head Group. Stratigraphic interval of study shown by black arrows. Figure modified from (Knight 2007).

The lower limestone member of the Catoche Formation is a well bedded, dark grey, dolomitic, bioturbated limestone that weathers as a series low cliff and steps when examined upward on coastlines. (Plate 2.2.1) (Knight et al. 2007). It contains skeletal and peloidal wackestones and packstones, which display stylonodular to uneven fabric, are the dominant lithology in the lower member. Gastropods, large straight and coiled cephalopods, brachiopods, crinoids, and trilobites composed most of the macro fauna in the lower limestone (Boyce 2000). Simple tubular burrows occur almost everywhere and sparse lenses of skeletal, grainstone, and rudstone occur in the mud dominated facies (Haywick 1984). Most of these grainy lenses contain starved ripple marks, sinuous and straight, or planed ripple marks (Plate 2.2.1). Rudstones in the first 20 m of the lower member typically contain discoidal, centimeter size pebbles of pink to red lime mudstone. Recessive weathering beds of sparsely bioturbated associated with low diversity fauna of large trilobites and graptolites are periodically intercalated in the bedded lower member limestone (Lane, 1990). Several beds of thrombolitic microbial boundstones ranging in size are present in the lower member limestone, but most occurrences are in the upper half of the member. Sponges, receptaculitids, trilobites, and large mollusks are common in the mound structures with grainstone fringes/intermound fills (Plate 2.2.1).

The middle member of the Catoche Formation is ~ 50 m thick and weathers tan-gray. The member is ubiquitously mottled and is highly dolomitized. In outcrop, large domal mounds are preserved in the dolostone associated with intermound dolarenite (Plate 2.2.2). Porosity in this unit varies, but includes intercrystalline, vuggy cavernous, and breccias porosity (Baker, 1993). Highest porosity in the middle member is associated

with the coarse hydrothermal dolomite. It is speculated that the middle dolostone member, from its large number of complex microbial mounds, is part of a mound belt that formed a substantial barrier complex on the shelf system in Arenig time.

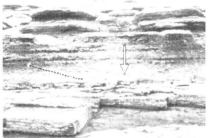
The Costa Bay Member of the Catoche Formation is a unit of well bedded, off white, clean, grainy limestone that is readily mapped around the Port au Port Peninsula (Knight 2007). The member is of economic significance due to high purity limestone it contains (Plate 2.2.2). In the western region of Port au Port, the member loses purity and transitions in to deeper water, fossil rich, cyclic limestone overlain by a thick porous dolostone (Boyce 2000). Porosity in this dolostone cap can range as high as 10%. On the western side of the Northern Peninsula, the Costa Bay Member is extensively dolomitized and is host to the Daniel's Harbour Zinc mine in a region where it is rich hydrothermal dolomite complexes. The Costa Bay member was also host to an exhumed oil field in the Port au Choix area (Cooper et al. 2001). Specifically on the Port au Port Peninsula, the Costa Bay Member consists of white to cream, and occasionally pink and green, stylonitic limestones that range from crossbedded, peloidal grainstone, to burrowed packstone, to fenestral limestone laminate, and finally nodular to burrow- mottled lime mudstone and wackestone (Baker, 1993). Locally on the Port au Port the member can comprise sixteen coarsening and shallowing upward parasequences that comprise burrowed wackestone to grainstone. Porous dolostone marks to top of the parasequences in some locations (Plate 2.2.2). Glossy, bright green shale lenses are observed in some beds among stylolites, vugs, and rubble zones where limestone appears to be dissolved

(Boyce, 2000). The Catoche Formation is conformably overlain by the primary formation of interest in this study, the Aguathuna Formation.

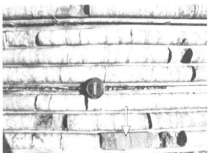


Plate 2.2.1: LOWER MEMBER OF THE CATOCHE FORMATION. (Figures are modified from Knight 2007).

A.) Sinuous, widely spaced, ripple marks composed of intraclastic skeletal grainstone and rudstone. Lower limestone, Catoche Formation. Meter stick for scale.



B.) Cross-stratified rudstone, 65 cm thick, bounded by planar surfaces and flat-lying burrowed dolomitic lime wackestones. Black dashed line displays forests. The white arrow displays wackestone drapes that interrupt the foresets. Lower Limestone, Catoche Formation.



C.) Bioturbated dolomitic limestone from the Lower Catoche Formation. Lens cap is 6 cm.

A

B

C



Plate 2.2.2: UPPER DOLOSTONE,
COSTA BAY MEMBER,
CATOCHE
FORMATION. (Figures
are modified from
(Knight, 2007).

A.) Peloidal, fenestral laminated limestone (white arrow) lying next to clean white stylolitic, fine grainsstone (Black arrow) of the Costa Bay Member, Catoche Formation, Port Au Port Peninsula. (Lens cap is 6cm.)

A



B.) Sucrosic Dolostone cap in the Upper Dolostone of the Catoche Formation. Porosity in this unit ranges widely, but contains measurements up to 10%. Hammer for scale.

B



C.) Dolomitized Thrombolitic Mounds from the Middle Catoche Formation. Hammer is 32 cm long.

C

2.3 Lithostratigraphy of the Aguathuna Formation

The Aguathuna Formation (Figure 2.2.1) is a stacked succession of cyclic, meter thick platform limestone and dolomites present everywhere in the western Newfoundland autochthon. The lithology of the formation varies considerably with location in western Newfoundland. In some locations, such as Port au Choix to Daniel's Harbour, it is exclusively finely crystalline dolostone with minor shale (Knight 1987). On the Port au Port Peninsula, limestone is intercalated with dolostones and shales (Plate 2.3.1) (Azmy et al. 2008). Detailed studies of the Aguathuna Formation from Port au Choix to Daniel's Harbour have shown it is composed of two informal members separated by the St. George Unconformity (Lane, 1990 Azmy et al. 2008). The Lower Member of the Aguathuna Formation is preserved and mapped in all of western Newfoundland, however, the only area which both members are preserved is the region between Port au Choix and Daniel's Harbour (Knight 1987). On the Port au Port peninsula, only the lower member of the Aguathuna Formation is preserved and varies in thickness from the amount of erosion associated with the St. George Unconformity. For the context of this study only the Lower Member will be discussed in this section.

The Lower Member of the Aguathuna Formation from Port au Choix to Daniel's Harbour consists of a stacked succession composed of meter thick beds of burrow-mottled dolostone, dololaminite which is locally shaly, beds of stromatolitic dolostone, and some units of green-grey shale (Lane, 1990) (Plate 2.3.1). In this region, the Member is up to 60 m thick, but may be as thin as 6 m as a result of erosion from the St. George

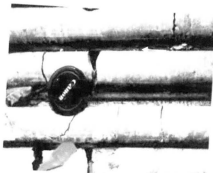
Unconformity. A distinctive burrowed-mottled, basal marker four to twelve meters thick occurs in the Daniel's Harbour zinc mine area known as the "Dark Grey Dolomite" (Lane, 1990). (Lane,1990) describes the lithology in the Lower Member as a series of repetitive deposition cycles. The cycles begin with a truncation surface or erosional surfaces, sharply overlain by unfossiliferous, mudcracked shales and dololaminites. Burrow mottled to massive dolomite, partially to completely burrowed and two-tone dark grey to buff weathering appearance, overlie the dololaminate indicative of deepening upward facies. *Thalassinoides* burrows occasionally completely rework beds in the cycles (Sheenan, 1984). The burrows range in size up to 50 mm in cross-section and vertically penetrating 10-50 mm. Shelly fossils a rare in this unit with brachiopods, pelecypods, gastropods, and bryozoans. Conodonts recovered from this unit represent the Midcontinent late Ibexian E fauna and occur in very limited numbers. This is partially indicative of a restricted, hypersaline, shallow depositional environment (Knight et al. 2007). Occasionally, the top of the sequences in the Lower Member are marked by siliclastic pebble conglomerate and chert breccias at the erosional surfaces. The lithology documented by (Knight 1987; Lane 1990; Knight 2007) in the Lower Member from the Port au Choix can be correlated with the Lower Member on the Port au Port peninsula.

On the Port au Port peninsula, only the Lower Member of the Aguathuna Formation is present. The Upper Member has likely been removed by erosion associated with the St. George Unconformity. Here, the Lower Member consists of repetitive depositional cycles similar to the Port au Choix cycles, however, there is abundant limestone intercalated with the dololaminites. The thick regions of the Lower Member

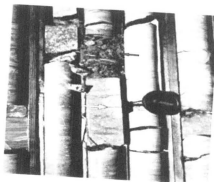
are up to 103 m despite evidence of substantial erosion from removal of the of the Upper Member (Haywick,1984). Limestone forms six marker units in the lower 85 m of the Lower Member, two to five meters in thickness. The limestone units are typically grey to off-white, burrow-mottled, unfossiliferous mudstones and wackestones. Locally, sparse skeletal, peloidal, oolitic, and oncolitic grainstones and packstones are observed. The skeletal components of these limestones are composed of trilobites, brachiopods, and ostracods. The most prominent limestone is located 20 m above the base of the Aguathuna Formation where it is host to a wide variety of fossils, dominantly oncolites. This unit can traced for over 15 km along the south west section of Port au Port (Boyce, 2000). Stromatolites occur in the limestones of the Lower Member, but are most common in the upper part of the member.

Dolostones in the Lower Member of the Aguathuna Formation on the Port au Port peninsula are characterized by burrow-mottled and laminated depositional fabrics similar to the Port au Choix sections. In exposure, the dolostone appearance varies from multicolored striped fabrics, to lumpy fabrics containing irregular wispy, argillaceous seams (Haywick, 1984). Mudcracks, small tepee structures, rare white quartz nodules, cross lamination, thin beds of dolomitized rudstone, and local pockets of breccias are all present (Knight, 2007). Green and grey shale lenses are common on the Port au Port peninsula intercalated in the dololaminites. (Plate 2.3.1) The shale units are centimeter thick and occur as partings, with the thickest shale beds being 0.75 m (Plate 2.3.1). This thick shale lies at the 85 m mark, just 17 m from the top of the Aguathuna Formation. The thick shale lies upon an irregular surface which the dolostone below is extensively

brecciated and fractured, implying a disconformity (Knight et al. 2007). Above this 85 m mark in the Aguathuna Formation, the lithology is almost exclusively dolostone and can be traced for 22 km in outcrop below the St. George Unconformity on the eastern Port au Port Peninsula. (Plate 2.3.1) Paleo-dissolution cavities in bedding planes of the upper dolostone suggest limestones once occupied the cavity space and have been dissolved.



A



B



C

Plate 2.3.1: LOWER MEMBER
AGUATHUNA
FORMATION.
(Figures are modified
from (Knight 2007).

A.) Clean burrowed
dolomite above the 85
meter mark in the upper
section of the Lower
Member of the
Aguathuna Formation.
(Lens cap is 6cm for
scale) (Core is from
RND 001 from the Port
Au Port Peninsula.)

B.) White arrow points to an
oncolite horizon at the
top of a thick grainstone
that dominates the
middle part of a
shallowing upward
limestone unit, 20 m
above the base of the
Aguathuna Formation.
Red arrow points to
green shale lying on the
grainstone bed. Core to
the right of the lens cap
is a typical rudstone of
the Aguathuna. (Lens
cap is 6cm)

C.) Dololaminites (white
arrows) and Burrow
mottled dolostones
(black arrows) of the
Aguathuna Formation.
(Core from the RND 001
drill hole, Port Au Port
Peninsula). Lens cap is
6cm for scale.

2.4 St. George Unconformity and Table Point Formation

The St. George Unconformity marks the upper boundary for the St. George Group Carbonate Succession and the Western Newfoundland Passive Margin Megasequence defined by (Cooper et al. 2001). The St. George Unconformity has a major influence on the development of porosity and paleo-erosion of reservoir strata, making it important this study. Previous researchers have suggested the St. George Unconformity was part of a multi-continental event marking a global eustatic drop (Azmy et al 2008). Although the St. George Unconformity does mark the Sauk/Tippecanoe Boundary in western Newfoundland, it does not correlate with other Laurentian coeval unconformities (Knight et al. 1991). This anomalous character of the St. George Unconformity suggests local tectonism controlled its development and extent.

The St. George Unconformity developed primarily due to a tectonism shift along the paleocontinental margin of Laurentia in the Middle Ordovician/Taconic Orogeny. During the Middle Ibexian (Ordovician), prior to relative sea level fall, the transformation causing cessation of sedimentation on the Passive Margin Megasequence began. The passive margin transformed into a convergent plate boundary due to Taconic-related development of a forebulge complex ultimately responsible for porosity development in the St. George Group (Knight et al. 1991). As development of the convergent margin continued and the forebulge axis migrated toward the carbonate platform, paleorelief in the carbonate platform was elevated subaerially (Figure 2.4.1). Deposition of the Aguathuna Formation continued at the time of forebulge migration, however deposition

was terminated as paleo-relief and exposure occurred. Karst features, collapse dolines, and massive erosion took place on the carbonate platform during this time (Knight et al. 1991).

Due to meteoric water ingress, and subaerial exposure of the St. George Group platform carbonates, major diagenetic and erosional changes occurred near the surface of the St. George Unconformity. These changes can be classified into three categories: 1). Spatial, thickness, and facies variation of overlying and immediate underlying sediments. 2). Surface paleokarst features. 3). Subsurface paleokarst features.

Erosion along the unconformity caused significant spatial, facies, and thickness changes to strata directly above and below the surface. In areas where paleo-highs are present (Port au Port Peninsula, Cape Norman), the Upper Member of the Aguathuna Formation has been completely eroded and very thin successions of the Table Point Formation uncomfortably lie on Catoche Formation (Knight et al. 1991). Conversely, in areas of paleo-lows (Port au Choix, Maria Islands) the Table Point Formation is at its thickest and the unconformity is immediately underlain by the Upper Member of the Aguathuna Formation (Knight, 1989). Lithofacies in the Table Point Formation (see discussion in later in section) and changes are related to thickness of the succession. Two small disconformities occur in the Springs Inlet Member of the Table Point Formation as separate depressions merging with St. George Unconformity (Knight et al. 1991). The disconformities are represented by surfaces of erosional relief and abrupt, disconformable changes in lithology.

Surface karst features along the St. George Unconformity include smooth and planar surface karren as a result of solution sculpture. Small irregular connected flutes and depressions up to 0.2 m in length occur incised 40-60 mm in interbedded dololaminite in the Aguathuna Formation (Knight et al. 1991). Larger karren, up to 0.6 m long with 0.1 m troughs, occur on gently inclined surfaces. Karren features are rare on the uniformity surface most likely due to either the lack of any significant slope or the impervious nature of the microcrystalline Aguathuna Formation dolostones (Knight, 1989). Rubble breccias, another surface karst feature, also occur along the St. George Unconformity. Rubble breccias contain the lithology of the underlying strata and are similar to weathering and soil profiles on top of Mississippian karstified carbonates in New Mexico (Kerans, 1989). Locally, at Cape Norman where the St. George Unconformity lies on top of Catoche Formation, the rubble breccia is composed of burrow mottled dark grey dolostone derived from the Catoche Formation. On the Port au Port peninsula, the rubble breccia is composed of yellow to buff weathering dolostone derived from the Aguathuna Formation. Sub-surface karst features are more common than surface karst features. Sub-surface karst features include shallow fracture systems, porosity development, geopetal sediment, local removal of limestone beds, bedding/structurally controlled caves, rock matrix breccias, and subsidence and collapse dolines. 30 mm - 0.3 m irregular doglegged, anastomosing networks of fractures occur in the Costa Bay Member (Catoche Formation) are common in the Pistolet Bay Area and Hare Bay, but are not present in the overlying Aguathuna Formation (Knight et al. 1991). These fracture networks provide conduits for corrosive meteoric water ingress.

Millimeter to 10's of millimeter scale, irregular, laminar, and fabric selective porosity filled with fine dolomite silt is also common immediately below the unconformity in respective members of the St. George Group underlying the unconformity. Preferential dissolution to limestone beds creates undulating topography along the unconformity and also produced tabular caves as noted on the Port au Port Peninsula (Knight et al. 1991). Faults and fractures were enlarged by fluid ingress at the unconformity and signs of solution enlargement occur up to 120 m below the level. The resulting solution seams are filled with mineralized precipitates, composed of cherts/ dolomites from the Upper Aguathuna Formation, and dolomitization zones up to 0.6 m from the fault surfaces (Knight, 1989). The presence of debris from the Upper Aguathuna Formation confirms the filled fractures and faults were associated with the unconformity. Rock matrix breccias near the unconformity are characterized by a matrix of fine- to medium-crystalline grey dolomite crystals and predate epigenetic breccias with saddle dolomite cement (Lane, 1990). The breccias related to the unconformity are stratabound bodies that lie parallel to bedding, commonly involve several beds, and can be several hundred meters along strike. Also, the breccias can form vertical discordant 1 m to 150 m wide bodies along faults and fractured that crosscut several hundred meters of stratigraphy at a time (Knight et al. 1991). The composition of the breccias varies spatially, but basically is constrained to two types: polymictic and oligomictic breccias. (Figure 2.4.2) The polymictic breccias are characterized by discordant, rubble to matrix rich, granule to block sized clasts of light grey, burrow mottled to massive dolostone. Dark chert is variably abundant and encased in vitreous, dark fine grained dolomite and some clasts are

displaced 50m from their (Knight et al. 1991). Oligomictic breccias are typically stratabound and characterized by fragments of burrow mottled dolostone and chert. Collapse breccias are also abundant and found in greatest abundance in dolines and infilled cave structures. (Figure 2.4.2)

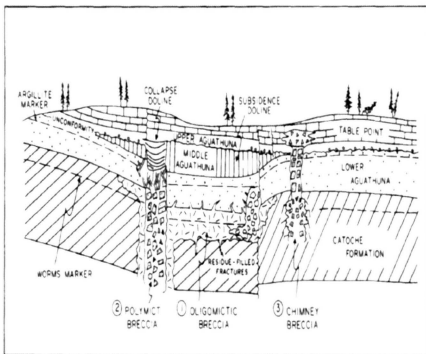


Figure 2.4.2: Schematic diagram displaying various karst features located along the St. George Unconformity. Areas of subsidence show lenses of Middle Aguathuna and thick Table Point. Figure modified from (Knight et al. 1991).

Dolines occur in the St. George Group as a result of the karstification of limestones, and from subsidence produced as the axis of the forebulge migrated. Subsidence dolines are typically characterized by the presence of the anomalously (10-70 m) thick Middle Member of the Aguathuna Formation. These dolines form mostly above the oligomictic breccias but below the unconformity surface. Collapse dolines are formed from northeast trending high angle faults penetrated from the unconformity to the Upper Catoche Formation. Polymictic breccias fill the vertical collapse dolines and fill from the unconformity surface up to a depth of 50 m (Knight et al. 1991). The formation of dolines and rock matrix breccias has been documented in the following sequence of events: 1). Deposition of the Lower Aguathuna Formation. 2). Partial subsurface dissolution of the Upper Catoche Limestone and stratabound collapse of interbedded dolomites to form oligomictic breccias. 3). Subsurface dissolution concomitantly with tectonically enhanced sagging of strata to create broad subsidence dolines during deposition of the middle Aguathuna (Lane, 1990). Sedimentation generally kept pace with subsidence during the deposition of the Middle Aguathuna. 4). Faults crosscut and displaced oligomictic breccias and localized upward stoping into the lower Aguathuna to form narrow polymictic breccias. 5). Lower and Middle Aguathuna collapsed into the solution cavities in the Catoche Formation, forming collapse dolines up to 50 m deep at the unconformity (Knight et al. 1991). To conclude, the St. George Unconformity was an erosional and karst event, controlled primarily by a migrating forebulge associated with the Taconic Orogeny tectonism, leading to significant diagenetic and structural changes in the Aguathuna and Catoche Formation of the Upper St. George Group. In the next part of

this section, the depositional thickness of the Table Point Formation on top of the St. George Unconformity topography as a significant indicator of paleo-relief and porosity development is discussed.

The Table Head Group comprises three formations (Figure 2.4.3) of foreland basin carbonates deposited after the collapse of the Cambro-Ordovician Carbonate Platform. The specific unit of interest is the Table Point Formation (Figure 2.4.3) and how its thickness correlates with the paleo-relief along the St. George Unconformity. The Table Point Formation is a shallow marine, massive-to-thick bedded, grey limestone with minor interbedded dolostone in the basal 10 m. Limestones exhibit stylo-nodular to pseudoconglomeratic fabric (James et al. 1980; Stenzel 1990). The limestones contain a diverse number of shelly fauna including illaenid and bathyurid trilobites, articulate brachiopods, ostrocods, and other high-spined gastropods, echinoderms, bryozoans, and cephalopods (Boyce, 1997). The thickness of the Table Point varies quite markedly amongst its spatial distribution. In the Port au Port Area, it varies in thickness from 160 m at Cape Cormorant, to 43 m at the Aguathuna Quarry (Stenzel, 1990). Despite spatial thickness variation, lithofacies is similar in most areas.

The facies of the Table Point Formation is interpreted to be of shallow water, marine environment synchronous and following the fragmentation, uplift, and erosion of the platform carbonates of the St. George Group. The thickness of the Table Point Formation is entirely controlled by, and indicative of topography amongst, individual

fault blocks and subsidence dolines of the underlying platform. Synsedimentary slumping and sliding confirms deposition during seismically active times.

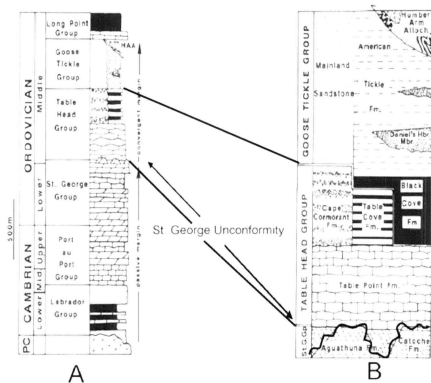


Figure 2.4.3 A) Generalized stratigraphy section of the early Paleozoic autochthonous sedimentary strata in western Newfoundland. B) Localized stratigraphy of the Table Head Group and overlying Middle Ordovician siliclastics. St. George Unconformity in blue. Figure modified from (Stenzel 1990).

2.5 Structural Framework

The western margin of Newfoundland, specifically the Ordovician St. George Group, has undergone polyphase deformation associated with the Taconic, Salinic, and Acadian Orogenies. Each of the four wells (A-09, A-36, PAP-1 and M-16) in this study targets a specific structural region on the Port au Port Peninsula and will be discussed in detail in this section. The structural history of the Humber zone of western Newfoundland is incredibly complex, and therefore, only events pertinent to the development of porosity and reservoir quality on the Port au Port Peninsula will be discussed in this study.

The earliest recorded Taconic tectonism in the Humber zone was recorded in the metamorphic sole of the ophiolitic rocks in the St. Anthony Complex at 490 Ma. Tectonism in the St. George Group began during the Taconic Orogeny with, as previously discussed, the St. George Unconformity as a peripheral bulge migrated across the platform from loading of the Humber Arm Allochthon. As the basin was uplifted and then subsided, normal extensional faults were created. They would later become pathways for the thin skinned thrust stack systems (Waldron et al. 1998). During the Salinic Orogeny, deformation shifted from thin skinned extensional faulting to regional metamorphic fabric development. However, during the Salinic Orogeny, most metamorphism was constrained to the Humber Arm Allochthon in development of cleavage and fold fabrics, leaving the rocks of the Upper St. George Group largely unaffected (Figure 2.5.1). Amphibolite and Greenschist facies were common temperature pressure conditions at this time. The formation of thrust stacks on the Port

au Port Peninsula were attributed to Acadian Orogenesis, late Silurian to early Devonian times (Stockmal et al. 2004) (Figure 2.5.1). The Ordovician carbonate platform underwent basin inversion during the Acadian orogeny which reactivated many normal faults in reverse sense. The basin inversion and multiple thrust stack systems compose the structural targets for the following exploration wells on the Port au Port. (Long Range A-09, Port au Port-1 PAP-1, Long Point M-16, and St. George's Bay A-36).

The four exploration wells targeted several different structural features in the Port au Port area. The first well to be drilled, the PAP-1 (Figures 2.5.2 and 2.5.3) targeted a small onshore structural trap in the Ordovician Platform down plunge of a larger offshore structure in the footwall on the Round Head thrust (Figures 2.5.2 and 2.5.3). PAP-1 demonstrated that the Round Head thrust had previous extensional history and footwall short cut anticlinal traps only developed in areas previously extended (Cooper et al. 2001). Well A-09 (48° 27' 51.21 N, 59° 14' 55.32 W) (Figure 2.5.2) is located approximately 1.5 km to the immediate southwest of the PAP-1 well in a slightly up plunge location. The structure in the PAP-1 and A-09 well is coeval (Figure 2.5.3). The M-16 (48° 45' 42.26 N, 58° 47' 24.84 W) well was directionally drilled from the northern tip of Long Point (Figure 2.5.2), eastward beneath Port au Port Bay. The well spudded in the northwest dipping Lourdes Formation (Figure 2.5.4) in the hanging wall of the Tea Cove thrust (Waldron, 1993). Cross section lines near the well show (Figure 2.5.4) the northwest dipping Long Point Group and younger strata of the Humber Arm Allochthon beneath the Tea Cove thrust (interpreted to be the basinward side of the triangle zone.) The well then passed through a series of imbricate thrust sheets within Humber Arm

Allochthon before finally penetrating the basal thrust at the bottom of the Humber Arm Allochthon as indicated by a shearzone on the Formation Microshear (FMS) logs (Cooper et al. 2001). The M-16 well eventually terminated in the Passive Margin Mega-Sequence below the shearzone where strata is dipping 15°NW and the PMMS is elevated above regional levels in the well. These geometries suggest some basement involved compression similar to the Round Head thrust, must have provided the uplift in the PMMS. Overall, the Long Point M-16 well demonstrates a cross sectional architecture of the triangle zone by a series imbricate thrusts in the Humber Arm Allochthon combined with thick skinned compressional faulting of the Ordovician Carbonate Platform (Cooper et al. 2001). Well A-36(48° 25'04.93N, 59° 19' 29.29W) (Figure 2.5.2) targeted the same short cut footwall anticline under the Round Head thrust as PAP-1 (Figure 2.5.5.). A-36 is located up plunge to the southwest, but due to thickness of the Table Point Formation (70 m), this is interpreted to be located on a paleolow along the Taconic forebulge deformation surface (St George Unconformity). The four wells aimed at specific structural traps on the Port au Port peninsula described in this section were targeting complex, heterogenous, porosity systems in the Upper St.George Group Carbonates. The diagenetic history and subsequent porosity development will be discussed in section 2.6.

W Late Devonian – Post Acadian Orogeny E
 Ophiolites gravitationally slide westward off uplift to east shortening HAA into triangle zone

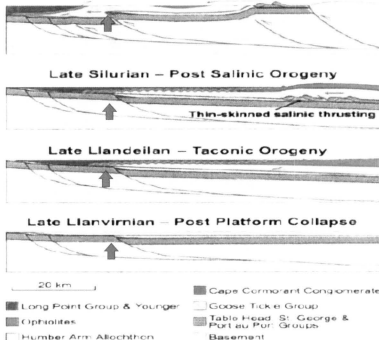


Figure 2.5.1 Schematic diagram displaying progression of deformation from the migration of forebulge, Taconic, Salinic, and Acadian Orogenies. Red arrow indicative of area of study. Lowest figure shows listric normal faulting from the migration of a forebulge axis westward. Onlap of allochthonous strata occurred during the Taconic. Metamorphism and thin skinned thrusting occurred during the Salinic mostly to the east of the Port au Port Peninsula. The Acadian brought about basin inversion in the Port au Port area and reverse sense reactivation of extension faults, along with the triangle zone formation, as the Humber Arm Allochthon was thrust into place. Figure modified from (Cooper et al. 2001).

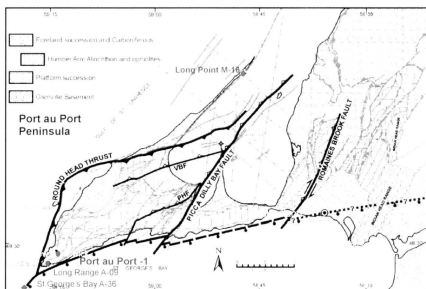


Figure 2.5.2. Structural and lithologic map displaying locations of wells, structural features, and surface lithology, Port au Port Peninsula, Western Newfoundland. Figure displays major faults, antiforms, and synforms. Existing seismic lines are shown in gray. VBF represents Voisey's Brook fault. Figure modified from (Cooper et al. 2001).

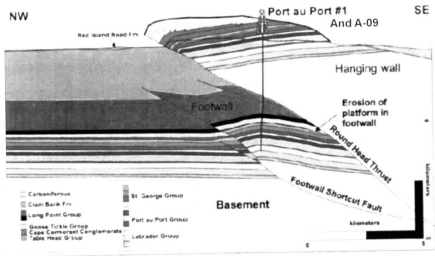


Figure 2.5.3 Cross section line trajectory and targets of the PAP-1 and A-09 wells. Both wells targeted the foot wall trap section of the Round Head Thrust. In the local vicinity, a short cut thrust fault, common named the St. George Fault, created the lower boundary of the trap antiform. Figure modified from (Cooper et al. 2001).

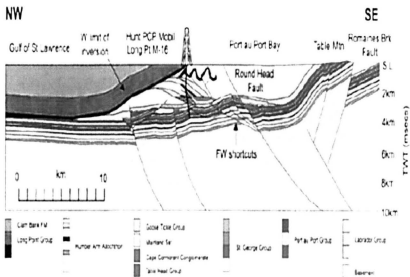


Figure 2.5.4 Interpreted structural and stratigraphic section well trajectory M-16. Cross section demonstrates the trajectory of the M-16 well as it is spudded on top of the Tea Cove Thrust. The well quickly penetrates in to the triangle zone into imbricate thrust sheets of the Humber Arm Allochthon. The well crosses a shear zone at the bottom of the triangle zone and terminates in the Ordovician Carbonate Platform. The triangle zone is bordered to the east by the Round Head Thrust and accompanying footwall shortcut faults. Figure modified from (Cooper et al. 2001).

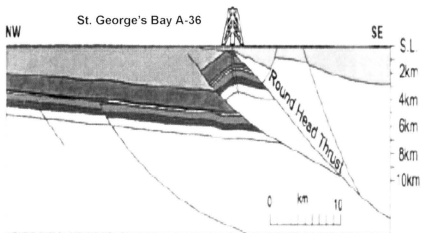


Figure 2.5.5. Interpreted stratigraphic and structural cross section well trajectory for A-36. Well A-36 targets a structural trap similar to PAP-1 and A-09 located in the carbonate platform bounded by the Round Head Thrust to the east and a footwall sort cut fault to the west. Picture uses same color scale as figure 2.6.4 Figure modified from (Cooper et al. 2001)

2.6 Diagenesis, Dolomitization, and Porosity Development

The Cambro-Ordovician passive margin carbonate platform was subjected to polyphase deformation during the Taconic, Salinic, and Acadian Orogenies. The effects of this complex tectonic history caused multiple phases of dolomitization, cementation, and porosity development in the Upper St. George Group. Several studies in recent time have documented (e.g. Collins 1975; Haywick 1984; Lane 1990; Baker 1993; Lavoie 2005; Knight et al. 2007; Azmy et al. 2008) the diagenetic history in the carbonate platform. The reservoir concept model in the Port au Port area is analogous both to the karst controlled reservoir model of the Ellenberger Carbonates in West Texas (Kerans, 1989) and structurally controlled hydrothermal dolomite plays described by (Davies, 2006). Heterogeneity is a major factor as structural events and diagenetic process have created a wide variety of reservoir facies. The paragenetic sequence of events that affected reservoir quality in the Upper St. George Group can be broken down in to dolomitization, cementation, mineralization, and solution events (Figure 2.6.1).

(Haywick, 1984; Lane, 1990) have identified three different generations of dolomite in the St. George Group Carbonates, specifically the Aguathuna and Catoche Formations. Chronologically, the first generation of dolomite (D1) was deposited in tidal mixing zones with a meteoric and seawater. Dololaminites in the Aguathuna Formation fall into this category of dolomites. These are composed of finely crystalline, uniformly luminescent, anhedral dolomicrite. Continued growth after burial is suggested by coarser, better zoned crystals in some dololaminites.

The second generation of dolomite (D2) comprises matrix and mottle dolomites. This postdates supratidal deposition at the beginning of burial and compaction of the St. George Group. Matrix dolomites in the fine grained limestones, and mottle dolomite in the (D2) form from long lived, mid-burial hydrothermal diagenetic events. Within mudstones and wackestones, matrix dolomite form clear euhedral, non-ferroan, finely crystalline (100 μm) (Haywick, 1984). Matrix dolomite (D2) in coarse grained limestones and packstones is coarser (200-500 μm) and has very irregular crystalline outlines where it abuts to other grains. Luminescence is zoned and color ranges from purple to red. The dolomite is pore-filling in grainstones, and postdates non-ferroan calcite cement (Haywick, 1984). It is likely, because of the varying nature of cathodoluminescent zonations that, Mn^{2+} and Fe^{2+} concentrations varied widely during dolomitization. Mineralized fluids were introduced through uncemented micro-porosity in the limestone and diagenetic fractures which allowed for prolonged formation of the matrix dolomites (Haywick, 1984). (D2) varies petrographically and in luminescence. Rhombs are fine to medium crystalline (50 to 150 μm), idiomorphic to xenotopic, non-zoned to exceptional well zoned, and range in luminescence from purple to bright red (Azmy, 2008). The degree of replacement of ichnofossils is variable. Some burrows are completely replaced while others are only partially replace, or not replaced at all. This suggests some of burrows were filled with xenotopic mosaic and then infilled in the center by spar calcite cement (Haywick 1984). Relationship to stylolites and evidence of dolomitization beyond cementation events suggests that D2 dolomitization was a late diagenetic event.

Feature	Marine	Meteoric	Burial	
			Shallow	Deep
Marine deposition (C1) & fibrous cements (C1b)	_____			
Uplift & meteoric equant Cements (C2)		_____		
Dolomite 1 (D1)			_____	
Solution seams			_____	
Dolomite 2 (D2)				_____
Stylolites				_____
Vertical fractures				_____
Saddle dolomite (D3)				_____
Pyrite mineralization				_____ Phase 1
Fracture-filling calcite (C3)				_____
Pyrite mineralization				_____ Phase 2
Silicification				_____

Figure 2.6.1. Chronologic diagram of paragenetic events occurring in diagenetic environments. Although not shown here, D4 dolomite developed during deeper burial. Figure from (Azmy et al. 2008)

Cavity filling saddle dolostone (D3) precipitated as exposure and erosion occurred on the St. George Group carbonate platform. The sediment that composes the cavity filling dolostone is mostly composed of pre-existing components such as anhedral dolomite, feldspar, micas, phosphate grains, and clays. Dolomite is by far the most abundant mineral, but other accessory minerals can make up to 15 % of the cavity fills. Crystals in the cavity dolostone range from 10 μm - cm scale and luminesce dully (Azmy et al., 2008). Paragenetically, the cavity filling dolostone postdates the D1 dolostone. Texturally, this is indicated by filling sediment being often penetrated in to the rocks by way of the boundaries along the D1 dolostone rhombs. Cavity filling dolostone also cross cuts algal structures in D2 dolomite in the Watts Bight Formation, but does not reach any higher. (Which indicates D3 postdates initial D2 dolomitization) (Lane, 1990). Pervasive D2 and D3 saddle dolomite developed as rapid burial of the platform occurred. Fractures associated with tectonism provided fluid flow pathways during the Acadian Orogeny. The mineralogy of the D3 saddle dolomite and the D2 dolostone are identical and therefore can be discussed as one. Dolomite in D3 saddle and D2 dolostone is medium crystalline (100 to 200 μm), forms xenotopic mosaics. Ichnofossils and gastropods are extremely well preserved. Intercrystalline pore space within the pervasive D2 dolostone is completely occluded by black organic rich, insoluble material. Despite similar composition, saddle dolomite occurred at different timing relative to D2 dolomite when tectonism was creating fracture networks in the St. George Group. The complete synopsis of dolomite systems in the St. George Group is complex for the scope of this thesis and the systems are simply introduced here aimed at visualizing complexity of

porosity development in the reservoir units. Cementation and solution seams also have significance in the diagenetic development of the reservoir units.

(Azmy et al. 2008) describes similar four generations of cementation, stylolitization and fracturing analogous to dolomitization events (marine, subaerial exposure/ meteoric, shallow burial and deep burial). Marine diagenesis accompanied the deposition of micrite and micritic algae cement (C1), skeletal components, and accretion of sediments. Also, isopachous fibrous marine cement (C1b) with internal sediments and microborings (Azmy et al. 2008) (Figure 2.6.1). Upon subaerial exposure and associated dissolution/development of secondary pore system into the underlying Aguathuna and Catoche Formations, non-luminescent meteoric equant cements (C2) precipitated below the water table. As the carbonate platform was initially buried, compaction features such as in-situ close packed grains, fitted fabrics, and microstylolites began to occlude porosity (Azmy et al. 2008). Higher amplitude stylolites formed with increasing burial depth along with pyrite mineralization in fractures and pores. Upon development of fractures in deep burial (late diagenesis), calcite cement (C3) occludes void space and engulfs pyrite crystals (Azmy et al. 2008). The listed diagenetic events are interpreted as synchronous to dolomitization events previously described. The seven types of cement and three generations of dolomite in the Upper St. George Group play a major role in the development of porosity, heterogeneity, and permeability of the reservoir units and the following discussion provides some detail about the reservoir characteristics from well information in this study.

2.6.1 Reservoir targets

The initial target reservoirs on the Port au Port peninsula were the Upper Aguathuna and Catoche Formations based on the subaerial exposure, karst involved model reservoirs of the Ellenburger Formation in West Texas (Kerans, 1989; Lucia, 1995). Based on outcrop and well data studies the karstification from the St. George Unconformity seems to be minor in the development of the porosity-permeability system. Most of the pore space created in these processes has been diagenetically replaced (Cooper et al. 2001). The dominant mechanism for reservoir development in the system is interpreted as hydrothermal dolomitization stemming from extensional collapse of the platform previously described. Some initial dissolution porosity developed at the timing of the St. George Unconformity along the tilted, subaerially exposed platform blocks, but was occluded by cementation and early dolomitization. In the Early to Middle Devonian, after burial by the Taconic and Salinic Foreland basins, Acadian tectonism was occurring in the east. Hydrothermal fluid migrated up the extensional fault pathways during this time as supported by isotopic evidence from (Lane, 1990) in the lead-zinc mineralization at Daniel's Harbour Mine. Hydrothermal fluid migrated upward in succession until they came into contact with a significant permeability barrier (Goose Tickle Group). As a result, the hydrothermally altered rocks are located on paleohighs of the fault blocks (Cooper et al. 2001) where the fluids preferentially altered the porous and permeable Aguathuna and Catoche Formations. Hydrothermal alteration and porosity development is greatest in the paleohighs having thinnest development of the Table Point Formation and poorest in paleolows (Knight, 2007) (Refer to Figure 2.6.2). It is important to note

only in the footwall sections of major thrust and extensional faults does porosity develop well enough to generate reservoir conditions. Rocks in the hanging wall sections are invariably tight and it is apparent hydrothermal fluids did not infiltrate these areas.

In the Port au Port I (PAP-1) (Figure 2.6.2) well, the strata in the hanging wall of the Round Head Thrust is similar to contiguous outcrop. Log porosities indicate a maximum of 4% with most areas close to zero. However, in the footwall section, there are several porous and permeable zones. The first is immediately below the St. George Unconformity in the Upper Aguathuna Formation. The zone is ~ 20 m in thickness, averages 10% porosity and 21 md in permeability (Cooper et al. 2001). Caverns below the St. George Unconformity appear on FMS logs. This reservoir interval produced oil at maximum rates of 1750-2400 bbl/day and approximate 25% water cut at pressures of 25 MPa. Several meters above and below the caverns are vuggy, sucrosic dolomites that have a possible zebra-dolomite texture. Drill cuttings contain abundant sparry white dolomite, pyrite, galena, and sphalerite. The well produced 5012 bbl of oil and 2737 bbl of water during a seven day test at variable rates with a gradual decrease in rate and pressure. The underlying Catoche Formation is also extensively dolomitized but not as porous, having 15 m of 9% porosity (Cooper et al. 2001). Some white dolospar is present in drill cuttings, but there is no indication of lead- zinc mineralization. The interval 3515-3600 m flowed 800 bbl/day of formation water. The Table Point Formation is thin in the footwall section of the PAP-1 well indicative of a paleohigh section on the faulted platform. Mineralization in the drill cuttings further indicates a paleohigh in well as hydrothermal dolomitization preferentially altered rocks in the vicinity.

The Long Range M-16 (Figure 2.6.2) well exhibits poorer reservoir quality than PAP-1. Both the Aguathuna and Catoche Formations are tight, the latter only slightly dolomitized (Cooper et al. 2001). The M-16 well lies in a structurally low region on the fault blocks of the platform indicated by a thick showing of the Table Point Formation and lack of any mineralized zones. Porosity and permeability are less than 3% and 2 md, respectively. The M-16 well was primarily drilled to prove the geometry of the triangle zone at the leading edge of deformation and was essentially a delineation well (Cooper et al. 2001). The St. George A-36 (Figure 2.6.2) well encountered a largely dolomitized, but tight interval at the top of the carbonate platform. Core taken from the Aguathuna Formation displays a tight, peritidal laminated mudstone to packstone that has pinpoint oil staining in the matrix and along fractures (Cooper et al. 2001). The thickness of the Table Point Formation is ~ 70 m and hydrothermal alteration is very low despite its 3 km proximity to the PAP-1 well. This lack of hydrothermal alteration is interpreted to account for the lack of porosity development in the well. In well Long Range A-09 (Figure 2.6.2) porosity and permeability are slightly developed and somewhat correlative to PAP-1 in the zones it occurs. The paleorelief is similar to the PAP-1 well, however, the amount of hydrothermal mineralization and dolomitization is less. Neither oil nor water shows were recovered from test in the A-09 well with only minimal gas cuttings (Cooper et al. 2001).

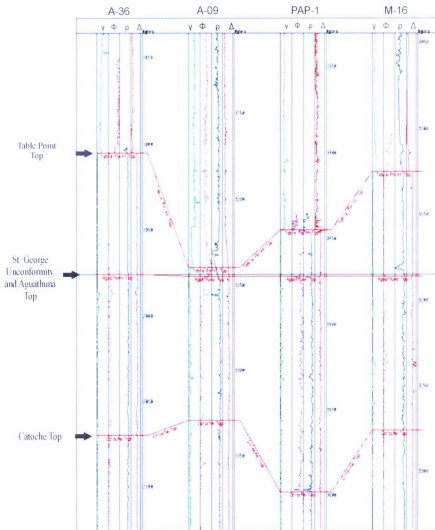


Figure 2.6.2 Correlation of A-36, A-09, PAP-1, and M-16. γ - Gamma Ray Φ - Neutron Porosity ρ - Bulk density Δ = Interval transit time (Sonic log). The major point of this figure is to show thickness variations of the Table Point Formation, indicative of paleorelief. St. George Unconformity Datum.

2.7 Facies Interpretation

The St. George Group (Ordovician) is a complex succession of limestone and dolostone, divided into two, third-order sequences of Tremadocian and Ibexian (Arenigian) age. (Knight 1987; 1989) and (Cooper et al. 2001) suggest these third order sequences are part of a Passive Margin Megasequence that is characterized by a three part internal architecture. This tripartite architecture includes a thin, lower peritidal unit, thick middle subtidal unit and thick upper peritidal unit. The youngest (Ibexian) Arenigian unit in the Upper St. George Group, that contain the units of interest in this study (Aguathuna and Catoche formations), is bounded below by the Boat Harbour disconformity and above by the St. George unconformity (Figure 2.7.2)(Knight et al 2008). Overall the carbonate intervals of the Upper St. George Group represent a small window, in a relatively large block time, of passive marginal shallow marine deposition. The Passive Margin Megasequence (PMMS) represents a period deposition, beginning with the Forteau Formation (Early Cambrian) (Figure 2.7.2) and ending with St. George Unconformity at the top of the Aguathuna Formation (Ordovician). Through time the lower PMMS progressively, upward deepens from shallow marine sandstones to reefal limestones (Devils Cove Member) into deeper marine shales. This transition likely occurred in response to thermal subsidence following cessation of active rifting (Williams,1987). The Hawke Bay Formation (Cambrian) (Figure 2.7.1) facies is shallow marine sandstone, transitioning eastward into thin sandstone turbidites and thick channel bound quartz arenites of the Penguin Cove, Summerside, and Irishtown formations. (Figure 2.7.1). In the upper PMMS, there is a facies shift to shelf carbonate deposition.

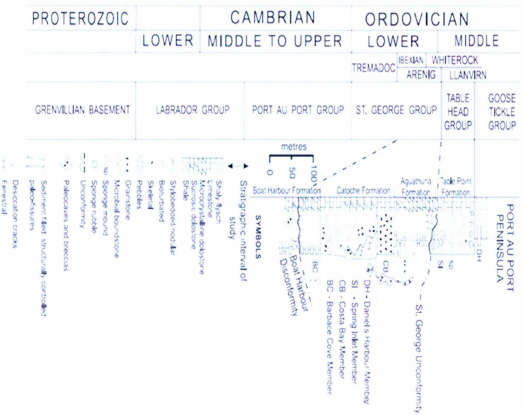


Figure 2.7.2: Lithostratigraphy of the Upper St. George Group and Table Head Group. Stratigraphic interval of study, shown by black arrows. Figure modified from (Knight 2007).

The upper PMMS is nearly exclusively carbonate and commences with the Lower Port Au Port Group (Cambrian) (Figure 2.7.2) (Chow 1992) and ends with the Upper St. George Group. The stage of the PMMS represents a termination of siliclastic deposition associated with a transgression that is likely eustatic (Knight et al. 2007). Strata in the PMMS record cycles of changing water depth on the carbonate platform, and also record the flooding of the platform in intercalated shaly carbonate layers of the Petit Jardin Formation (Figure 2.7.1) (Knight et al 2007). The rocks of the St. George Group represent deposition in a stable shelf environment. The stromatolitic and thrombolitic-rich, burrow mottled limestones and dolostones of the Watts Bight Formation (Figure 2.7.1) suggest that prior to regional dolomitization, these rocks were mostly likely deposited in a subtidal shelf facies (Knight, 1977; Levesque, 1978). The Catoche Formation of the middle St. George Group is dominated by lime mudstones and wackestones and regionally overprinted by dolomitization near the top. Depositional facies for the Catoche is also thought to be of subtidal conditions. The Boat Harbour and Aguathuna Formation, of the Middle and Upper St. George Group respectively (Figure 2.7.2), were deposited in shallower water facies than other formations because of the abundant dololaminite bed they contain. The interpretation of upper-tidal intertidal-supratidal facies has been suggested by (Levesque, 1978; Pratt, 1986) for those formations similar to present conditions forming in tidal flats. The dessication cracks, tepee structures, cryptalgal and millimeter scaled laminations, the lack of abundant body fossils, and no evidence of evaporate minerals leads to the interpretation of shallow water origin.

The interbedded dololaminite – limestone lithology of the Boat Harbour and Aguathuna formations, have been interpreted as the results of repeated shoaling upward cycles in a shoreline tidal flat (Levesque, 1978; Lane, 1990). The lithologic variation in these cycles (i.e. from mudstone to grainstone) was explained by (Levesque, 1978) as the periodic winnowing of subtidal muds, most likely through storm action. This winnowing is thought to result in laterally discontinuous grainstone that intermixes with the nearby mudstones and wackstones. A complete shoaling upward sequence would therefore consist of subtidal stromatolitic or thrombolitic burrow mottled rocks of the intertidal zone and finally into supratidal dololaminites.

The aims of this chapter were to introduce the complex geology of the (Ordovician) Upper St. George Group carbonates (Aguathuna and Catoche formations). This chapter has discussed the formations specifically, but also in the context of regional variation and relationship to strata above and below. In chapter three, data from the aforementioned wells will be analyzed for petrophysical relationships and meaningful petrophysical and porosity information will be used to build 1-D synthetic seismograms.

Chapter 3: Synthetic Seismogram Analysis

The scope of the study in chapter three is to develop a “key” for recognizing the effect of porosity in seismic wavelets across reflection horizons. The study begins with well data from the four well introduced previously: A-09, A-36, PAP-1, and M-16. In order to reveal the porosity effect on seismic data, the “effect” must be characterized. The way this study characterizes the effect of porosity is by integrating the porosity information into 1-D synthetic seismograms. Then, one can observe, over a multitude of complex trace attributes, the effect that porosity has on waveform character. The 1-D synthetic seismograms are generated from petrophysical well log data of the four aforementioned wells. The well curves analyzed are caliper, bulk density, sonic, gamma ray, and neutron porosity.

The caliper log is simply a tool inserted into the well bore with mechanical arms that measure the inner diameter of the well bore. This use of the tool in this study assists with assessing intervals of error in the well data, e.g. Intervals of borehole washout and log tool error.

The bulk density tool is used to compute the total density of the rock unit including fluid/gas and void space content. The tool measures electron density in the matrix of the formation by focusing charged photons from a gamma emitting source. When the photons interact with the electrons, they do not make it back to the log tool. Therefore, the greater the electron density, the less photons are recorded and the more

dense the rock (Bigelow, 2002). This tool is particularly useful for aiding lithology identification and can indirectly assist in measuring porosity.

Sonic log tools measure the acoustic interval transit time of the formation between a source and a series of receivers along the tool. Velocity is measured between the source and receivers as slowness, measuring the duration of travel/distance rather than distance/time (Bigelow, 2002). Porosity inherently slows acoustic velocity of sound in a rock by increasing void space and decreasing the acoustic connectivity in the matrix. Despite being sensitive to acoustic effect of porosity, the sonic tool should not be solely used to measure porosity due of numerous factors influencing the acoustic properties of rocks. The sonic tool is also useful for assisting in the interpretation of lithology.

Gamma ray and neutron logs function similarly by measuring the amount of natural radiation emitted from a formation. The gamma tool measures specifically gamma radiation emitted from potassium, uranium and thorium. These three minerals are most often associated with clay rich lithologies and make this tool a widely used lithology/VShale indicator.

The compensated neutron tool utilizes an artificial radioactive source to emit fast neutrons into the rock formation (Hallenburg, 1998). The fast neutrons propagate in a 360 degree pattern and interact with the atomic nuclei of the rock. The speed of the neutron emission is moderated by collisions in the rock's atomic matrix until the neutron either reaches epithermal or thermal energy, or is captured. Hydrogen is the primary source of neutron capture and is mostly contained within fluid such as water or

hydrocarbons (Hallenburg, 1998). When the neutron is captured by a hydrogen atom, a low energy capture gamma-ray is emitted. The tool contains two detectors, the epithermal and thermal sondes that detect the energy of the neutrons at a specific distance away from the source. The lower the neutron energy and the higher the amount of low-energy capture gamma rays detected, indicate a higher presence of hydrogen (Hallenburg, 1998). Since almost all formational hydrogen is in fluids, and fluids are located in void space, the tool used to measure porosity. Other factors, however, influence the compensated neutron tool reading.

Environmental factors and lithology matrix type affect the energy loss of the fast neutron and these must be corrected to obtain an accurate porosity reading. Since clay minerals and shales contain matrix bound water, it is important to apply a “shale” correction to mitigate the excess hydrogen present in the measurement. As the neutrons interact with the formation nuclei, the geometry directly affects the amount of collisions and energy loss of the artificial fast neutrons (Hallenburg, 1998). Therefore, it is important to apply matrix correction curves to the output of the tool as all measurements are recorded with a limestone matrix calibration.

The information provided in the well logs from the above mentioned tools will establish a correlation between the petrophysical properties and porosity so that 1-D synthetic seismogram models can be built. The intent of the synthetic seismograms is to simulate the acoustic response of a range of porosity conditions in the reservoirs. A series

of geostatistical assessments and data filters are necessary to reveal useful petrophysical relationships and eliminate erroneous data prior to generating synthetic seismograms.

3.1 Preliminary Statistical Assessment

In order to derive meaningful data from the reservoirs in this study, it was necessary to conduct an assessment of the relationship between porosity, density, sonic velocity, and acoustic impedance in the well logs. Porosity typically has predictable effects on the petrophysical properties of the rocks. Bulk density of rocks decreases when void space, or porosity, increases and acoustic velocity decreases when porosity increases. Revealing these relationships and distinguishing lithology in the well data is the primary goal of the statistical assessment. Without establishing a relationship between the petrophysics and porosity in the well data, continuation of this study would not be valid. By confirming and constraining the petrophysical correlation to porosity, petrophysical models could be built to simulate a variety of porosity conditions. The end goal of this chapter is to use these models to build and analyze 1-D synthetic seismograms. Also, it is necessary to eliminate areas of erroneous well data such as borehole washouts or tool malfunction. Errors in the well data are additionally quality controlled by using the caliper logs. Approximately 250 m of well data lithostratigraphy, from Table Head Group (Ordovician) to the lower St. George Group (Ordovician), are analyzed in petrophysical crossplots.

The first geostatistical analysis is standard X-Y linear regression cross plots of bulk density (RHOB), sonic interval transit time slowness (inverse velocity) (Δt), and

Acoustic Impedance (AI) vs. Matrix (Dolomite and Limestone) corrected Neutron Porosity (NPHI or NPOR). (All neutron porosity values in the well data were originally recorded by a Schlumberger compensated neutron tool calibrated for limestone matrix. The neutron tool responds differently to each type of lithology outputting different values based on calibration.) A database filter is designed to reveal lithology types to objectively observe each individual response to porosity. The primary mineralogy types, suggested by literature in chapter two (Knight et al 2007), that exist in the reservoir units are variations of calcite and dolomite. Limestone lithology (Calcite dominant) is separated in the well data by bulk density values in the range of 2.68 -2.74 g/cm³, gamma values <20 API, and sonic values in the range of 155-165µs/m. (values from (Bigelow, 2002)). Dolomite is separated by bulk density values of 2.82-2.87 g/cm³, gamma values of < 20 API, and sonic values of 142-155 µs/m (Bigelow, 2002). A Schlumberger supplied dolomite matrix porosity correction equation (Figure 3.2.1) is applied to the dolomite lithology to obtain accurate porosity readings. The following paragraphs discuss and illustrate the relationships between bulk density, sonic velocity, acoustic impedance, vs. porosity in separate X-Y plots.

Bulk Density (RHOB) is the first petrophysical property evaluated against corrected neutron porosity. Bulk density, in this study, is a computation of the total rock density including void space and pore fluids according to (Fetter, 2001). The intuitive expectation of this comparison is that increasing porosity yields less rock density as rock volume is replaced by gas or fluid filled volume. (Figure 3.1.2) demonstrates an example relationship between bulk density vs. porosity in well A-09. The trend overall, displays a

decreasing density with increased porosity which is intuitive. However, there is an increasing trend of density (2.68- 2.79 g/cm³) from 0 – 5 % porosity. This issue will be addressed in further detail later in section 3.2. The three other wells, M-16, PAP-1, and A-36, exhibits nearly identical character in the RHOB vs. NPOR X-Y plots as the A-09 well (Appendix A). This type of intuitive correlation is expected to occur in the Sonic Velocity (Δt) vs. NPOR X-Y plots as well.

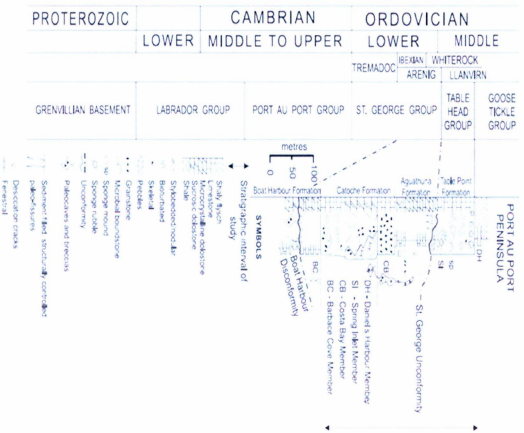


Figure 3.1.1: Lithostratigraphy of the Upper St. George Group and Table Head Group. Stratigraphic interval of study shown by black arrows. Figure modified from (Knigh 2007).

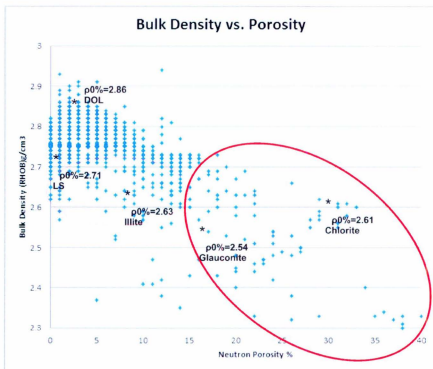


Figure 3.1.2: Standard X-Y Plot of Bulk Density (RHOB) vs. Corrected Neutron Porosity in well A-09 displaying the general trend of decreasing density with increasing porosity. The graph contains all lithology in the sample interval. Notice the red circles encompassing the outlying data. This region is interpreted to represent either undesirable mineralogy, log tool error, or bore hole wash out and removed from the data. Black text indicates different mineralogy represented at 0% true porosity in each mineral for reference. The neutron porosity is calibrated to limestone matrix.

Sonic velocity or in this case the reciprocal, interval transit slowness time (Δt), is another important petrophysical property used in this study to reveal porosity relationships. In the X-Y cross plots, the intuitive response is increasing interval transit time (decreased acoustic velocity) with increasing porosity due to the decrease in matrix connectivity (Rider, 1991). In the A-09 well, Δt vs. NPOR cross plot, the general trend is increasing transit time with increasing porosity (Figure 3.1.3). Again, there is an anomalous decrease initially from 145-165 $\mu\text{s/m}$ and 0-5% porosity. Outlying, higher porosity coinciding with very high transit times are again interpreted to represent either clay rich lithology or extremely vuggy pore space/ borehole washout in the sample interval. Results of the Δt vs. NPOR X-Y cross plots in the other three wells again show very similar results as the A-09 well (Appendix A). The final X-Y cross plot in this initial data assessment is the acoustic impedance (AI) vs. NPOR.

Acoustic impedance is a petrophysical property calculated from the product of bulk density and acoustic velocity (in this case it is calculated from $1/\Delta t$). This property is integral in the calculation of reflection coefficients and synthetic seismograms (Sheriff 1995). The linear relationship observed in the density and sonic slowness vs. porosity plots is not as prevalent in the acoustic impedance plots. However, acoustic impedance does decrease overall with increasing porosity (Figure 3.1.4), which corresponds with theory. There are outlying low acoustic impedance values in higher porosities, similar to the outlying nature of higher porosities in the density and sonic plots. This outlying data is interpreted again to be clay rich lithology or extreme vuggy porosity/ borehole

washout. Once again, redundant information is observed in wells A-36, PAP-1, and M-16 cross plots (Appendix A). Although a clear relationship is established between porosity and petrophysics in this study, one issue remaining unclear is the unexplained behavior of the X-Y plots between 0-5% NPOR. Furthermore, each porosity percentage had numerous petrophysical values correlating with it. A process is needed to determine the most accurate petrophysical values at any given porosity and this procedure will be discussed in section 3.3 and 3.4.

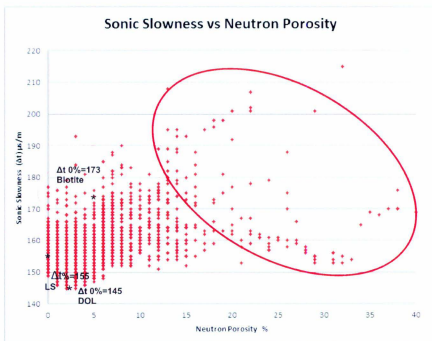


Figure 3.1.3: Standard X-Y plot of Sonic Slowness (Δt) vs. Corrected Neutron Porosity (NPOR) in well A-09 displaying the general trend of increasing interval transit time with increasing porosity. This graph contains all lithology types in the sample interval. Notice the red circles encompassing the outlying data. This region is interpreted to represent either differing mineralogy, log tool error, or bore hole wash out and was removed. Black text indicates sonic slowness of selected mineralogy at its respective 0% porosity.

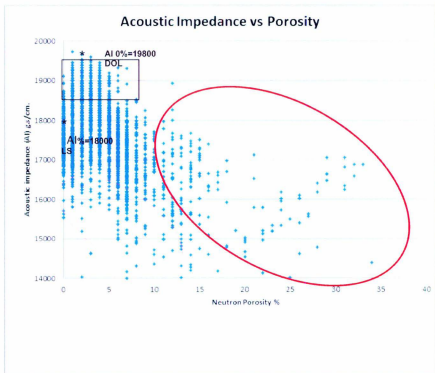


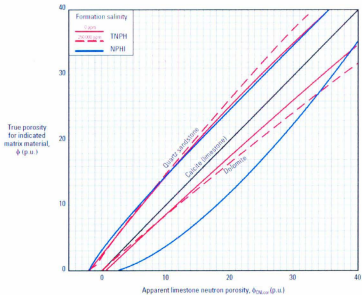
Figure 3.1.4: Standard X-Y plot of Acoustic Impedance (AI) vs. Corrected Neutron Porosity (NPOR) in well A-09 displaying the general trend of decreasing acoustic impedance with increasing porosity. This graph contains all lithology types in the sample interval. Red circles contains regions of undesirable data that has been removed. Black box indicates anomalous area. Black text indicates dolomite (DOL) and Calcite (LS) values at respective 0% porosities.

3.2 Lithologic Segregation in Well Data

A phenomenon in the data between 0-5% neutron porosity occurs in every RHOB, Δt , and AI vs. neutron porosity cross plot. In the A-09 bulk density plot (Figure 3.1.2); it occurs as an upward trend from 2.68- 2.79 g/cm³. In the A-09 sonic plot, it occurs as a downward trend from 165-145 μ s/m (Figure 3.1.3). Finally, the A-09 AI plot displays the phenomenon as a blocked region from 16000-19000 g.s/cm (Figure 3.1.4). This event is interpreted as a neutron porosity tool effect between dolomite and limestone (calcite). One can examine (Figure 3.2.1) to begin visualizing the effect on the anomalous plot character in (figures 3.1.2- 3.1.4). In (figures 3.1.2-3.1.4), each petrophysical property has been noted where each lithology would plot with 0% percent true porosity. The location of dolomite at 0% true porosity lies on 3% **neutron tool** porosity in the entire cross plots. This is precisely where dolomite with 0% percent true porosity lies on the neutron tool matrix correction plot (figure 3.2.1). This explains the anomalous break in linear trend noted above in the cross plots.

This separation of lithology in the cross plots can be further confirmed from an empirical study. A simple empirical model, based on core lithology data and chapter two literature, from the four wells specifically in the St. George Group (Aguathuna and Catoche Formations) is designed to separate lithology. Intervals of known lithology (either limestone or dolomite), from this data are plotted separate from bulk lithology on RHOB, Δt , AI, vs. neutron X-Y plots. For example, a clean dolomite from the upper Aguathuna Formation (Well A-09, 3310-3325m MD) and clean limestone from the

middle Catoche Formation (Well A-09, 3465-3475m MD). The data from selected lithology intervals is overlain on the bulk lithology X-Y plots to show lithology contrasts (Figure 3.2.2). The contrast between dolomite and limestone is particularly apparent in the overlays. The results are intermixed on the plot, however, because the formations themselves are composed of a mixture of dolomite and calcite. This model further rectifies anomalous behavior in the bulk lithology plots and allowed for continued interpretation of the porosity effects on different rock types. Lithology contrast grouping comparable to (Figure 3.2.2) are apparent in the remaining petrophysical properties (Δt and AI) X-Y plots and in all wells. Once the relationship between porosity and petrophysical properties is apparent, the next objective is assigning best representative values of petrophysical properties to certain porosity percentages. The results of this assessment are then used in creating block porosity models later on in this study.



TMMark of Schlumberger
© Schlumberger

Figure 3.2.1. Matrix correction plot from (Schlumberger, 2009). Diagram displays limestone (calcite) as the original neutron measurement. Sandstone and dolomite corrections are shown with various salinity plots. NPHI has been used in this study

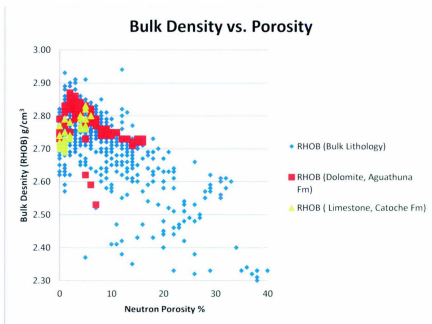


Figure 3.2.2: Example of a selected and bulk lithology X-Y cross plot of Bulk Density (RHOB) vs. Neutron porosity in well A-09. An overlay plot with the Dolomite and Limestone Intervals are denoted by color. Clean dolomite was recorded from 3310-3325m MD. Clean limestone was recorded from 3465-3475m MD. This diagram shows the clustering and separation of major lithology types. The intermixing between the dolomite and limestone on the plots is interpreted to be the nature of the rocks in this as suggested by literature.

3.3 Well Data Porosity Filter Analysis

A probability distribution analysis is designed to quantitatively constrain best representative values of RHOB and Δt at certain porosity percentages. The end objective of this filter analysis is to identify the petrophysical values representing porosity at 0, 5, 10, and 15%. By isolating petrophysical values at the above porosities, porosity can be modeled into reservoir zones on the well curves (This process will be discussed further sections 3.5-3.6). This filter is another step in building inputs for the 1-D synthetic seismic models.

This analysis is carried out in Microsoft Excel on the raw well data from the lower Table Head Group through the lower St. George Group (Figure 3.1.1). Preliminary database filters are designed to find bulk density and sonic velocity values in the bulk well curves occurring at selected porosity input. The following is an example of the process used to find bulk density values corresponding to a 5% neutron porosity input: The database filter scanned every depth interval and accompanying RHOB and neutron porosity values. If neutron porosity is equal to 5%, then the filter would return the value of RHOB at equal depth. If neutron porosity is not equal to 5%, then the filter would return FALSE at equal depth. This database filter is carried out for NPOR values of 0, 5, 10, and 15% returning corresponding RHOB and Δt numbers. Now, only bulk density and sonic velocity values coinciding with specified porosity remained in the filter columns and best representative values are selected by modal frequency analysis.

3.4 Frequency Analysis

A frequency distribution analysis on the filtered data is necessary to determine the best values of density and sonic interval transit time at selected porosities. The analysis is designed to graphically display (histogram) the frequency occurrence of a spread of values in a filter column. The range of values considered acceptable for density is 2.65-2.90 g/cm³ and 125-175 μ s/m for sonic interval transit time. These ranges eliminated the outlying values from interfering with desirable data. (Limestone and Dolomite). This statistical analysis is necessary due to variance in the range of density and acoustic velocity representing each porosity. (Figure 3.4.1) and (Figure 3.4.2.) display example histogram frequency analyses of RHOB and Δt , respectively, at 5% porosity in the A-09 well with standard deviation. Histograms, like figures 3.4.1 and 3.4.2, are generated in every well in the study at 0, 5, 10, and 15% porosity (Refer to Appendix A). The distribution is Gaussian on most histograms and low standard deviation and high degrees of confidence are common. The accuracy and high confidence of the Gaussian distribution is attributed to large numbers of data points available at selected porosity. Large amounts of data points are typically available in the wells at porosities between 0-5%. Porosities of 10-15% commonly did not provide as many sample data points for highly confident frequency histogram construction. The data in the 15% range, in some cases (Well M-16), did not contain enough sample points to build any degree of confidence and is not significantly valuable. Mean and modal values are recorded from each histogram with $\sigma_{std.dev.}$ (standard deviation) (Refer to Table 3.4.1 and Appendix C) These values are the best representative recordings of density and interval transit time at

0, 5, 10, and 15% porosity in the sample wells. The next step in the synthetic seismogram study involved generating block porosity models based on values from this frequency analysis.

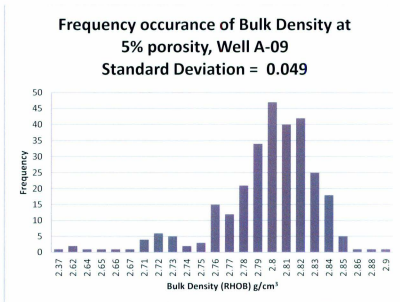


Figure 3.4.1: Graph displaying frequency distribution of Bulk Density (RHOB) at 5% Neutron Porosity (NPOR) Standard Deviation = 0.049. Mean= 2.79 g/cm³ Mode= 2.8g/cm³.

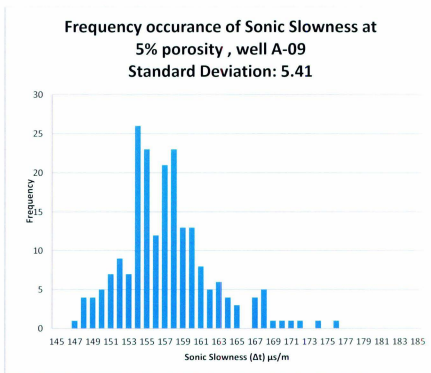


Figure 3.4.2: Graph displaying frequency distribution of Sonic Slowness (Δt) $\mu\text{s/m}$ at 5% Neutron Porosity (NPOR) Standard Deviation = 5.41, Mean= 157 $\mu\text{s/m}$ Mode= 154 $\mu\text{s/m}$.

	A-09	A-36	PAP-1	M-16
Δt,0%,Mean	157.064	155.835	157.388	155.125
Δt,0%,Mode	158.000	156.000	156.000	153.000
σstd. Dev. 0%Δt	3.074	2.327	2.515	6.718
Δt,5%,Mean	157.258	153.989	157.744	162.000
Δt,5%,Mode	154.000	152.000	152.000	157.000
σstd. Dev. 5%Δt	5.036	5.082	5.233	7.157
Δt,10%,Mean	164.163	162.688	165.273	158.778
Δt,10%,Mode	164.000	163.000	166.000	166.000
σstd. Dev. 10%Δt	7.339	6.519	7.273	6.180
Δt,15%,Mean	164.875	162.714	168.000	n/a
Δt,15%,Mode	164.000	160.000	169.000	n/a
σstd. Dev. 15%Δt	10.658	3.988	12.590	n/a
ρ,0%,Mean	2.747	2.740	2.741	2.730
ρ,0%,Mode	2.740	2.740	2.740	2.700
σstd. Dev. 0%ρ	0.023	0.017	0.043	0.059
ρ,5%,Mean	2.790	2.820	2.769	2.793
ρ,5%,Mode	2.800	2.830	2.790	2.830
σstd. Dev. 5%ρ	0.450	0.025	0.136	0.051
ρ,10%,Mean	2.700	2.759	2.731	2.730
ρ,10%,Mode	2.730	2.740	2.710	2.740
σstd. Dev. 10%ρ	0.070	0.024	0.067	0.017
ρ,15%,Mean	2.682	2.726	2.692	n/a
ρ,15%,Mode	2.730	2.730	2.690	n/a
σstd. Dev. 15%ρ	0.078	0.005	0.106	n/a

Table 3.4.1: Table displaying all frequency distribution analyses for the four wells in this study. P = Bulk Density, Δt= Sonic Slowness, σstd. dev. = standard deviation. Bulk density is displayed in g/cm³. Sonic Slowness is displayed in μs/m

3.5 Block Porosity Models

The best representative values for bulk density, sonic interval transit time, and acoustic impedance determined through the frequency analysis (Section 3.4) are used in generating block porosity well log models. The concept of a block porosity model in this study is quite simplistic. The models in this study are constructed in Landmark Geophysical software, Openworks/ Syntool on the density and sonic interval transit time well log curves. As previously mentioned, acoustic impedance is a controlling variable in the seismic response of a medium (Sheriff, 1995). Acoustic impedance is the product of velocity and bulk density of medium and therefore, changes in the velocity and density of a medium affect the seismic response. A block porosity model attempts to simulate porosity effects on sonic and bulk density well log data by altering the numeric data of well log curves to reflect changes associated with porosity. Reservoir architecture from e.g. (Cooper et al. 2001; Knight et al. 2007; Azmy et al. 2008) is maintained in a 25 m interval of the upper Aguathuna Formation and a 25 m in the lower Aguathuna and upper Catoche Formation in the models. Aguathuna and Catoche Formation reservoir porosity zones are mirrored from the four well log suites to simulate seismic changes from known porous zones in the models (Refer to Figures 3.5.1, 3.5.2 and 3.5.3, and Appendix B for neutron porosity correlation curves). Construction of models in reservoir units is homogenous and fixed on input values of density and sonic interval transit time determined from the frequency analysis at a specified porosity. However, prior to placing the models on the well curves, a calibration model is necessary to validate the block modeling theory.

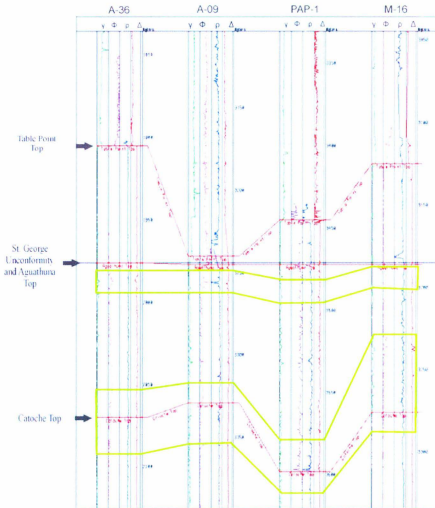


Figure 3.5.1 Correlation of A-36, A-09, PAP-1, and M-16. γ = Gamma Ray Φ = Neutron Porosity ρ = Bulk density Δ = Interval transit time (Sonic log). Note thickness of Table Point Formation indicative of paleo-relief. St. George Unconformity Datum. Green outline represent approximate reservoir intervals.

The calibration of the block porosity models is completed to demonstrate the model structure could successfully reproduce the seismic response of the original, unmodeled, synthetic seismograms. If the original seismic response can be reproduced by the calibration block porosity model, then the calibration models are valid. This ability is indicative that the model is sensitive enough to generate the acoustic contrasts produced by the lithology from the original well data. The construction of the calibration models involved taking an average of each petrophysical property (bulk density and sonic slowness) in the reservoir interval. Then, the next step is taking these averages, and using them to represent the entire anticipated block model interval in the reservoir (Figure 3.5.2). With the average values in place in the reservoir intervals, synthetic seismograms are generated from the calibration well curve block models. Synthetic seismograms from the calibration models are compared to the synthetic seismograms from the original well curves for waveform correlation. (Figures 3.5.2 and 3.5.3) The resultant seismograms, (from the models) successfully reproduced the reflection character of the original seismograms within reason. The slight variation between the two scenarios is attributed to placing a single average value along the reservoir model intervals and removing the multiple differences in the original data in the reservoir. The objective here is to demonstrate that the reservoir could indeed be assigned a data driven average value to represent the entire unit and still reproduce the original seismic response. This process validates the concept of the modeling procedure and allowed for developing block porosity models to best represent 0, 5, 10, and 15% porosity in the petrophysical data.

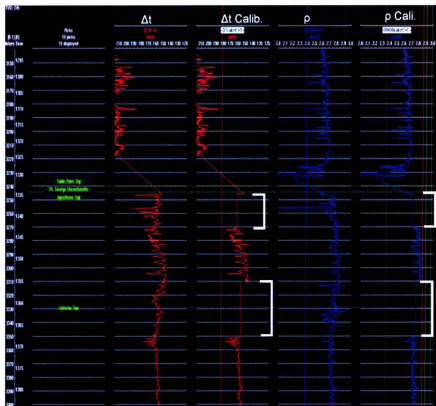


Figure 3.5.2. Diagram displaying comparison of the original and calibration block model interval transit time (Δt) and bulk density curves (ρ). The left, red curve is the original Δt curve. The right, red Δt curve features the calibration block model derived from the average values of data over the reservoir interval. The left, blue is the original (ρ) curve. The right, blue curve is the calibration block model curve for (ρ). Reservoir intervals of interest is denoted by white brackets.

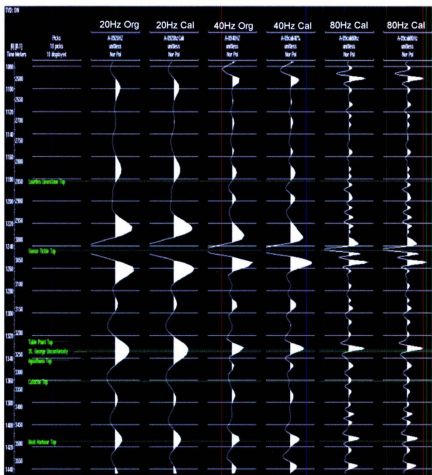


Figure 3.5.3 Synthetic seismogram comparison between original and calibration block models at 20, 40, and 80 Hz. Normal polarity, + reflection in white, Ricker wavelet. Notice the similarity in reflection patterns and waveform attributes between the original and calibration block model seismogram at all dominant frequencies.

The logical reasoning for homogenizing models in the whole reservoir deals with the resolution of typical seismic data and the scope for this study. Conceptualizing the reservoir units as one homogenous entity rather than continuously varying layers in depth, recognizes the minor contribution of very thin beds to the overall seismic response (Kallweit, 1982; Sheriff, 1995). Furthermore, most resolution of thin units cannot be imaged at the resolution of typical seismic waves. The reservoir units of the Aguathuna and Catoche Formations contain high porosity zones ranging between 10-30 m. These zones fall below the level of typical seismic resolution of about one quarter wavelength, 30-50m unit thickness . Therefore, the effects of this model will only manifest as subtle changes in wavelet attributes rather than additional reflections. By modeling the entire reservoir units as one consistent value, the subtle effect on the wavelet is maximized for observation. These subtle differences in attribute values are used as proxies for porosity across reflection horizons in 2-D data in Chapter Four of this study. The scope of the study in Chapter Three is simply developing a “key” for recognizing porosity effects in wavelets across reflection horizons. The design of the block models is employed for values representing 0, 5, 10, and 15% (Figure 3.5.4 and 3.5.5, and Appendix D) porosity in each of the four well data suites on bulk density and interval transit time curves. The objective in generating this model array is to create a mixing model scenario in which porosity models, and the subsequent synthetic seismograms, could be compared and contrasted at different porosity levels simultaneously. Synthetic seismograms generated from the porosity block models are processed and discussed in empirical and complex attribute analysis in section 3.6 of this chapter.

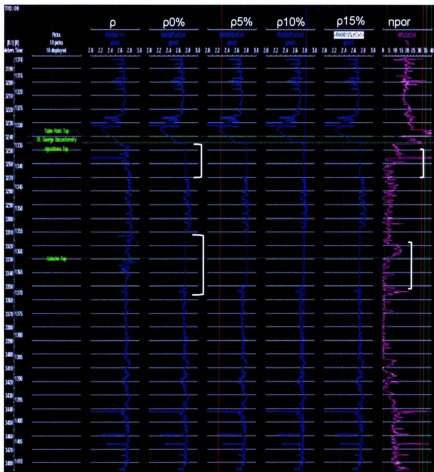


Figure 3.5.4. Block modeled well curve diagram for bulk density in well A-09 with Neutron Porosity correlation curve. Models (shown in blue) progress from original bulk density curve (ρ) to models at 0, 5, 10, and 15% porosity. Values for the porosity blocks in the models are taken from frequency analysis section 3.4. Notice in the Neutron log (purple curve) zones of higher porosity. These zones have been used for the block model construction. Green lines represent stratigraphic formation tops. White brackets indicate interval of interest.

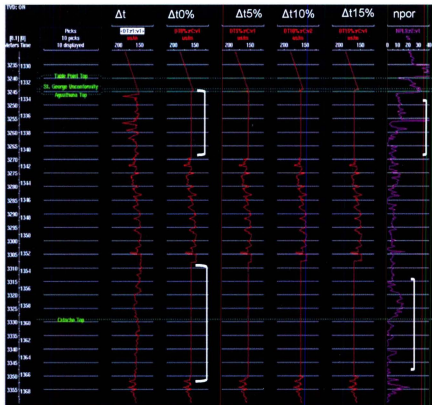


Figure 3.5.5. Block model well curve diagram for sonic interval transit time (AT) in well A-09 with Neutron Porosity correlation curve. Models (shown in red) progress from original AT curve to models at 0, 5, 10, and 15% porosity. Values for the porosity blocks in the models are taken from frequency analysis. Notice in the Neutron log (purple curve) zones of higher porosity. These zones are used for the block model construction. Green lines represent stratigraphic formation tops. White brackets indicate interval of interest.

3.6 Synthetic seismogram analysis

The purpose of generating one - dimensional synthetic seismograms in this study is to provide a model that is well data controlled, for complex trace attribute analysis, to understand the seismic response of different geology on porosity. Complex trace attribute analysis has been employed in exploration seismology since the late 1970's. Complex attribute analysis was spurred by so called "bright spot" exploration in the 1960's when interpreters realized apparent brightness of seismic reflectors on a true amplitude display depended on several factors besides geology (Barnes 2007). In particular, it was recognized differences in reflection polarity, or phase, obscure and change the amplitude of reflectors. Initially, interpreters tried to correct this problem by plotting seismic data twice; first with normal polarity then with reverse (Sheriff 1988). This approach did not take into account the effect of phase on the data and was awkward due to the spread of information over two displays. Nigel Anstey then invented a technique by combining the amplitude information from reverse and normal polarity that displayed the complete trace envelope independently of phase. This technique was classified as reflection strength and contained the amplitude of the original trace without phase information. A wide spectrum of attributes, using the Hilbert transform (quadrature trace) (Figure 3.6.1), were created since Anstey's initial technique for use in seismic interpretation. The Hilbert transform applies a 90 degree phase shift to the original signal and forms a quadrature trace (White 1991). Instantaneous attributes of the complex trace (quadrature trace) will be used in this study to reveal the subtle changes in waveform and amplitude in the synthetic seismograms from the effects of porosity.

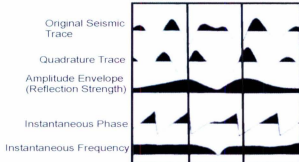
This study will utilize three complex trace attributes: instantaneous amplitude (reflection strength), instantaneous phase, and instantaneous frequency (Plate 3.6.1). These three attributes are commonly computed from the complex seismic trace and displayed as colored sections (variable density) or overlays on seismic traces to aid with interpretation. These attributes can be defined from the complex trace by (Equation 3.6.1 and Plate 3.6.1).

$$x_2 = \text{Re}\{A_1 \exp(j\theta_1)\} \quad \text{Equation 3.6.1}$$

Recorded seismic trace:	x_1
Complex trace or analytic signal:	$A_1 \exp(j\theta_1)$
Quadrature trace:	$\text{Im}\{A_1 \exp(j\theta_1)\}$
Amplitude envelope or instantaneous amplitude:	A_1
Instantaneous phase:	θ_1
Instantaneous frequency:	$(1/2\pi) d\theta_1/dt$

In equation 3.6.1, x_1 represents the real component of a complex signal $A_1 \exp(j\theta_1)$. A_1 is the amplitude envelope or instantaneous amplitude (reflection strength). The imaginary part of the complex signal is called the quadrature trace and is formed by applying a 90° phase shift (Hilbert transform) to the real trace. A_1 and θ_1 are the two basic instantaneous attributes (Barnes 2007) and are derived from the relationship between the quadrature trace and seismic trace by a Cartesian – polar conversion (Plate 3.6.1). From these two attributes, all others can be derived through various functions.

A



B

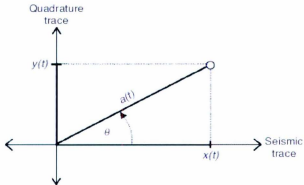


Plate 3.6.1

A.) Diagram displaying the derivation of attributes from a seismic trace using the Hilbert transform. Modified from (White 1991)

B.) Cartesian and Polar plot showing the derivation of $a(t)$ instantaneous amplitude (reflection strength) and θ Instantaneous phase. Figure from (Barnes 2007)

(E.g. instantaneous frequency can be derived from the differential of instantaneous phase (Barnes 2007)) (Equation 3.6.1 and Plate 3.6.1). This separation of amplitude information from phase data in a seismic signal is essentially the purpose of complex trace analysis. Instantaneous attributes describe the shifting, or partitioning, of energy at given sample points along a complex trace. They are excellent aids when trying to interpret changes laterally across reflection horizons on seismic data. However, with the exception of isolated gas sands, they should not be used for direct interpretation because of the many different interference effects on the seismic signal involved in the generation of attributes. The meaning of each attribute is not always straight forward and has room for exploration of definition.

Instantaneous amplitude (reflection strength) measures, in theory, the dimensions of the trace envelope and by design, measures the strength of a reflection. All amplitude information in the seismic trace is contained within the reflection strength analysis and quantifies it independently of phase and polarity (Barnes, 2007). Instantaneous phase essentially represents the seismic trace with all amplitude information removed and acts as the perfect automatic gain control (AGC) (Barnes, 2007). Its values refer to the apparent position of the cosinusoid for which peaks on the seismic trace 0° phase, troughs have 180° phase, downward zero crossings have a 90° phase, and upward zero crossing have -90° phase. Instantaneous frequency is measure of apparent spacing between reflections and gives the interpreter an idea how the seismic wave is partitioning or convolving. There are several other types of complex trace analysis, however in this study only the aforementioned three are used. The complex mathematics and theory of

complex trace analysis is beyond the purpose scope of this study and will not be discussed in further detail. The purpose for complex trace analysis in the study is simply to gain a qualitative understanding on waveform changes so the observed attributes can be used as proxies for porosity on real seismic data.

The one dimensional synthetic seismograms produced use minimum phase Ricker wavelets. A Ricker wavelet is placed on the original trace data at 20, 40, and 80 Hz peak frequency to best quantify low, medium and high frequency in the seismic data. The nature of this study is largely exploratory, examining multiple variables to see which produce a forward and meaningful result. The reason for using multiple Ricker wavelets does not differ from the initial exploratory nature. The aim is to observe the frequency range that displays the most change in attributes from the effects of porosity. The following is pictographic discussion of the results of the synthetic seismogram complex trace attribute analysis study.

3.6.1 Qualitative and Quantitative analysis of Synthetic Seismograms

For each of the four wells (PAP-1, A-09, A-36, and M-16), a synthetic seismogram is generated at 20, 40, and 80 Hz Ricker wavelet from the original data and 0-15% porosity block modeled bulk density and sonic curves. The actual synthetic seismogram traces are overlaid upon the complex trace attribute analysis to show correlation and the position of attribute changes. Empirical measurements of waveform geometries are graphically shown as correlations to the change in attributes. The standard format of each instantaneous attribute analysis is as follows: Each suite contains

overlain synthetic seismograms generated from block porosity models indicated by label at the bottom of each pane. (e.g. A-09 20Hz represents the synthetic generated from the original well curves at 20Hz Ricker wavelet. A-09 10p 20Hz represents synthetic from well A-09 generated from the block modeled well curves at 10% porosity (10p) , 20Hz Ricker wavelet) Original un-modeled curves at left, progressing up to 15% block modeled porosity at far right. The amount of panes in each suite is dependent on the amount of data controls in each well for a given porosity. (E.g. in well M-16 porosity is only modeled up to 10%, due to lack of reliable data in the 15% range.) An important note prior to examining the following attribute analysis is to realize the wells in this study are spaced far enough apart that the geology varies considerably between them. The most important change between the wells is the varying thickness of the Table Point Formation along the St. George Unconformity. This variation allows the large amplitude Table Point-Goose Tickle reflector to affect the reservoir response in the Upper Aguathuna Formation when the Table Point Formation is thin.

3.6.2 Synthetic Seismogram Analysis of well A-09

Well A-09 contains reliable well data control points in the frequency analysis up to 15% porosity. Refer to following guided, annotated graphs for results of the attribute analysis. Note in this well, the 80Hz Ricker wavelet is found to contain no significant characteristics in instantaneous phase, instantaneous frequency, or reflection strength. The changes in attribute character show either too subtle or no significant changes that can be differentiated between the block porosity modeled synthetics. Therefore, the 80Hz

will be either shown illustrating the insignificance, only listed in the appendices, or not shown altogether. A-09 displays unique ambiguity between the 0% and 10% porosity model synthetics in most of the attributes analysis. It is important to note the Table Point Formation is very thin in this well, allowing for the large, dominant reflector from the Goose Tickle- Table Point interface to affect the reservoir intervals.

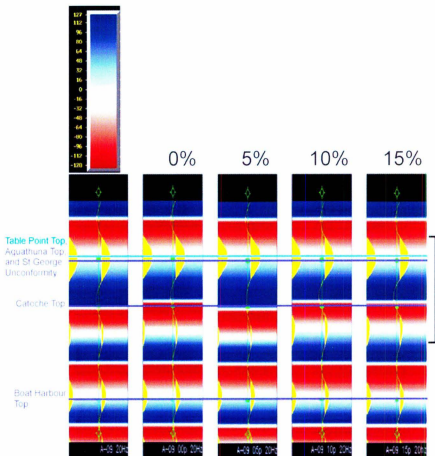


Figure 3.6.2.1. Instantaneous Phase analysis of well A-09 (synthetic seismic traces in yellow), Ricker wavelet 20Hz, Lower Table Head Group – St. George Group. Original data on left and porosity models from 0-15% (p) to right. Black bracket represents zone of interest. Wavelets in models 00p (0%) and 10p (10%) indicate ambiguity in phase shift patterns. Model 05p (5%) represents the most noticeable phase shift pattern. Overall, The detail at 20Hz in well A-09 does not show a great deal of distinguishing information in instantaneous phase and it can be inferred instantaneous phase at 20Hz in well A-09 does not display the level of resolution needed to be useful in this study.

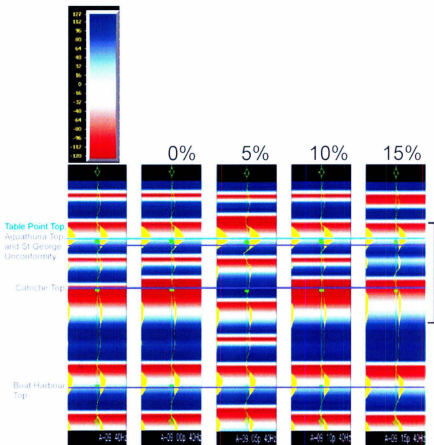


Figure 3.6.2.2. Instantaneous Phase analysis of well A-09 (synthetic seismograms in yellow), Ricker wavelet-40Hz. Lower Table Head Group – St. George Group. Original data on left and porosity models 0-15% (p) to right. Models 00p (0%) and 10p (10%) display similar phase shift patterns as the negative trough energy of the reflector in the middle Aquathuna Formation is diminished and show ambiguity. Model 05p (5%) displays a phase shift pattern resembling the original at far left, indicative that actual porosity in the well is relatively close to 5%. Model 15p (15%) displays decreased phase shift activity, most likely from decreased crest to trough spacing. Overall, with increasing porosity, the decreasing negative trough reflector energy below the major Table Point-Goose Tickle interface causes decreased phase shift activity.

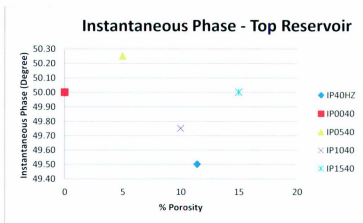


Figure 3.6.2.3. Empirical measurement of instantaneous phase on the peak amplitude, A-09 40 Hz Ricker wavelet, Original to 15% porosity models. In the legend, IP40HZ - Original synthetic, instantaneous phase. IPXX40 equals a specified porosity modeled synthetic. Top reservoir is indicative of the Upper Aguathuna reservoir. Bottom reservoir indicates the Lower Aguathuna -Catoche reservoir. These graphs illustrate the numeric change between phase values in the models at peak crest or trough amplitude in the reservoir interval. However, it does not display the exact location of phase shift as the variable density graph 3.6.2.2 does. Therefore, the affect porosity has on instantaneous phase can be optimally viewed in the variable density graphs.

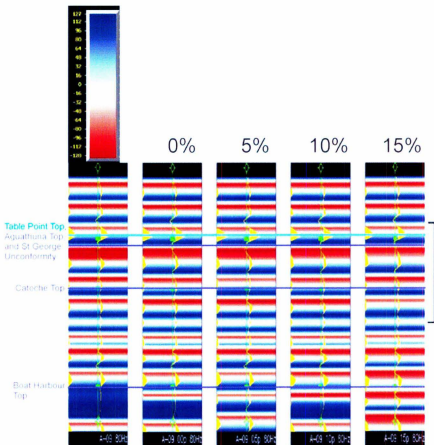


Figure 3.6.2.4. Instantaneous Phase analysis of well A-09 (synthetic seismograms in yellow), Ricker wavelet 80Hz, Lower Table Head Group – St. George Group. Area of interest in black bracket. Original synthetic data on left and porosity models from 0-15% (p) to right. It is clear that at 80 Hz dominant frequency, porosity does not noticeably affect changes in phase shift intervals, nor does it affect the shifting of energy much in the yellow seismic trace. No empirical correlation is made for this suite of synthetics because of the indifferent effect of porosity on the attribute.

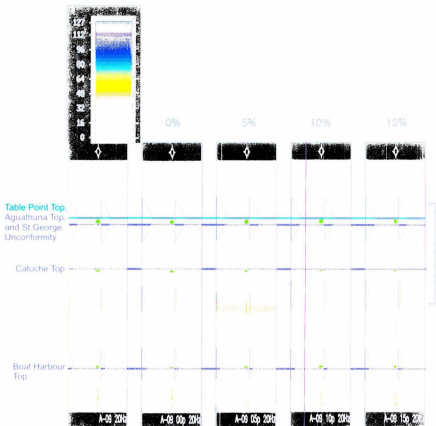


Figure 3.2.2.5: Vertical Profile Progression (meters of ice) A-BK, projected ice progression (vertical) Superimposed 20% Lower Table (Red Group – St George Group, Orange) data on all well cores by month. Note 0-176 to right leads to an RL zone of interest to West. Location: This is a plot at 20% ice class. The primary data set produce any immediate potential results to be observed, compared to reference top, which are (shown) were again in the higher percentages. The regional cover also means for this rate of synthesis. Because of the potential effect of severity in this section.

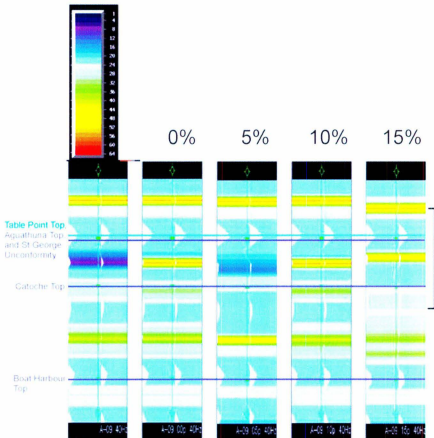


Figure 3.6.2.6 Instantaneous Frequency analysis of well A-09, (synthetic seismograms in white), Ricker wavelet 40Hz. Lower Table Head Group – St. George Group. Original data on left, and porosity models from 0-15% (p) to right Scale is in Hz. Black bracket is interval of interest. There again is ambiguity in between the 0% (00p) and 10% (10p) models. The 05p 5% model again shows the largest difference in pattern while 15p 15% model also has a distinguished difference. Instantaneous frequency at 40Hz shows potential to be used in mapping 2-D reflection changes .

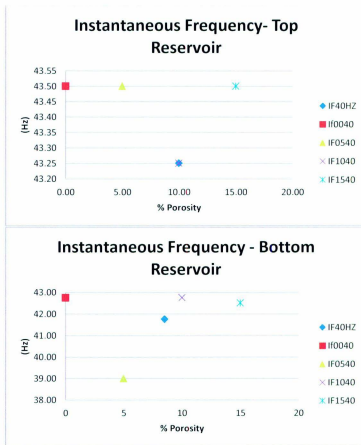


Figure 3.6.2.7. Empirical measurement of instantaneous frequency on the peak amplitude. A-09 40 Hz Ricker. Original to 15% porosity models. In the legend, IF40HZ = Original synthetic, instantaneous frequency. IFXX40 equals a specified porosity modeled synthetic. Top reservoir is indicative of the Upper Aguathuna reservoir. Bottom reservoir indicates the Lower Aguathuna –Catoche reservoir. These graphs illustrate the numeric change between instantaneous frequency values in the models at peak crest or trough amplitude in the reservoir intervals. In the top reservoir, it is interesting the original and 10p 10% porosity model match identically. This confirms that the models do indeed work by showing the ability to match original data in attributes. However, the lack of change in the other porosity models shown and very subtle frequency change is discouraging for attribute tracing in the 2-D study. In the bottom reservoir, ambiguity exists in the 0040 0% and 1040 10% models again with subtle variation in the 1540 15% model. It is interesting the original 40Hz contains 8% porosity and falls somewhere in between the 5% model and 10% model in frequency value. This is expected, and again confirms the models are indeed functional.

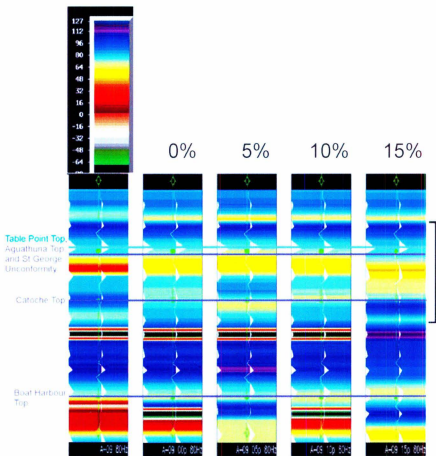


Figure 3.6.2.8 Instantaneous Frequency analysis of well A-09, (synthetic seismograms in white). Ricker wavelet 80Hz. Lower Table Head Group – St. George Group. Black bracket is interval of interest. Original data on left and porosity models from 0-15% (p) on right. Scale is in Hz. Negative values are interpreted as errors. This analysis at 80Hz dominant frequency produces very subtle changes in values, but is still considered when mapping 2-D data. Ambiguity still exists between the 0% and 10% porosity models.

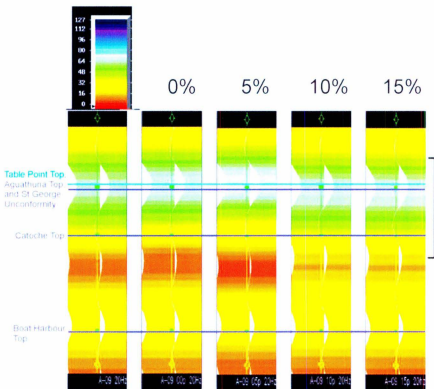


Figure 3.6.2.9. Reflection Strength analysis of well A-09, Ricker filter 20Hz, Lower Table Head Group-Upper St. George Group. Black bracket is interval of interest. Original data on left and porosity models from 0-15% to right. The results here show there is subtle difference in reflection strength along the models. The difference is marginally acceptable and will be considered for use in the 2-D modeling. In the middle of the Aquathuna Formation there is an overall increase in reflection strength.

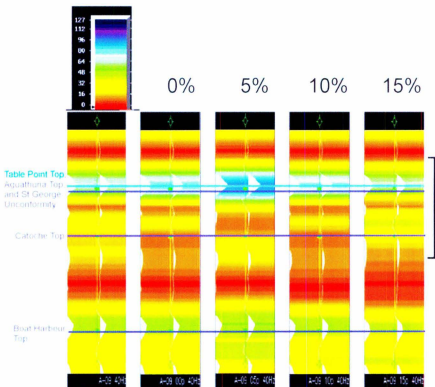


Figure 3.6.2.10. Reflection Strength analysis of well A-09, Ricker wavelet 40Hz, Lower Table Head Group- Upper St. George Group. Black bracket is interval of interest. Original data on left, and porosity models from 0-15% (p) to right. Model 05p displays the strongest change of reflection strength in the Table Point- Goose Tickle Reflection. Again, models 00p and 10p are nearly identical, as in instantaneous phase and frequency. A noticeable increase occurs in the middle Aquathuna with increasing porosity. Reflection strength in this well at 40Hz is used as a traceable attribute in the 2-D study in chapter 4.

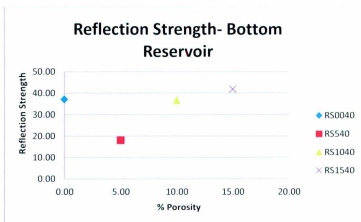
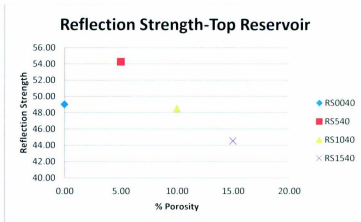


Figure 3.6.2.11, Empirical measurement of reflection strength on the peak amplitude, A-09 40 Hz. Ricker, 0 to 15% porosity models. In the legend, RS40HZ= Original synthetic, reflection strength, RS0040 equals a 0 % porosity modeled synthetic. Top reservoir is indicative of the Upper Aguathuna reservoir. Bottom reservoir indicates the Lower Aguathuna –Catoche reservoir. These graphs illustrate the numeric change between reflection strength frequency values in the models at peak crest or trough amplitude in the reservoir intervals. The changes in this attribute with porosity are represented well by empirical plotting rather than variable density representation. Although ambiguity exists once again between the 0 and 10% models, there is significant variation between the other models making this attribute appropriate to use in the 2-D modeling study. In the top reservoir, there is decreasing reflection strength with porosity while the bottom reservoir is the inverse. The interpretation between the ambiguity in the 0 and 10% models will be addressed in detail in the discussion section this chapter.

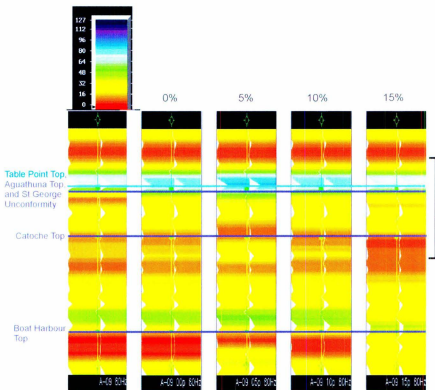


Figure 3.6.2.12. Reflection Strength analysis of well A-09, Ricker filter 80Hz, Lower Table Head Group-Upper St. George Group. Black bracket is interval of interest. Original data on left and porosity models from 0-15% to right. Unlike the previous 80Hz attributes, a noticeable shift in reflection strength occurs at 80Hz. Model 05p displays the largest increase in the Upper Aguathuna reservoir while highest porosity cause decreases in strength. There is a noted increase in reflection strength in the middle Aguathuna. Again, models 00p and 10p correlate.

3.6.3 Synthetic Seismogram Analysis of well A-36

Well A-36 contained a thick succession of the Table Point Formation and the dominant reflector of the major interface does not occlude as much reservoir reflection information. 80 Hz in this well does display some favorable results. An empirical calculation of instantaneous phase at 40 Hz is not displayed because instantaneous phase is best displayed as variable density plots. The data again is responding to the 40Hz wavelet with the most useful information.

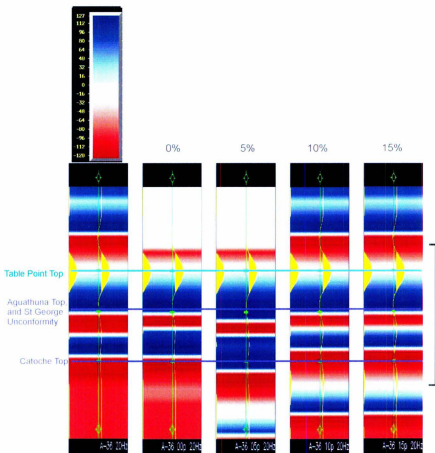


Figure 3.6.3.1. Instantaneous Phase analysis of well A-36, Ricker wavelet 20Hz, Lower Table Head Group-Upper St. George Group. Original at left and 0-15% porosity models to right. Interval of interest in black bracket. Unlike the A-09 well, ambiguity does not exist between the 00p 0% and 10p 10% models. There is no difference between the 10p 10% and 15p 15% models, so the use of this attribute at 20Hz for modeling purposes is problematic. There is also not much difference in between 0% and 10-15%. However, this attribute could possibly be used to distinguish zones of higher porosity from lower porosity.

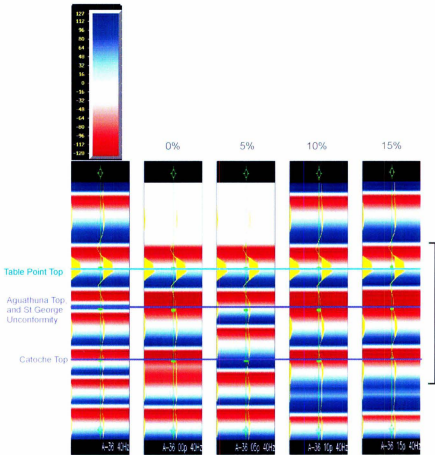


Figure 3.6.3.2. Instantaneous Phase analysis of well A-36, Ricker wavelet 40Hz, Lower Table Head Group-Upper St. George Group. Original at left and 0-15% porosity models to right, Interval of interest in black bracket. At 40 Hz, there are some noticeable trends in phase shift with increasing porosity. However, 10p 10% and 15p 15% are still identical. The 40Hz analysis of this attribute yields some change with increasing porosity, but 10p 10% and 15p 15% are still the same along with its similarity to the 20Hz figure 3.6.3.1

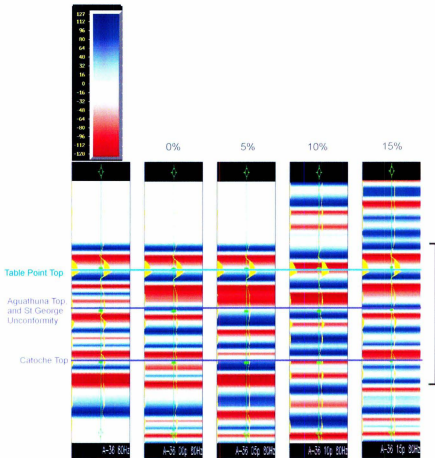


Figure 3.6.3.3. Instantaneous Phase analysis of well A-09, Ricker wavelet 80Hz, Lower Table Head Group- Upper St. George Group. Original at left and 0-15% porosity models to right At 80 Hz, there some noticeable trends in phase shift with increasing porosity. Models 00p and 10p do share similar, but not identical attributes. Model 10p and 15p are again nearly identical in phase shifts making dissociation difficult. Instantaneous phase is a valid attribute analysis in well A-36 at 80Hz, however changes are very subtle. Area of interest in black bracket.

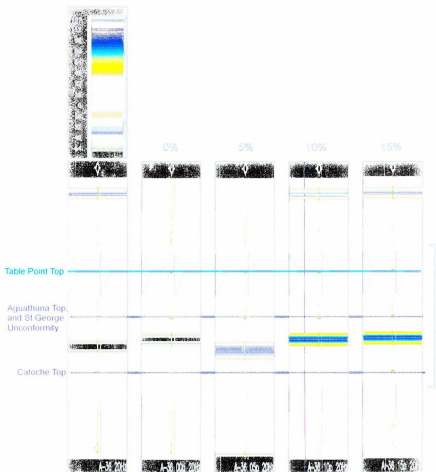


Figure 4.1.4 Interfacial Frequency analysis of the A-05, Baker wells in 2019. Lower Table Point Group - Upper St. George Group. Original at reduced 0-15% permeability. On right, interval of interest by your choice. In general, decrease in permeability increases the amplitude of the signal, but there is still amplitude in the higher frequency modes. This is possibly due to the wave reflecting off the boundary with zones of higher permeability, but there is no net increase in energy between 0 Hz and 12 Hz. Negative values are interpreted as noise.

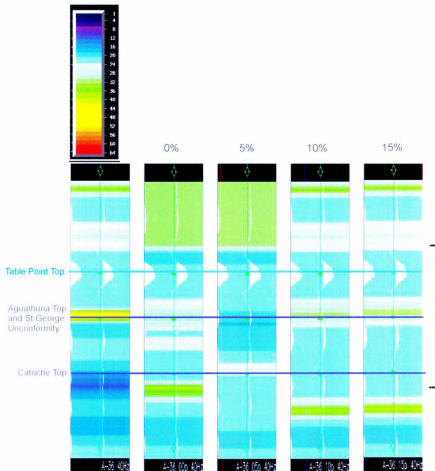


Figure 3.6.3.5 Instantaneous Frequency analysis of well A-36, Ricker wavelet 40Hz, Lower Table Head Group- Upper St. George Group. Original at left and 0-15% porosity models to right. Interval of interest in black bracket. Instantaneous Frequency 40 Hz shows some mapable character as porosity increases, however the recurring lack of dissociation between 10p and 15p continues. It is reasonable to assess the difference between 00p and 05p as a significant change that could be mapped. The petrophysics in the 10p and 15p are very similar in this well leading to the similar models. The subtle nature of the change is somewhat problematic for implement this attribute in 2-D reflection changes.

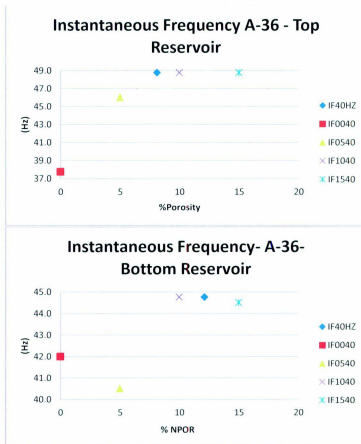


Figure 3.6.3.6. Empirical measurement of instantaneous frequency, A-36 40 Hz Ricker, Original to 15% porosity models. In the legend, IF40HZ= Original synthetic, instantaneous frequency. IF0040 equals a 0 % porosity modeled synthetic. Top reservoir is indicative of the Upper Aguathuna reservoir. Bottom reservoir indicates the Lower Aguathuna –Catoche reservoir. These graphs illustrate the numeric change between instantaneous frequency values in the models at peak positive crest or negative trough amplitude within the reservoir intervals. In the top reservoir measurement, there is an abrupt, then subtle increase in instantaneous frequency. The original porosity in the interval is 8.9% and it is assuming that it has comparatively the same instantaneous frequency as the 10% model. The 15% model only displays a very slight increase in frequency. The bottom reservoir interval exhibits similar behavior to the top reservoir interval, with the only exception being the 0% model. This analysis illustrates the subtle differences between the higher porosity models. It may be the case that this attribute in well A-36 is best suited to distinguish zones of low porosity from high porosity.

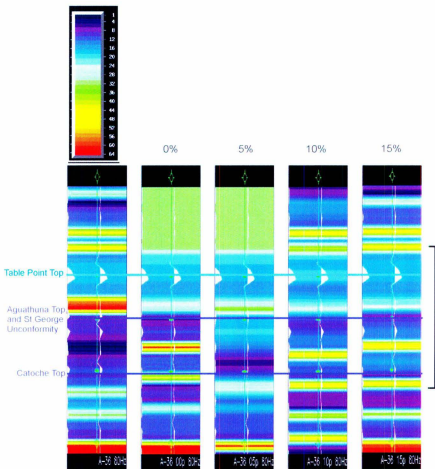


Figure 3.6.3.7. Instantaneous Frequency analysis of well A-36, Ricker wavelet 80Hz. Lower Table Head Group- Upper St. George Group. Original at left and 0-15% porosity models to right. Interval of interest in black bracket. In the 80Hz analysis, there are some subtle differences between the models and may be useful for the 2-D study in chapter four.

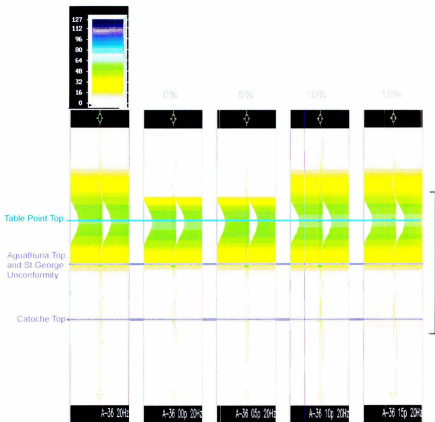


Figure 3.6.3.8. Reflection Strength analysis of well A-36, Ricker wavelet 20Hz. Lower Table Head Group-Upper St. George Group. Black bracket is interval of interest. Original data on left and porosity models from 0-15% to right. There is no significant change in the reflection strength in the majority of the range of the 20Hz analysis. The Table Point Reflector is the dominant event in this type of analysis at 20Hz and it does not provide much other information.

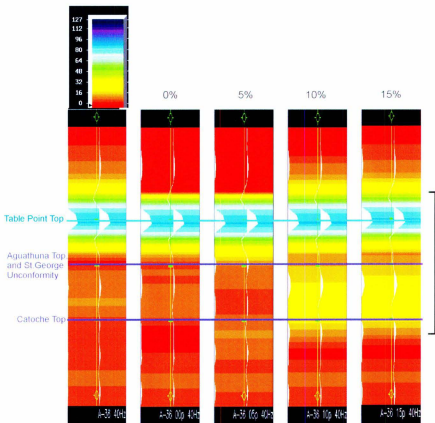


Figure 3.6.3.9. Reflection Strength analysis of well A-36, Ricker wavelet 40Hz, Lower Table Head Group-Upper St. George Group. White bracket is interval of interest. Original data on left, and porosity models from 0-15% to right. Interval of interest in black bracket. In this well there are only minute changes in reflection strength with the largest porosity models. However the distinction between zones of low porosity and higher porosity is apparent.

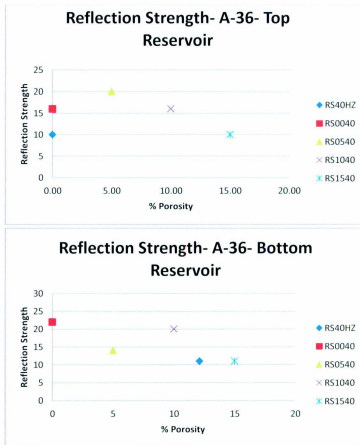


Figure 3.6.3.10. Empirical measurement of reflection strength, A-36 40 Hz, Ricker, 0 to 15% porosity models. In the legend, RS40HZ= Original synthetic, reflection strength. RS0040 equals a 0 % porosity modeled synthetic. Top reservoir is indicative of the Upper Aguathuna reservoir. These graphs illustrate the numeric change between reflection strength values in the models at peak positive crest or negative trough amplitude within the reservoir intervals. Bottom reservoir indicates the Lower Aguathuna –Catoche reservoir. The top reservoir interval displays a slight decrease in reflection strength as porosity increases while the bottom reservoir, at the point of measurement, increases then decreases with increasing porosity. It is important to note that in the variable density plot figure 3.6.3.8, the reflection strength increases with increasing porosity in the Middle Aguathuna. This suggests the 40Hz reflection strength is best viewed on a variable density plot.

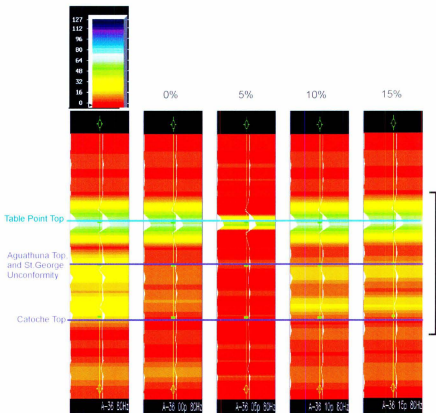


Figure 3.6.3.11. Reflection Strength analysis of well A-36, Ricker wavelet 80Hz , Lower Table Head Group- Upper St. George Group . White bracket is interval of interest. Original data on left, and porosity models from 0-15% to right. Interval of interest in black bracket. The reflection strength changes in this 80Hz prove to be too subtle and similar for use in the 2-D study in chapter 4.

3.6.4 Synthetic Seismogram analysis of well M-16

Well M-16 only contains reliable, confident well data control in the frequency analysis up to 10% porosity, so 15% models are not included. 80 Hz attribute analyses are excluded from this section because of non-useful information in the models. 40Hz continues to be the frequency best displaying the changes in attribute character. Empirical plots are utilized on the 40Hz instantaneous frequency and reflection strength. The Table Point Formation in this well is again thick enough to allow the reflection character of the Upper Aguathuna reservoir to be un-observed by the dominant Goose Tickle- Table Point reflector.

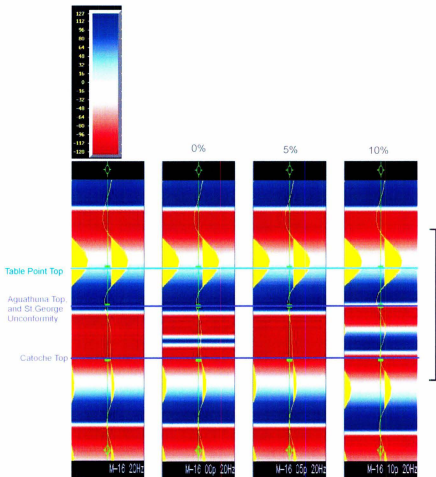


Figure 3.6.4.1 Instantaneous Phase analysis of well M-16, Ricker wavelet 20Hz. Lower Table Head Group-Upper St. George Group. Original at left and 0-15% porosity models to right. Interval of interest in black bracket. The M-16 well only contained reliable and sufficient data for up to 10% porosity modeling. At 20Hz, instantaneous phase has discernable difference between the porosity models, however it is not systematic. Model 10p has a similar phase pattern as 00p, but is slight more exaggerated in the middle of the Aguathuna Formation.

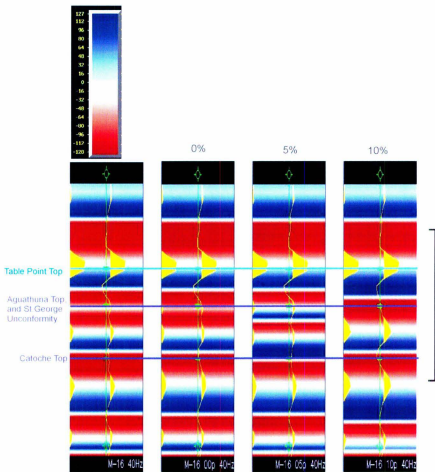


Figure 3.6.4.2 Instantaneous Phase analysis of well M-16, Ricker wavelet 40Hz, Lower Table Head Group-Upper St. George Group. Original at left and 0-15% porosity models to right. Interval of interest in black bracket. The original trace shows clear correlation to a porosity in the range of the 00p 0% model. The two positive reflections near the top and bottom of the Aguathuna Formation merge and gain amplitude in the 10p model. The difference in instantaneous phase shift patterns between the porosity models is clear and this analysis provides a positive phase shift proxy for porosity in the 2-D study in chapter four.

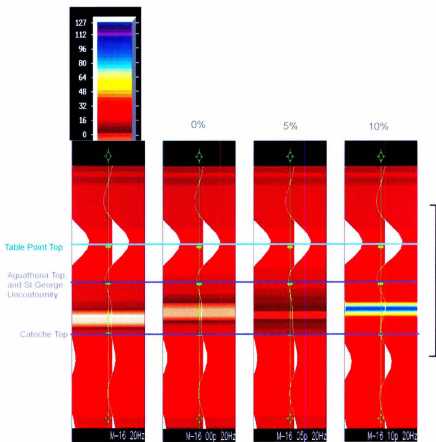


Figure 3.6.4.3. Instantaneous Frequency analysis of well M-16, 20Hz Ricker filter. Lower Table Head Group- Upper St. George Group Original on left with 0-10% porosity models on to right. Interval of interest in black bracket. A gradual increase in instantaneous frequency content with increasing porosity occurs at 20Hz in the middle of the Aquathuna Formation. This attribute appears to be a strong choice to trace along seismic horizons.

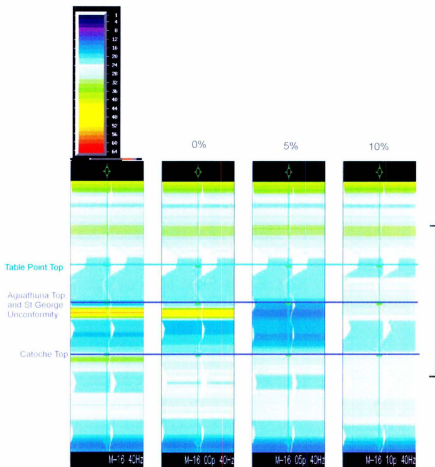


Figure 3.6.4.4 Instantaneous Frequency analysis of well M-16, 40Hz Ricker filter. Lower Table Head Group- Upper St. George Group Original on left with 0-10% porosity models to right. Interval of interest in black bracket. There are subtle but definite changes in instantaneous frequency as porosity increases. It seems to be an overall decrease in frequency looking at the 10p model. These systematic changes make this a desirable attribute for 2-D reflection modeling, but the subtle nature of the change may not be observable when tracing reflection changes laterally.

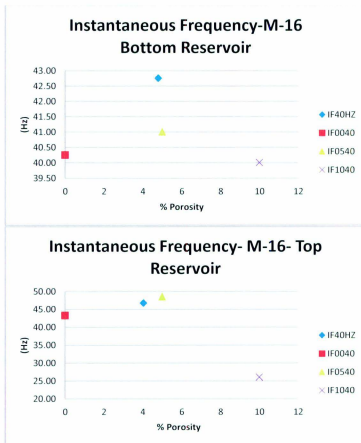


Figure 3.6.4.5. Empirical measurement of instantaneous frequency on the peak crest or trough amplitude within the reservoir intervals, M-16 40 Hz Ricker, Original to 10% porosity models. In the legend, IF40HZ = Original synthetic, instantaneous frequency. IF0040 equals a 0 % porosity modeled synthetic. Top reservoir is indicative of the Upper Aguathuna reservoir. Bottom reservoir indicates the Lower Aguathuna –Catoche reservoir. There is an overall decrease in instantaneous frequency with increasing porosity. The original IF40HZ in the bottom reservoir does not seem to correlate well with any of the models.

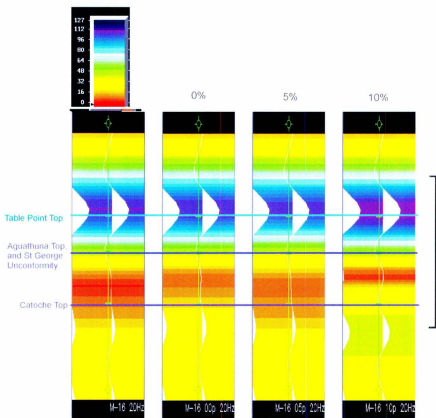


Figure 3.6-4.6 Reflection Strength analysis of well M-16, 20Hz Ricker filter. Lower Table Head Group-Upper St. George Group Original on left with 0-10% porosity models to right. Interval of interest in black bracket. The changes in this attribute could be useful in determine zones of higher and lower porosity in lateral 2-D horizon mapping. Although, there is an increase in the highest porosity model.

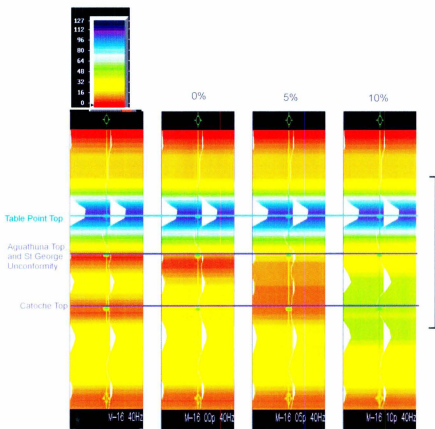


Figure 3.6.4.7. Reflection Strength analysis of well M-16, 40Hz Ricker filter, Lower Table Head Group-Upper St. George Group Original on left with 0-10% porosity models on to right. Interval of interest in black bracket. There is very sharp increase in reflection strength with increasing porosity. This attribute will be very useful in mapping porosity changes in the 2-D study, although it may only be useful for distinguishing zones of higher and lower porosity.

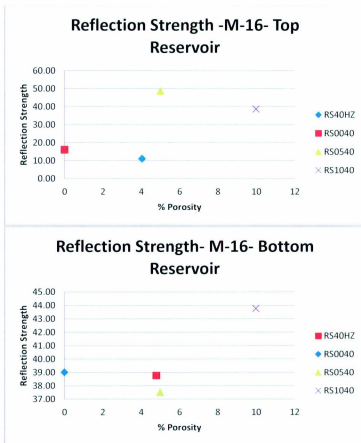


Figure 3.6.4.8. Empirical measurement of reflection strength on the peak crest or trough amplitude in the reservoir intervals, M-16 40 Hz Ricker, Original to 10% porosity models. In the legend, RS40HZ= Original synthetic, reflection strength. RS0040 equals a 0 % porosity modeled synthetic. Top reservoir is indicative of the Upper Aguathuna reservoir. Bottom reservoir indicates the Lower Aguathuna –Catoche reservoir. Both reservoir intervals show increases in reflection strength with increasing porosity. In this attribute the best scope of the change may be best visualized in the variable density plots.

3.6.5 Synthetic Seismogram analysis of well PAP-1

Well PAP-1 contained reliable data in the frequency analysis up to 15% porosity. Note that in this well, the 80Hz Ricker wavelet has no significant characteristics in instantaneous phase, instantaneous frequency, or reflection strength. It is important to note that the Table Point Formation is again thinner in this well, allowing for the large, dominant reflector from the Goose Tickle- Table Point interface to affect the reservoir intervals. However, it does not interfere with the waveform information in the Upper Aguathuna reservoir interval as much as in the A-09 well. This is likely because the Table Point Formation is slightly thicker in this location.

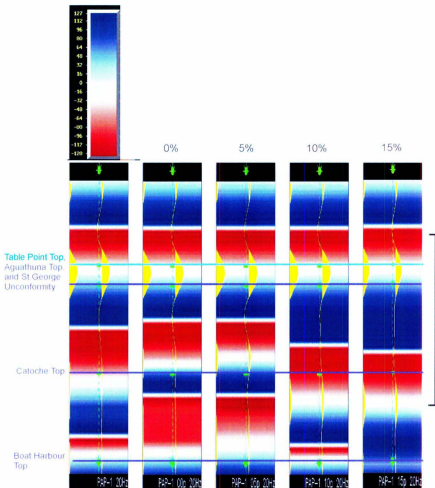


Figure 3.6.5.1. Instantaneous Phase analysis of well PAP-1, Ricker wavelet 20Hz, Lower Table Head Group- Upper St. George Group. Original on left with 0-15% porosity models to right. Interval of interest in black bracket. The instantaneous phase analysis displays perhaps the best systematic progression of phase shift pattern at 20Hz than in any of the other wells. The major phase shift progressively moves toward the top of the Catoche Formation as the energy of the second major positive reflector (below the Goose Tickle- Table Point interface) is shifted down. The results of this analysis makes a superb proxy for porosity for lateral reflection mapping later on in the study.

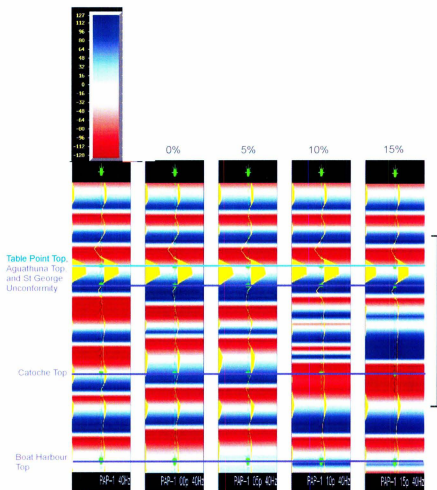


Figure 3.6.5.2. Instantaneous Phase analysis of well PAP-1, Ricker wavelet 40Hz, Lower Table Head Group- Upper St. George Group. Original on left with 0-15% porosity models to right. Interval of interest in black bracket. It is clear that with increasing porosity, the phase shift intervals increase in number of distinct phase shifts and then reduce in number as the amplitude of the reflectors in the middle to lower Aguathuna Formation decrease.

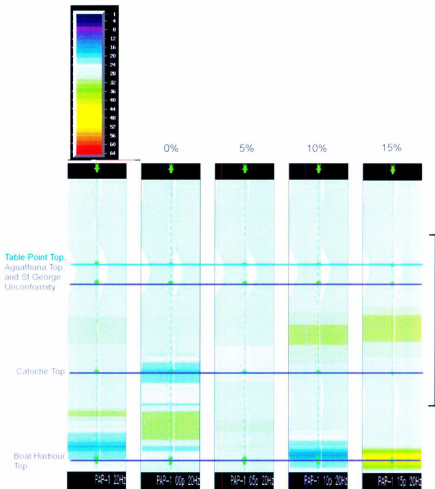


Figure 3.6.5.3. Instantaneous Frequency analysis of well PAP-1, Ricker wavelet 20Hz. Lower Table Head Group- Upper St. George Group. Original on left with 0-15% porosity models to right. Interval of interest in black bracket. Although very subtle, there are marked increases in instantaneous frequency in middle of the Aquathuna Formation with increasing porosity. This trend could provide useful information in mapping of attributes in chapter four. The largest attribute contrasts are between low (0-5%) and high (10-15%) porosity.

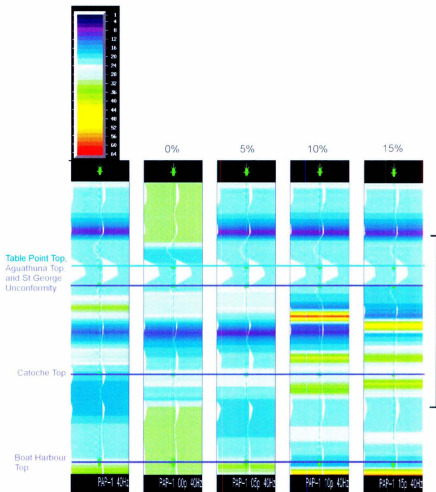


Figure 3.6.5.4 Instantaneous Frequency analysis of well PAP-1, Ricker wavelet 40Hz, Lower Table Head Group- Upper St. George Group. Original on left with 0-15% porosity models on to right. Interval of interest in black bracket. Only a subtle difference between the 00p and 05p models exists, however there is a larger difference between the 10p and 15 p models. The subtle nature of the change between 0 and 5% may not be detectable along a 2-D horizon, but in this well, there is a clear difference between low and high zones of porosity.

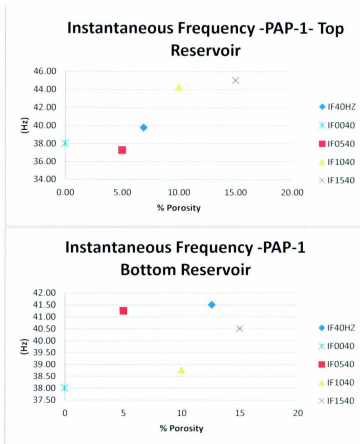


Figure 3.6.5.5. Empirical measurement of instantaneous frequency on the peak crest or trough amplitude within the reservoir intervals, PAP-1 40 Hz Ricker, Original to 10% porosity models. In the legend, IF40HZ- Original synthetic, instantaneous frequency, IF0040 equals a 0 % porosity modeled synthetic. Top reservoir is indicative of the Upper Aguathuna reservoir, Bottom reservoir indicates the Lower Aguathuna -Catoche reservoir. The top reservoir interval displays one of the best linear regressions in the entire analysis with instantaneous frequency increasing with increasing porosity. The bottom reservoir interval, however, does not contain any cohesive relationships between the porosity models. Even though it is not as linearly organized as the top interval, the bottom interval does display difference in the models.

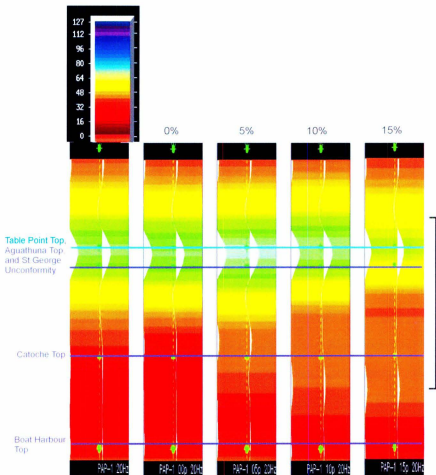


Figure 3.6.5.6 Reflection strength analysis of well PAP-1, Ricker wavelet 20Hz, Lower Table Head Group- Upper St. George Group. Original on left with 0-15% porosity models to right. Interval of interest in black bracket. There is only a subtle difference between the 00p and 05p models, however there is a larger difference between the 10p and 15 p models. Overall, the subtleness of the reflection strength attribute suggests this is not be a great proxy for porosity in the chapter four study.

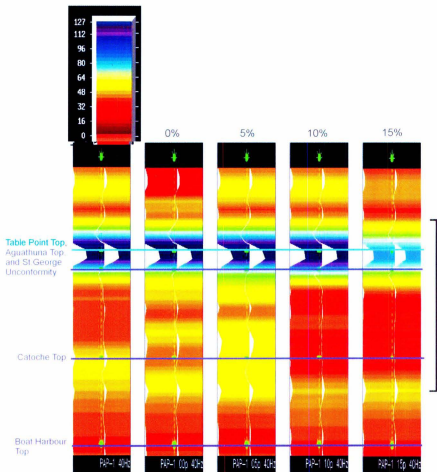


Figure 3.6.5.7 Reflection strength analysis of well PAP-1, Ricker wavelet 40Hz, Lower Table Head Group-Upper St. George Group. Original on left with 0-15% porosity models on to right. Interval of interest in black bracket. There is an overall decrease in reflection strength as porosity increases. Even though the increase is subtle, this attribute would still be applicable for separating zones of low porosity from high porosity.



Figure 3.6.5.8. Empirical measurement of reflection strength on the peak crest or trough amplitude within the reservoir intervals, PAP-1 40 Hz Ricker. Original to 10% porosity models. In the legend, RS40HZ= Original synthetic, reflection strength. RS0040 equals a 0 % porosity modeled synthetic. Top reservoir is indicative of the Upper Aguathuna reservoir, Bottom reservoir indicates the Lower Aguathuna –Catoche reservoir. The top reservoir again has a good example of a systematic linear regression with reflection strength decreasing with increasing porosity. The bottom reservoir interval also shows decreased reflection strength with increasing porosity with the anomalous original at 12% porosity. However, this anomalous value decreases the confidence of this attribute as a porosity proxy in the 2-D modeling.

3.7 Discussion of Synthetic Seismogram Analysis

The quantitative and qualitative assessment of the synthetic seismograms in this study provide a variety of different information based on the well and attribute of interest. Before discussing the ultimate conclusion for this chapter, it is important to address some complications with this type of reservoir and its effect on the attributes. The first major issue is the presence of mixed lithology within the reservoir intervals. As stated before, this reservoir is a hydrothermal dolomite play and contains zones of porosity developed in regions of alteration, rather than laterally continuous reservoir “beds”. Also, in the Aguathuna and Catoche Formations, the lithology varies from dolomite to limestone and presents an ambiguous situation throughout the study. Consistently during the attribute analysis in well A-09, the 0% and 10% porosity block models, and corresponding complex trace attributes, produced nearly identical character in all attributes. The hypothesis behind this phenomenon is interpreted to be petrophysical similarities between a “tight” limestone and ten percent porosity dolomite. The data from well A-09 suggests a limestone with around 0% porosity contains a bulk density of 2.71 g/cm^3 and interval transit time of $155 \mu\text{s/m}$. Also, the data suggest dolomite with 10% percent porosity most frequently contains bulk density of 2.72 g/cm^3 and a most common interval transit time of $153 \mu\text{s/m}$. The similarity between the two sets of petrophysical properties is carried directly into the response of the seismic attributes. The result is that two conditions look very similar, and sometimes indistinguishable, in the block porosity models and attribute comparisons as previously discussed. This fact must be considered when analyzing attributes laterally across reflection horizons in seismic data. One must carefully consider

alternate sources of information, such as all available lithologic logs, outcrop data/samples, and available literature, to determine lithology of a zone of interest, rather than simply relying on petrophysical data. Wells A-36 and PAP-1 also display ambiguity in the 10% to 15% porosity modeled attribute analysis. This is interpreted as a limitation from the frequency analysis data. The best representative petrophysical values at 10% and 15% porosity are either similar in the above wells or the amount of data control was insufficient in the frequency analysis at higher porosities.

The second major issue, as mentioned previously, is the importance of varying thickness of the Table Point Formation along the St. George Unconformity and the overlying position of the Goose Tickle- Table Point Interface. The transition of argillaceous clastics of the Goose Tickle Formation into tight limestone of the Table Point Formation creates a dominating reflection interface. This interface directly overlies the St. George Unconformity and thus, the top of the Aguathuna Formation reservoir units. The St. George Unconformity itself does not create a large reflection interface due the similar lithology of the Table Point and Aguathuna Formations. The large amplitude and wavelength of the Goose Tickle- Table Point interface occludes the effects of interfaces within the upper Aguathuna Formation. Therefore, the effect porosity has on the wavelet through the upper Aguathuna reservoir emerges as subtle changes **within the reflection** of the Goose Tickle – Table Point reflection.

The complex trace and synthetic seismogram analysis of the four exploration wells (PAP-1, A-09, A-36, and M-16) reveal unique reservoir scenarios and model

responses. The changing geologic constraints in each well have great effect on what frequency and resolution attributes respond to on the model analysis. The objective of this analysis is to find a series of attributes transferrable to a seismic processing program useful for mapping similar attributes on real seismic data. (Finding similar character on the 2-D seismic data is interpreted as porosity equivalent to the modeled proxies.) This complex trace analysis matching technique is ultimately used as a predictive tool for porosity in the immediate vicinity of the wells.

In well A-09, the best quality responses did not occur in all Ricker wavelets. At 20Hz instantaneous phase (Figure 3.6.2.1), there is no discernable difference in phase shift pattern from the original to 5% porosity and 10%-15% porosity. 40Hz instantaneous phase (Figure 3.6.2.2) was the only analysis to show a difference between the models and 80 Hz (Figure 3.6.2.3) did not show sufficient variation for mapping lateral changes. As stated before, a recurrent characteristic in the A-09 well was the similarity of the 0% and 10% models in all complex trace analysis. The instantaneous frequency analysis of well A-09 20 Hz again reveals no discernable difference between models. 40Hz displays similarities between 0% and 10% models, yet displays notable frequency changes in the 5% and 15% models. The empirical graph (figure 3.6.2.7) effectively displayed the changes between the porosity models and also displayed the correlation of the original data. At 80Hz (figure 3.6.2.8), the instantaneous frequency analysis does resolve very subtle difference between the models. It is questionable if this attribute is sensitive enough to map lateral changes later in this study. Reflection strength, in this well, displayed distinguishing character between zones of low and high porosity in the 20 and

40 Hz plots. The overall trend in the Table Point-Goose Tickle reflector is decreasing reflection strength with increasing porosity, while the middle Aguathuna Formation interval displays increased reflection strength with increasing porosity. The empirical plots (Figure 3.6.2.11) display changes in the reflection strength strongly and provide another useful tool in quantifying the changes in the attribute. In well A-09, where the Table Point Formation is thin, the bulk of the change in reflection strength is contained in the area of the dominant reflector on the Goose Tickle-Table Point Interface. There are smaller scale changes in the middle of the Aguathuna Formation as well. At 80 Hz (figure 3.6.2.12), the reflection strength in this well mirrored the changes in the 40Hz analysis, only at a smaller scale.

The complex trace analyses in well A-36 yield a greater frequency range of useful results than well A-09. Both 20 and 40Hz instantaneous phase and frequency analyses produce significant changes between the porosity models in large enough resolution to be used as proxies for porosity. The most useful trait of the 20 and 40 Hz instantaneous phase (Figures 3.6.3.1 and 3.6.3.2) is the ability to distinguish zones of higher and lower porosity. 80 Hz instantaneous phase (Figure 3.6.3.3) did provide useable data in this well unlike well A-09. Instantaneous frequency, in the 20 and 40 Hz analysis (Figures 3.6.3.4 and 3.6.3.5), also produces a distinction between zones of lower and higher porosity consistently. The empirical plot (Figure 3.6.3.6) of instantaneous frequency at 40Hz confirms the distinct difference between 0-5% and 10-15% models. At 80 Hz, instantaneous frequency displays significant variation between the porosity models, unlike any other well. Reflection strength produces very subtle change, and only

produces change in the higher porosity models. At 20Hz (Figure 3.6.3.7), reflection strength does not show any significant change within the reservoir units. 40Hz (Figure 3.6.3.8) reflection strength only provides very subtle increases in reflection strength in the 10% and 15% models. The empirical plot (Figure 3.6.3.9) illustrates the subtle nature of the reflection strength changes at 40Hz in this well. Perhaps the most important trait about the A-36 analysis is the ambiguity all three attributes share between the 10 and 15% porosity models. The overall results of attribute study in well A-36 conclude this well only shows difference between lower and higher porosity zones rather than individual percentages.

The M-16 well reveals defined changes in attributes in instantaneous phase, instantaneous frequency, and reflection strength. However, due to the lack of available petrophysical data in the 15% porosity range, only models up to 10% are displayed in the M-16 well. In this well, 80 Hz analyses provide no useable results and therefore aren't discussed. Both 20 and 40 Hz analyses display mapable changes with increasing porosity. Both the 20 Hz and 40 Hz (Figures 3.6.4.1 and 3.6.4.2) instantaneous phase display significant phase shift pattern changes within the models as the reservoir interval seismic amplitudes increase overall with increasing porosity. Instantaneous frequency is the strongest changing attribute analyzed in this well, changing noticeably in the empirical and variable density plots. (Figures 3.6.4.5, 3.6.4.3 and 3.6.4.4) Instantaneous frequency, overall, decreases with increasing porosity along the models and best displays changes in the 20Hz variable density plot. Reflection strength in the 20 and 40Hz (Figures 3.6.4.6 and 3.6.4.7) display similar changes by increasing reflection strength with increasing

porosity. The empirical plot (Figure 3.6.4.8) confirms the large reflection strength increase in lower reservoir units of the Lower Aguathuna – Upper Catoche. It is noteworthy that the Table Point Formation is thicker here, as in well A-36.

The PAP-1 well displays the most systematic progressions in the attribute analysis. The behavior of the instantaneous phase analysis was predictable in the 20 and 40Hz (Figure 3.6.5.1 and 3.6.5.2). In the 20Hz, the most significant phase shifts occur in the Aguathuna Formation as the large negative (blue) phase interval increased in duration with increasing porosity. The 40Hz analysis of instantaneous phase displayed the best resolution of phase shift in the Aguathuna Formation. As porosity increases, the duration of each phase shift is shorter as the complexity of signal decreases. The same types of systematic attribute changes are noted in instantaneous frequency at 20 to 40Hz (Figures 3.6.5.3 and 3.6.5.4). Each porosity model displays significant changes and, overall, instantaneous frequency increases with increasing porosity. Reflection Strength proves to be a useful attribute in this well at 40Hz (Figure 3.6.5.7) and displays decreasing reflection strength between zones of low and high porosity (0-5% and 10-15%). The 20Hz (figure 3.6.5.6) reflection strength attribute change is too subtle for use for mapping across lateral horizons. The reflection strength attribute trends are confirmed using the empirical plot (Figure 3.6.5.8). To restate, the 80 Hz complex trace attributes in wells M-16 and PAP-1 did not provide useful information and are not included in this discussion.

Overall, the results of this chapter study provide a series of proxies for porosity that can be implemented on a specific location basis in the vicinities of wells on real

seismic data. It is very important, as evident from this study, that one must carefully evaluate each well independently at a variety of frequency resolution and all complex trace analyses. This type of analysis is not a regional solution but a tool to extend borehole information away from existing wells to aid in predicting porosity in the immediate vicinity. A variety of frequency resolution is important as some of the best attribute responses were constrained to either the 40Hz Ricker wavelet or only revealed at 20Hz. Yet, other attributes are equally represented in the 20 and 40 Hz frequencies. Rarely, the 80Hz Ricker wavelet provided useful results but it was still important to recognize the useful data it did contain. The best resolution of attribute change in this study is displayed consistently at 40Hz and will be used in the modeling study of chapter four. The depth of procedure in this study must be evaluated on well-by-well basis based on feedback from the initial well data, each frequency resolution, and each attribute analysis. The objective of this chapter was to reveal, visually and numerically, the changes in seismic attributes stemming from porosity fluxes that could be mapped on seismic data.

Chapter 4: 2-D Seismic Line Complex Trace Attribute Analysis

4.1 Introduction to 2-D Seismic Attribute study

The ultimate objective of this research is to determine if a correlation exists between porosity and complex trace attributes in the St. George Group carbonates and to determine if attribute changes associated with porosity could be mapped laterally on real seismic data. The first step in this work focused on seismic attribute information from 1-D synthetic seismograms derived from petrophysical data. The initial intention of the second phase of this project was to obtain real 2-D seismic lines shot over the Port au Port Peninsula, containing the four wells in this study as well ties, and run complex trace attribute analyses. However, examination of the 2-D seismic data available raised several concerns with respect to data suitability.

The first major issue was the quality of data itself. The nature of the complex structure in the Ordovician Carbonate sequence on the Port au Port Peninsula area affects the data quality immensely. Each one of the four wells selected in this study was drilled through thrust fault complexes to penetrate the footwall blocks. The drilling strategy in this area was aimed at hydrothermally altered footwall blocks of thrusts where literature suggested porosity potential exists (e.g. Cooper et. al 2001). The deformational nature of strata near each line location resulted in imperfect imaging along the deformed zones and loss of amplitude information. This loss of reliable amplitude information proved to be problematic in recovering accurate reflection information to conduct complex trace

attribute analyses. Reflectors are often untraceable laterally in regions of distortion caused by the significant structural deformation. Survey quality and line location were also additional contributing issues in the 2-D data quality.

Most of the 2-D seismic lines available in the public domain at the CNLOPB (Canada-Newfoundland and Labrador Offshore Petroleum Board) are older, lower resolution lines with no availability of 3-D data. Moreover, the number of lines intersecting the wells directly was low. Only two of the four wells, PAP-1 and A-36, feature lines traveling through the well bore. The remaining M-16 and A-09 wells do have lines traversing in the near vicinity, but the well locations need to be extrapolated to lie on the lines. After viewing the available 2-D seismic data, it was decided the study needed to pursue an alternate path for correlation of attributes in 2-D with the synthetic seismogram study in chapter three.

4.2 Simulated, Variable Porosity 2-D seismic line generation

Since real 2-D seismic data could not be utilized, an alternate method of comparing well and seismic data attributes is employed. This involved developing synthetic, simplistic reservoir models containing laterally varying reservoir porosity zones. The aim of this model was to simulate lateral porosity variability in the carbonate reservoir. The model is then used to generate synthetic 2-D seismic data upon which complex trace attributes are measured and correlated to the results of chapter three. In the absence of real data, the models visually display how reflection attributes within the reservoir zones change with porosity and reveal the sensitivity of the attributes to noise.

The design theory behind the 2-D models was quite simplistic. The aim is to create a data driven model that simulates a variety of geologic conditions. Since the models are built from well data, the primary objective is to document how the seismic complex trace attributes change in response to lateral porosity variations and determine if attribute analysis might provide a predicative tool. The following geologic parameters were satisfied in the models:

1) varying thickness conditions of the Table Point Formation and the overlying proximity of the Goose Tickle-Table Point Interface. Two different models were made with a thin and thick succession of Table Point Formation 2) the models honoured the original reservoir architecture described in the literature and demonstrated in the analysis of the well logs. 3) the models contained realistic lateral porosity variations within the reservoir zones 4) the models simulate the velocity of the reservoirs, non-reservoir carbonates, and argillaceous/siliciclastic rocks in the interval of study.

4.2.1 Model building parameters and procedure for the 2-D synthetic seismic models

The models are designed using the reservoir architecture known from literature and well logs analysis documented in chapter three of this study. The reservoir porosity zones are assigned two, 30 m thick intervals in the Upper Aguathuna Formation and Lower Aguathuna- Upper Catoche Formations, respectively, with 45 m spacing in between the reservoir porosity zones (Figures 4.2.1 and 4.2.2). Non- reservoir strata between the reservoir zones in the St. George Group are assigned a constant velocity.

Also, the Table Point Formation is represented by constant thickness and shares the same velocity as the non-reservoir zones in the St. George Group. This relationship is established from examining well data in chapter three observing the petrophysical similarity. Two models with differing thickness of the Table Point Formation are constructed with thin (Figure 4.2.1) and thick (Figure 4.2.2) occurrences. The argillaceous Goose Tickle Group is assigned a separate velocity to represent the significant contrast from the underlying carbonates. Dimensionality information is assigned to the models and reservoir zones to provide a realistic scale to the synthetic seismic models.

The dimensions of the seismic line models are set to 2 km laterally and 0.6 km in thickness to provide an adequate range of data above and below the reservoir zones to capture all important reflection information within the models. Each velocity in the models is assigned based on the zone represented, determined through the statistical analysis in chapter three. Average velocities are determined from all four wells in the reservoir carbonates, non-reservoir carbonates, and argillaceous silliclastics (Table 4.2.1). The velocities values are averaged from the entire data set to keep the model general.

Well	0%	5%	10%	15%	Average Sonic St. George/Table Head Carbonates	Average Goose Tickle
PAP-1	157.39	157.74	165.27	168.00	160.85	220.00
M-16	155.13	157.00	158.78	162.00	155.43	221.00
A-36	155.83	153.99	162.69	162.71	155.82	218.00
A-09	157.06	157.26	164.16	164.88	159.00	220.00
Average	156.35	156.08	162.73	165.20	157.77	219.75
Average Velocity (m/s)	6395.79	6406.87	6145.33	6053.40	6338.17	4545.45

Table 4.2.1. Table displaying the average interval transit time (sonic slowness) ($\mu\text{s}/\text{m}$) and converted average acoustic velocities (m/s) of the four wells in this study. 0-15% sonic values are derived from the frequency distribution analysis of chapter three. Average St. George/Table Point Carbonates are taken from non-reservoir interval average sonic slowness of the St. George Group and Table Point Formation in this study. Average Goose Tickle represents the average sonic slowness in the Goose Tickle Formation. The average velocities listed above are used to substitute for gray scale values in the velocity model.

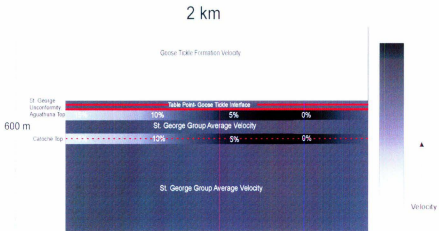


Figure 4.2.1. 2-D gray scale model representing a thin succession of the Table Point Formation. Note velocity scale within the reservoir units (denoted by porosity percentages). Major interfaces shown in red. Velocity information is substituted for gray scale values in the finite difference model.

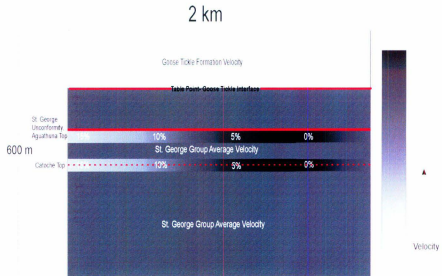


Figure 4.2.2. 2-D gray scale model representing a thick succession of the Table Point Formation. Note velocity scale within the reservoir units (denoted by porosity percentages). Major interfaces shown in red. Velocity information is substituted for gray scale values for the finite difference model.

A 2-D finite difference modeling program is used to generate 2-D synthetic seismic profiles for attribute analysis. Grid spacing is set to 5 m in the finite difference model to adequately sample the aforementioned velocity models and to satisfy the stability conditions of the modeling program at 10 grid nodes/ shortest wavelength for a maximum frequency of 100Hz. The model source is a plane wave with a Ricker wavelet resulting in a simulation of a normal incidence seismogram. The frequency spectrum of the source wavelet had a peak of 40Hz and maximum frequency of 100Hz. The data is filtered with an Ormsby bandpass filter (4-8-80-100Hz) to emulate the best frequency resolution of the attribute analysis in chapter three (40Hz Ricker wavelet). Lateral changes in porosity zones are simulated by varying, gradational velocities. This gradational change is included so abrupt change in velocity does not occur between each porosity zone. Without these gradational changes, edge reflections are produced between porosity zone vertical boundaries and affect amplitude information on the horizontal reflection responses. Not only did the gradational porosity zones attenuate the edge effects, but it also simulated actual geologic conditions in this type of reservoir. The reservoir intervals are separated into 0, 5, 10, and 15% porosity zones (Figure 4.2.1 and 4.2.2). The seismic lines generated from this procedure are imported into Landmark software to analyze complex trace attribute changes with porosity in the final part of this study.

4.3 Synthetic 2-D Seismic Model Complex Trace Attribute Analysis and Correlation

Instantaneous phase, instantaneous frequency and reflection strength are analyzed on the 2-D seismic models, analogous to the 1-D synthetics seismograms in chapter three.

The following discussion examines the results of the attribute analyses and the correlation between various attributes and reservoir porosity. The data are first examined without the addition of any noise to confirm the consistency with the 1-D analyses. Then, a sensitivity analysis is carried out to determine the robustness of the attributes in the presence of random noise. From this point on, the two synthetic seismic models will be referred to as “the *thick* and *thin* models”, referring the varying thickness of the Table Point Formation within them.

4.3.1. 2-D seismic model quality assessment

The synthetic seismic models are designed to remove artifacts produced from the imperfect structure of the model. Reflections from the sides of the model and in between reservoir porosity zones interfere with amplitude information in the horizontal reflections and are removed in the design process. Figure 4.3.1.1 is an example of artifacts that are removed from the seismic lines. The reflection events in the models are examined for sufficient strength prior to proceeding the complex trace attributes analysis. Refer to (Figures 4.3.1.2 and 4.3.1.3 for final versions of 2-D synthetic seismic lines.

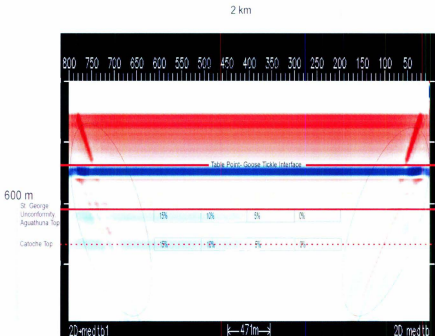


Figure 4.3.1.1. 2-D synthetic seismic model, **thick** Table Point Formation. This diagram is showing the edge reflections due to imperfect absorbing boundary conditions. (black circles) The original model was extended 1km on either side out past the 2 km bracket to move these refractions outside the area of interest (reservoir porosity percentage zone boxes).

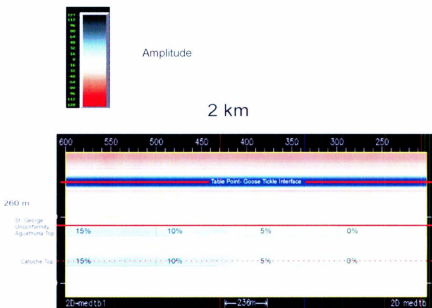


Figure 4.3.1.2. 2-D synthetic seismic model, **thick** Table Point Formation. Major contacts are in red. Porosity zone boxes denote area of reservoir modeling. Notice how the reflection packages change with varying porosity.

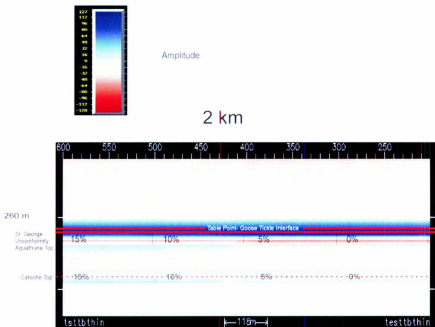


Figure 4.3.1.3. 2-D synthetic seismic model, thin Table Point Formation. Major contacts are in red. Porosity zone boxes denote area of reservoir modeling. Notice how the dominant reflection from the Table Point-Goose Tickle Interface is now interfering with the upper reservoir interval.

4.3.2 Instantaneous Phase analysis of the modeled 2-D seismic models

In general, instantaneous phase displays significant lateral changes with varying porosity for both cases of Table Point Formation thickness. The most notable changes are phase shifts between zones of high and low porosity. This relationship is consistent in both Upper Aguathuna and Lower Aguathuna-Upper Catoche reservoir units. For both cases of the models, the largest scale attribute change occurs at the transition between 5% and 10% porosity zones. Despite similar major phase pattern themes the thickness models are quite different in minor phase shift patterns.

The **thin** model (Figure 4.3.2.1) displays short wavelength phase polarity shifts below the Table Point-Goose Tickle Interface. It is clear that with increasing porosity, the number of phase polarity shifts decreases. This attribute change is identical to the patterns observed in wells A-09 and PAP-1 in chapter three. The largest phase shifts occur within the Aguathuna Formation where the negative (red) phase completely shifts to positive (blue) in porosities above 5%. In the upper reservoir porosity zone of the Aguathuna Formation, the magnitude of the negative phase is only subtly affected by the increasing porosity. In the lower reservoir unit of the Aguathuna-Catoche Formations, phase is shifted from positive to negative between the 5% and 10% models. This model shows positive correlation to the attributes mapped in chapter three and reveals a bound between 5% and 10% porosity.

The **thick** model (Figure 4.3.2.2) does not display the amount of instantaneous phase attribute robustness as the **thin** model. The significant attribute difference occurs

between zones of high porosity and lower porosity within the reservoir porosity zones and largely between 5% and 10% porosity. The multiple polarity shifts present in the **thin** model are not present and polarity shift information between the 0% and 5% reservoir zones is very subtle. The subtleness of the phase shift pattern and dominance of negative phase values is correlative to the M-16 and A-36 well where the Table Point Formation is thicker. Phase patterns do not change substantially between each porosity zone. Despite, the subtle change of instantaneous phase within the **thick** model, it appears to correlate to the well information and provide distinguishable change with lateral variation in porosity. The key characteristics in both models is the major polarity pattern shift between the 5% and 10% porosity zones.

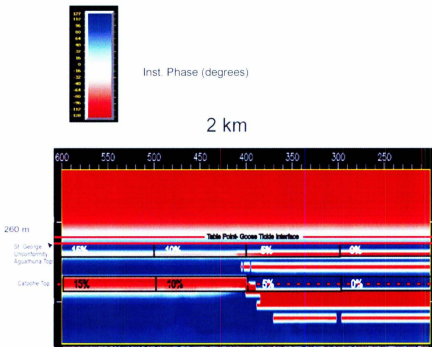


Figure 4.3.2.1. Instantaneous Phase Analysis on the **thin** model. Major interfaces shown in red. Porosity zones indicated by black boxes and percentages. Notice the major phase shift pattern between zones of high and low porosity.

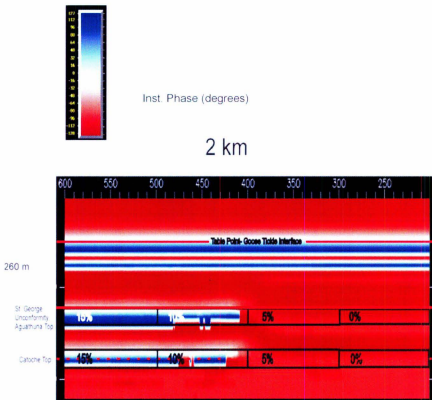


Figure 4.3.2.2. Instantaneous Phase analysis of **thick** model. Major interfaces shown in red. Porosity zones indicated by black boxes and percentages. Notice the major phase shift pattern between zones of high and low porosity.

4.3.3 Instantaneous Frequency analysis of the modeled 2-D seismic models

Instantaneous frequency successfully displays differences between zones of high and low porosity in both seismic model cases. Again, the largest scale attribute changes occur between the 5% and 10% porosity zones. Effects of the gradational model design are apparent in the instantaneous frequency analyses as variations within the porosity zones. Again, both seismic models differ in the robustness and change patterns of the instantaneous frequency attribute.

The **thin** model (Figure 4.3.3.1) displays robust changes in instantaneous frequency between zones of low and high porosity. The upper reservoir in the Aguathuna Formation interestingly shows highest instantaneous frequency values below the reservoir porosity zones between the 0-5% ranges. The high values shift up into the reservoir zones between the 10-15% ranges. High instantaneous frequency values anomalously fluctuate within the 10% reservoir porosity zones. This change within a porosity zone is most likely attributed to the gradational velocity changes designed into the models and is related to the effect of gradually changing porosity. The bottom, Lower Aguathuna- Upper Catoche Formation reservoir porosity zones do not lie within the regions of largest attribute change. The largest attribute changes lie directly above the (0-5% zones) and below the (10-15% zones) (see figure 4.3.3.1). The major attribute events in the reservoir porosity zones correlate with events in the PAP-1 well. The A-09 well shows some correlation to this model, but it is weak.

The **thick** model (Figure 4.3.3.2) again features more subtle attribute changes in the lower porosity zones (0-5%). There are overall, more intervals of higher instantaneous frequency in the lower porosity (0-5%) zones, but the difference between 0% and 5% is very subtle. The lower porosity zones (0-5%), in both top and bottom reservoirs units, do not lie within the intervals of largest attribute change. In contrast, the higher porosity zones (10-15%) do lie within regions of largest attribute change and appear to have decreased instantaneous frequency. The 10% porosity zone in the Lower Aguathuna-Upper Catoche Formation reservoir unit again changes value internally. The instantaneous frequency attribute is graphically displaying how wavelength is changing in response to porosity and in both models cases, the changes are not always within the porosity zones. The attribute changes in the **thick** model do not share correlation with events in wells A-36 and M-16 (wells with thick Table Point Formation).

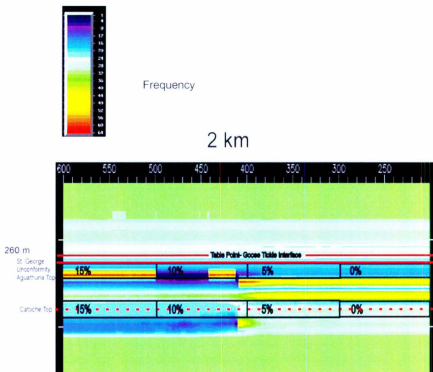


Figure 4.3.3.1. Instantaneous Frequency Analysis on the 2-D **thin** model. Major interfaces shown in red. Porosity zones indicated by black boxes and percentages. Notice the major difference in instantaneous frequency between zones of high and low porosity. Also, note variation in instantaneous frequency within the 10% porosity zones.

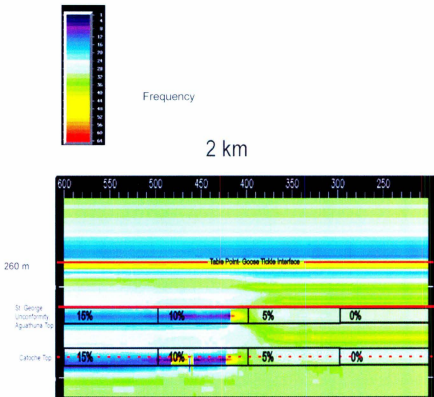


Figure 4.3.3.2. Instantaneous frequency analysis on 2-D **thick** model. Major interfaces shown in red. Porosity zones indicated by black boxes and percentages. Notice the major difference in instantaneous frequency between zones of high and low porosity. Additionally note, the variation in instantaneous frequency within the 10% porosity zones.

4.3.4 Reflection Strength analysis of the modeled 2-D seismic models

Reflection strength is a predictor of porosity in both seismic models. It displays strong lateral attribute changes at the Table Point-Goose Tickle Interface and within the reservoir porosity zones. Again, the major theme of this attribute reveals strong contrast between areas of higher and lower porosity. Overall, reflection strength increases with increasing porosity. This relationship is identical in all four of the wells previously examined in chapter three. The **thick** seismic model produces a more subtle resolution in attribute response than the **thin** model. The **thin** seismic model produces strong reflection strength changes at the dominant Table Point-Goose Tickle Interface.

The **thin** seismic model (Figure 4.3.4.1) reveals a clear attribute distinction between reservoir porosity zones and displays increasing reflection strength with porosity. Porosity has an effect on the attributes of the Table Point-Goose Tickle Interface reflector by increasing reflection strength abruptly between the 5% and 10% porosity zones. The bottom reservoir unit also displays an increase in reflection strength between the 5% and 10% porosity zones. There is some distinction between each individual porosity zones in both top and bottom reservoir units. Although very subtle, the difference manifests as minor increases in reflection strength with increasing porosity. The attribute changes in this model correlates to events in well A-09, however the events in well PAP-1 do not correlate.

The **thick** model (Figure 4.3.4.2) displays subtle, but resolvable changes in reflection strength. The major attribute change again occurs between zones of higher and

lower porosity. Both top and bottom reservoir units in between 0-5% porosity zones did not resolve significant attribute change within the porosity zones or other areas of the model. There is subtle difference in both top and bottom reservoir units amongst the 10% and 15% porosity zones. Overall, reflection strength increases with increasing porosity. No reflection strength attribute changes are observed in this model at the Table Point-Goose Tickle interface. The reflection strength patterns of the **thick** model correlate to the patterns observed in wells M-16 and A-36.

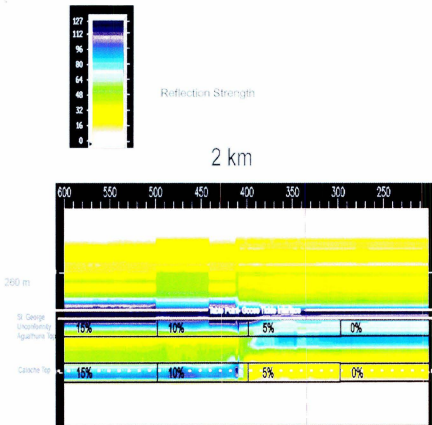


Figure 4.3.4.1. Reflection Strength analysis on the 2-D thin model. Major interfaces shown in red. Porosity zones indicated by black boxes and percentages. Notice the major reflection strength increase between zones of low and high porosity.

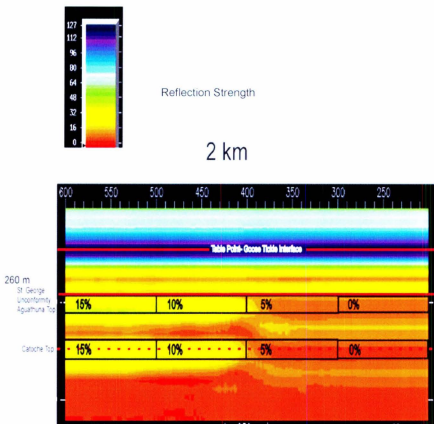


Figure 4.3.4.2. Reflection Strength analysis on the 2-D **thick** model. Major interfaces shown in red. Porosity zones indicated by black boxes and percentages. Although more subtle, there is a reflection strength increase between zones of low and high porosity.

4.3.5 Discussion of Complex Trace Attributes in the 2-D seismic models

One of the major aims of this chapter is to determine if porosity variations can be mapped laterally using complex trace attributes. The attributes examined on both seismic models prove changing porosity conditions manifest in the complex trace attributes. The distinction between zones of low porosity (0-5%) and high porosity (10-15%) is the most outstanding characteristic in all three complex trace attributes and in the **thin** and **thick** seismic models. All attributes are most robust in the **thin** seismic model while attribute changes are more subtle **thick** model. Each attribute provides a unique sensitivity to changing porosity conditions but the overall result is consistent for all attributes.

Reflection strength displays attribute changes along major interfaces and within the reservoir porosity zones. The reflection strength attribute does show subtle variation between individual zones of porosity, but the major attribute change is sharp contrast between the 5% and 10% porosity zones. This was expected because the 5 and 10% zones had the largest petrophysical contrast of any zones. Correlation to the major changes, in both seismic models, was made to three of the four wells in chapter three. The PAP-1 well was the only well to not correlate to attribute events in the seismic models.

Major patterns of instantaneous phase in both models are correlative with patterns in the wells. Minor phase patterns did not correlate however, but is not surprising because the data in the seismic lines is built from averages of all wells. Instantaneous phase show clear distinction between zones of higher and lower porosity (major contrast between 5%

and 10% porosity zones) in both seismic models, but does not reveal attribute changes between 0- 5% and 10-15% porosity zones .

Instantaneous frequency is the least useful of the attributes in this study, not only in this chapter, but in the well analysis of chapter three. It does not readily correlate to major frequency attribute changes in any of the wells, nor does it provide a change pattern with predictable trends. There is distinction between zones of higher porosity and lower porosity, with major contrast between 5% and 10% porosity zones. The major changes instantaneous frequency occurred outside of the reservoir porosity zones and this must be accounted for by the interpreter using this attribute. Interpretation difficulty is increased when using this attribute because the major attribute changes would occur outside of the suspected porosity zones in some porosities, and inside the porosity zones at other porosity values. Instantaneous frequency does correlate with the overall changes in instantaneous phase with a decrease in both attributes with increasing porosity.

Overall, the results demonstrate the ability to distinguish zones of higher ($\geq 10\%$) and lower ($\leq 5\%$) porosity laterally along horizons in seismic data by using complex trace attributes. The attributes cannot resolve the subtle changes between individual porosity zones, but the applicability of this tool is still useful in the initial stages of reservoir development. Particularly in reservoirs where the play is exploring for oil, it is not generally useful to distinguish between zones of 0% and 5% porosity. Typically at porosities below 5%, a tight carbonate reservoir will not flow economically viable amounts of oil. Therefore, knowing the specific porosity value below 5% is not relevant

information. It is also somewhat unnecessary to know exactly the distinction between zones 10% and 15% porosity, because either zone is desirable. The important distinction, initially in reservoir delineation, is to gain knowledge where the “high” (10-15%) and “low” (0-5%) porosity zones occur and plan future well locations from this distinction. This study successfully contributes to the knowledge base and toolset available to the interpreter. (exploring with this study’s scope of data), when attempting to reveal lateral variation in seismic attributes caused by porosity.

4.4 Noise sensitivity analysis of 2-D seismic model complex trace attributes

The attribute analysis presented in the previous section demonstrates useful characteristics, but the true test of applicability requires an assessment of attribute robustness with respect to noise. Real seismic data contain a significant amount of noise that may mask subtle changes in the attribute character. The following discussion determines the quantity of noise in the data at which useful attribute character is no longer resolvable in the three complex trace attributes employed in this study.

The amount of noise is measured by signal-to-noise ratio and is applied to the seismic models in Landmark software. The synthetic noise is applied with uniform noise generation over an amplitude range with equal probability of occurring at each amplitude. The calibration of the signal to noise ratio is based on the maximum peak and minimum trough signal amplitudes contained within the reservoir units. In other words, for the purpose of this discussion, the signal to noise ratio is defined by the signal strength within the reservoir zones. For example, to generate noise at a 2:1 signal to noise ratio, signal

information in the reservoir units with an amplitude of +/- 28 would yield noise at +/- 14. The following is a pictographic discussion separated into two subsections: 1) signal to noise sensitivity of the **thin** Table Point Formation seismic model with corresponding attributes. 2) signal to noise sensitivity of the **thick** Table Point Formation seismic line with corresponding attributes.

*4.4.1 Noise Sensitivity of the **thin** Table Point Formation seismic model*

The maximum and minimum amplitude in the signal of the reservoir units is measured at +/- 28. Signal to noise ratios of 2:1, 1:1, 0.7:1, and 0.5:1 are applied to the seismic data prior to attribute analysis in the **thin** model. Reflection strength attributes are coherent to a 2:1 signal to noise ratio displaying the major difference between high and low porosity zones (10%-5%) (Figure 4.4.1.1) and marginally coherent at 1:1 signal to noise ratio (Figure 4.4.1.2). At 0.7:1 and 0.5:1 (Figures 4.4.1.3 and 4.4.1.4, respectively), there are no longer recognizable attribute changes.

Attribute changes are resolvable in instantaneous phase at 2:1 (Figure 4.4.1.5) and 1:1 (Figure 4.4.1.6) signal to noise ratios. 2:1 signal to noise ratio displays major phase shifts without losing much resolution from the original model. At 0.7:1 (Figure 4.4.1.7) signal to noise ratio, very faint major phase shifts in the high porosity zones are still recognizable, but most of the information in the lower reservoir porosity zones is masked by noise. 0.5:1 (Figure 4.4.1.8) reveals no useful information and all important phase shifts are attenuated by noise.

Instantaneous frequency is not a reliable attribute when noise is introduced. 2:1 (Figure 4.4.1.9) signal to noise ratio is marginal at displaying original attribute character, but does distinguish zones of higher and lower porosity in the upper reservoir porosity unit. The resolution in the lower reservoir porosity zones is marginal and not reliable. 1:1, 0.7:1 and 0.5:1 (Figures 4.4.1.10-12, respectively) do not display any useful information and all attribute information has been attenuated by noise.

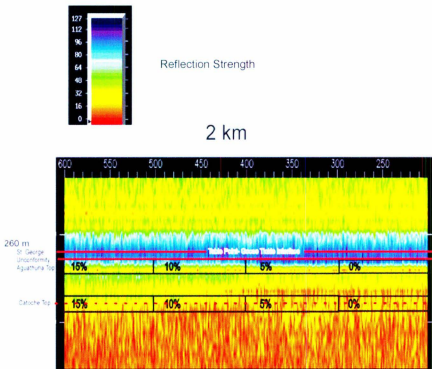


Figure 4.4.1.1. Reflection strength analysis of the **thin** model with a 2:1 signal to noise ratio. Major interfaces in red, reservoir porosity zones in black boxes. The major change between low and high porosity zones is still recognizable.

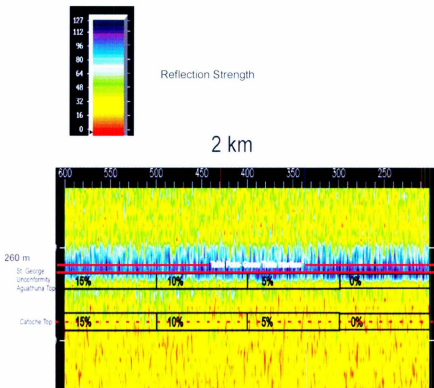


Figure 4.4.1.2. Reflection strength analysis of the **thin** model with a 1:1 signal to noise ratio. Reservoir porosity zones in black boxes. The attribute information in the lower reservoir porosity zone is unrecognizable. Some attribute information is retained in the upper reservoir porosity zone, but only in the higher porosity ranges.

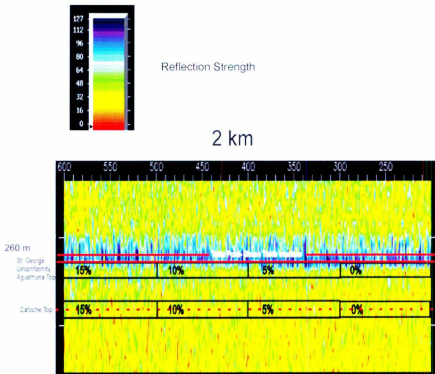


Figure 4.4.1.3. Reflection strength analysis of the **thin** model with a 0.7:1 signal to noise ratio. Reservoir porosity zones in black boxes. All use attribute information has been lost

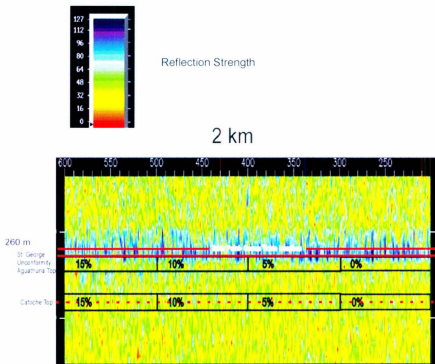


Figure 4.4.1.4. Reflection strength analysis of the **thin** with a 0.5:1 signal to noise ratio. Reservoir porosity zones in black boxes. All use attribute information has been attenuated by noise.

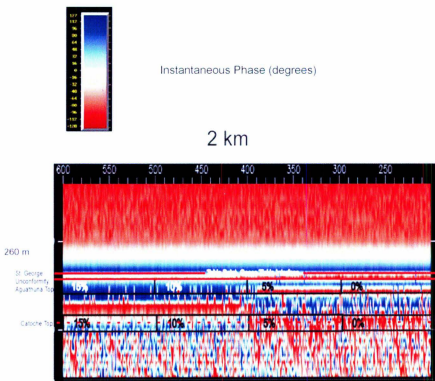


Figure 4.4.1.5. Instantaneous phase analysis of the **thin** model with a 2:1 signal to noise ratio. Major interfaces in red, reservoir porosity zones in black boxes. The major phase shifts are still recognizable and preserved in good detail in the upper reservoir porosity zone.

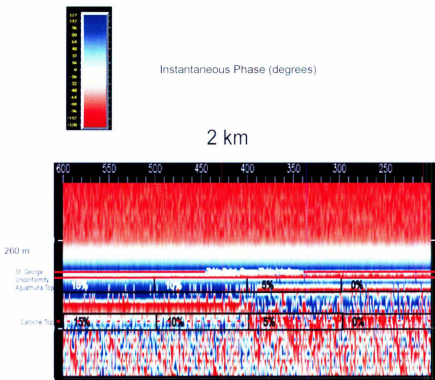


Figure 4.4.1.6. Instantaneous phase analysis of the **thin** model with a 1:1 signal to noise ratio. Major interfaces in red, reservoir porosity zones in black boxes. The major shifts in phase between the 5% and 10% porosity zones is marginally recognizable, but all other important information has been attenuated by noise.

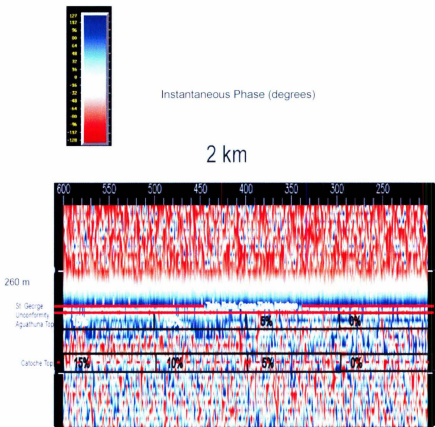


Figure 4.4.1.7. Instantaneous phase analysis of the **thin** model with a 0.7:1 signal to noise ratio. Major interfaces in red, reservoir porosity zones in black boxes. The major shifts in phase between the 5% and 10% porosity zones is marginally recognizable in the top reservoir zones, but all other important information has been attenuated by noise.

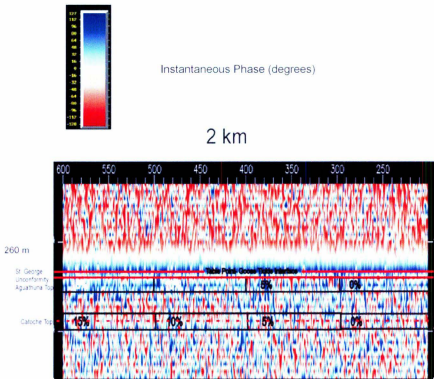


Figure 4.4.1.8. Instantaneous phase analysis of the **thin** model with a 0.5:1 signal to noise ratio. Major interfaces in red, reservoir porosity zones in black boxes. All recognizable phase shifts have been lost under the St. George Unconformity.

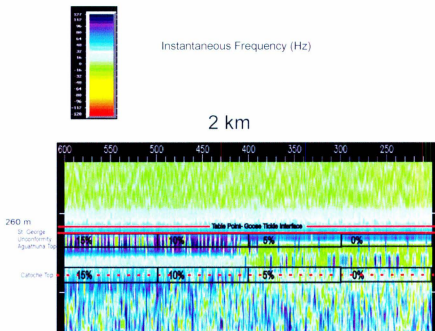


Figure 4.4.1.9. Instantaneous frequency analysis of the **thin** model with a 2:1 signal to noise ratio. Major interfaces in red, reservoir porosity zones in black boxes. It is very difficult to recognize the major pattern change between zones of lower and higher porosity, but the relationship is still subtly apparent.

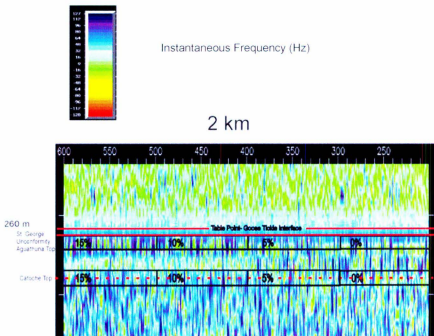


Figure 4.4.1.10. Instantaneous frequency analysis of the thin model with a 1:1 signal to noise ratio. Major interfaces in red, reservoir porosity zones in black boxes. All recognizable attribute information has been attenuated with noise at this ratio.

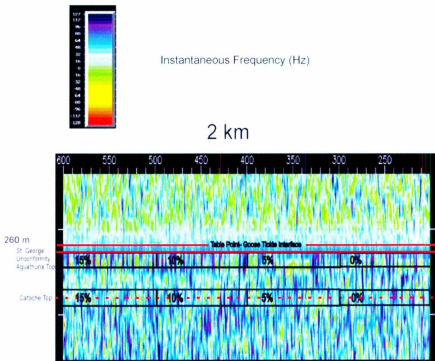


Figure 4.4.1.11. Instantaneous frequency analysis of the **thin** model with a 0.7:1 signal to noise ratio. Major interfaces in red, reservoir porosity zones in black boxes. All recognizable attribute information has been lost at this ratio.

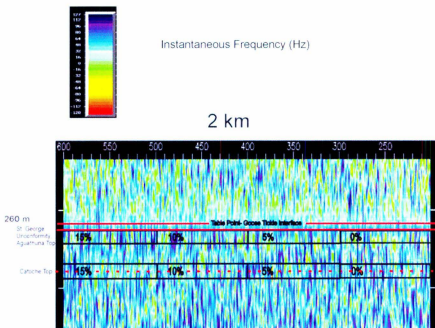


Figure 4.4.1.12. Instantaneous frequency analysis of the **thin** model with a 0.5:1 signal to noise ratio. Major interfaces in red, reservoir porosity zones in black boxes. All recognizable attribute information has been lost at this ratio.

*4.4.2 Noise Sensitivity of the **thick** Table Point Formation seismic model*

The maximum and minimum amplitude of the signal in the reservoir units was measured at ± 30 . Signal to noise ratios of 2:1, 1:1, 0.7:1, and 0.5:1 are applied to the seismic models prior to attribute analysis. Reflection strength attribute changes are resolvable when 1:1 and 2:1 signal to noise ratios are applied to the data. (figure 4.4.2.2 and figure 4.4.2.1, respectively) The 0.7:1 (figure 4.4.2.3) signal to noise ratio only marginally reveals the increase in reflection strength in the higher (10-15%) porosity zones. At 0.5:1 (Figure 4.4.2.4), there are no longer recognizable attribute changes and all important information is attenuated by noise.

Attribute changes are recognizable in instantaneous phase as low as 1:1 (Figure 4.4.2.6) signal to noise ratio. 2:1 (Figure 4.4.2.5) signal to noise ratio displays the major phase shifts without losing much resolution from the original analysis. 1:1 signal to noise ratio still retains the major phase shifts between zones of higher and lower porosity, but loses a good deal of fine detail attribute information. At 0.7:1 (Figure 4.4.2.7) signal to noise ratio, faint major shift patterns in the high (10-15%) porosity zones are marginally recognizable, but almost all other attribute information in the reservoir porosity zones is masked by noise. 0.5:1 (Figure 4.4.2.8) reveals no useful information and all important phase shifts are attenuated.

Instantaneous frequency again, is not a reliable attribute when noise is introduced. 2:1 (Figure 4.4.2.9) signal to noise ratio is marginal at displaying resolvable information from original attribute character, but slightly resembles the original data in higher

porosity zones (10-15%). The resolution in the lower porosity zones (0-5%) is marginal and not reliable. 1:1, 0.7:1 and 0.5:1 (Figures 4.4.2.10-12, respectively) do not display any useful information and all attribute information is attenuated by noise.

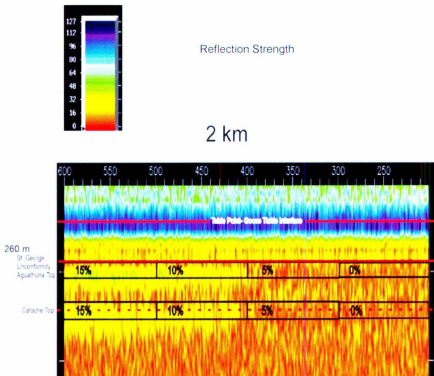


Figure 4.4.2.1. Reflection strength analysis of the **thick** model with a 2:1 signal to noise ratio. Major interfaces in red, reservoir porosity zones in black boxes. The major change between low and high porosity zones is still readily recognizable.

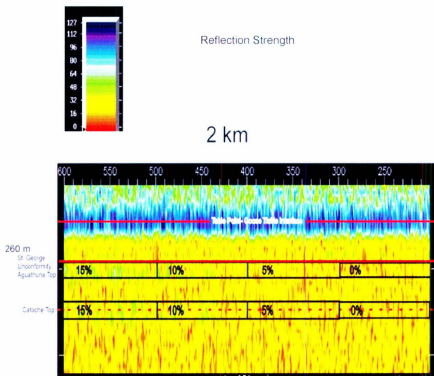


Figure 4.4.2.2. Reflection strength analysis of the **thick** model with a 1:1 signal to noise ratio. Major interfaces in red, reservoir porosity zones in black boxes. The increase in reflection strength is still marginally visible with increasing porosity. (green areas in reservoir porosity zone boxes)

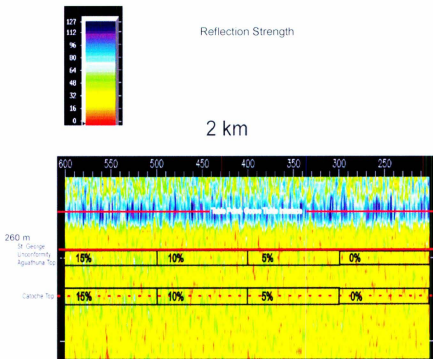


Figure 4.4.2.3. Reflection strength analysis of the **thick** model with a 0.7:1 signal to noise ratio. Major interfaces in red, reservoir porosity zones in black boxes. The increase of reflection strength (green areas) within the reservoir porosity zones is still faintly visible, but mostly not useful.

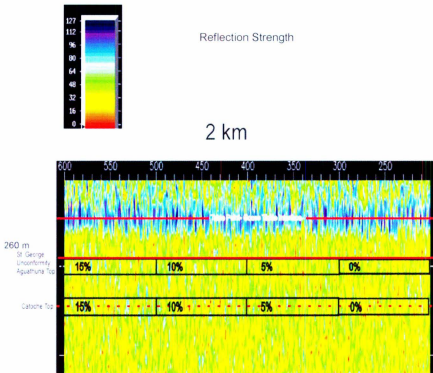


Figure 4.4.2.4. Reflection strength analysis of the **thick** model with a 0.5:1 signal to noise ratio. Major interfaces in red, reservoir porosity zones in black boxes. All useful information from attributes is lost.

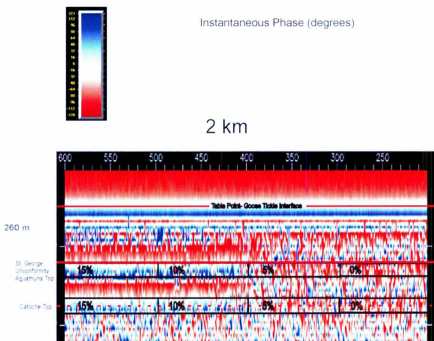


Figure 4.4.2.5. Instantaneous phase analysis of the **thick** model with a 2:1 signal to noise ratio. Major interfaces in red, reservoir porosity zones in black boxes. The major phase shift intervals within the 10% and 15% porosity zones are still readily visible. The distinction between the lower and higher porosity zones is also resolvable.

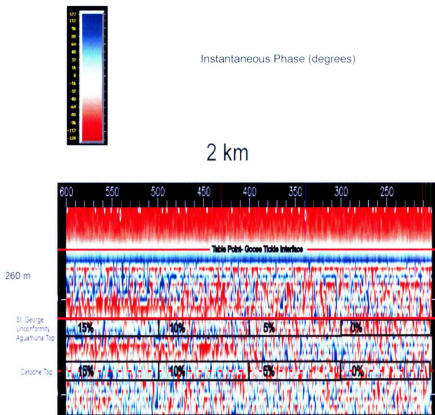


Figure 4.4.2.6. Instantaneous phase analysis of the **thick** model with a 1:1 signal to noise ratio. Major interfaces in red, reservoir porosity zones in black boxes. The major attribute changes between zones of lower and higher porosity are not as easily recognizable, and only the higher reservoir porosity zones display distinguished phase shift interval information.

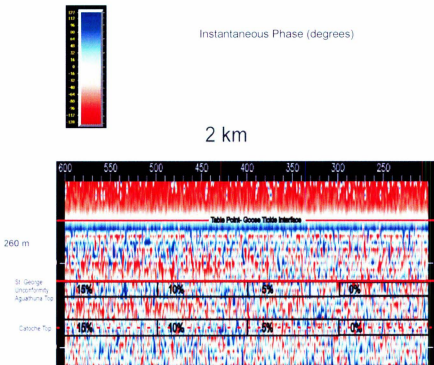


Figure 4.4.2.7. Instantaneous phase analysis of the **thick** model with a 0.7:1 signal to noise ratio. Major interfaces in red, reservoir porosity zones in black boxes. Most useful information is occluded by noise.

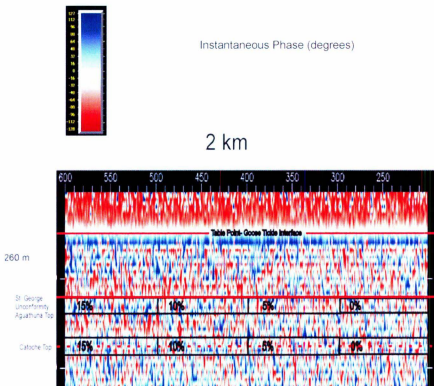


Figure 4.4.2.8. Instantaneous phase analysis of the **thick** model with a 0.5:1 signal to noise ratio. Major interfaces in red, reservoir porosity zones in black boxes. Most useful attribute information has been attenuated by noise. Only large phase shifts at the Table Point-Goose Tickle Interface remain.

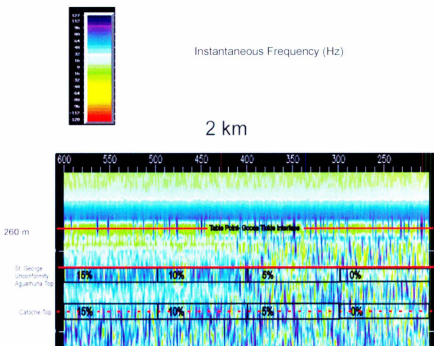


Figure 4.4.2.9. Instantaneous frequency analysis of the **thick** model with a 2:1 signal to noise ratio. Major interfaces in red, reservoir porosity zones in black boxes. Only instantaneous frequency values in the higher porosity reservoir zones are recognizable of the original data, but are marginal in quality.

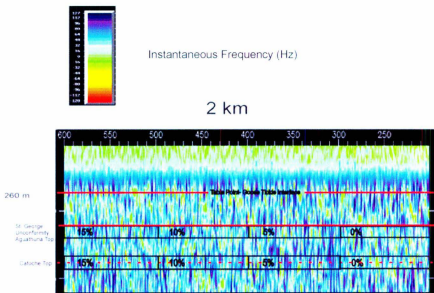


Figure 4.4.2.10. Instantaneous frequency analysis of the **thick** model with a 1:1 signal to noise ratio. Major interfaces in red, reservoir porosity zones in black boxes. All recognizable attribute information has been lost at this ratio.

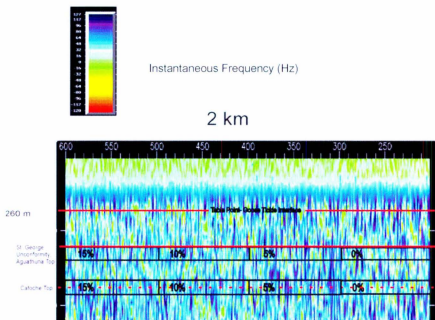


Figure 4.4.2.11. Instantaneous frequency analysis of the **thick** model with a 0.7:1 signal to noise ratio. Major interfaces in red, reservoir porosity zones in black boxes. All recognizable attribute information is attenuated at this ratio.

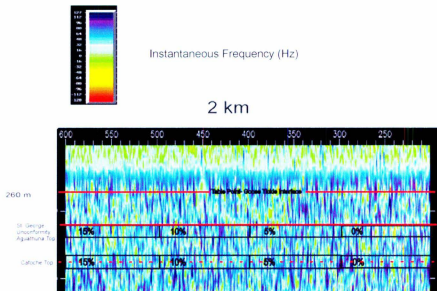


Figure 4.4.2.12. Instantaneous frequency analysis of the **thick** model with a 0.5:1 signal to noise ratio. Major interfaces in red, reservoir porosity zones in black boxes. All recognizable attribute information is attenuated by noise at this ratio.

4.5 Discussion of noise sensitivity analysis of 2-D seismic model complex trace attributes

Both variations of the seismic models display attribute resolution at reasonable signal to noise ratios that can be obtained in real seismic data applications. Instantaneous phase attributes are resolvable down to 1:1 in the **thin** and **thick** seismic models. Instantaneous frequency is most susceptible to noise attenuation and attribute character was marginally recognizable at 2:1 signal to noise ratios in both seismic models. Reflection strength produces recognizable attribute changes at 1:1 in the **thick** seismic model and only 2:1 in the **thin** seismic model.

This type of sensitivity analysis proves that complex trace attributes can reveal lateral effects of porosity on waveform character and maintain robustness in the presence of noise. Despite the subtle nature of the attribute changes of **thick** model, the robustness of attribute character held up slightly better than the **thin** model in the presence of noise. The difference between the two models is most likely attributed to the effects and proximity of the Table Point-Goose Tickle Interface. The interpreter must be aware of these relationships when applying this technique.

Chapter 5: Conclusions and future recommendations

5.1 Conclusions

The methodology in this thesis is iterative and exploratory regarding the wide variety of constraints and attributes tested. This section restates the geology, techniques, and results from this thesis. The purpose of this study is to demonstrate a technique, using complex trace attributes, to reveal lateral changes in seismic data from varying porosity in heterogeneous carbonates in the immediate vicinity of wells. The raw data, specifically petrophysical well data and background geologic information, is acquired from outside sources for use used in this study.

The reservoir units of interest in this study are constrained to the St. George Group (Ordovician) carbonate reservoirs of the Port au Port Peninsula, western Newfoundland. In particular, this study examined the hydrothermally altered, dolomitized rocks of the Aguathuna and Catoche Formation. The Aguathuna and Catoche Formations were subjected to complex diagenetic and structural evolution. The peritidal reservoir units underwent three generations of dolomitization and four generations of cementation, complicating the porosity development history with multiple phases of occlusion and replacement. Three, separate, polyphase deformational events occurred in the Passive Margin Megasequence on the Port au Port Peninsula. Processes associated with this structural deformation provided the main mechanism for hydrothermal fluid ingress and porosity development in the Aguathuna and Catoche Formations. Porosity initially developed, from the migration of forebulge, along subareally exposed paleohighs

in the extensional fault blocks of the carbonate platform in the Taconic Orogeny. Secondary porosity developed from hydrothermal fluid flow during the Salinic and Acadian Orogenies. The reservoir intervals, or porous zones, within the Aguathuna and Catoche Formations are on the order of 25-30 meter thickness. The four exploration wells used in this study targeted porosity enhanced footwall blocks beneath the Round Head reactivation thrust fault. All models and geophysical analysis were built from petrophysical data from wells: St. Georges Bay A-36, Port au Port-1, Long Range A-09, and Long Point M-16.

A preliminary statistical assessment is designed to correlate petrophysics to porosity. Furthermore, data filters are designed to determine which petrophysical values best represent any given porosity. The filters specially display results at 0, 5, 10, and 15 % porosity. Statistical analysis provided the mean, mode, and standard deviations for bulk density and sonic slowness (interval transit time) for the above mentioned porosity values. The results of the preliminary statistical assessment are summarized by the following statements; An anomalous trend from 0-5% porosity occurred in all petrophysical properties is noticed. The trend is represented by counter intuitive linear regression in the plots from 0 to 5%. I.e. A rise in bulk density with increasing porosity between 0 and 5%. This is interpreted to be combination effects of two rocks types in the plots and the plotting effect of the compensated neutron porosity tool. The two rocks types, dolomite and limestones, are grouped together in this type of plots and therefore overlap. The two lithologies were distinguished by using a numeric lithology filter derived from intervals of known rock types in the wells and using the compensated

neutron tool correction equation. Once the data separation of lithology was completed, correlations are determined between the crossplots. As anticipated, bulk density decreased overall with increasing porosity and interval transit time increased with increasing porosity. Acoustic impedance, by definition a product of interval transit time and bulk density, displayed a decrease overall with increasing porosity. After the preliminary assessment, a frequency distribution analysis selected the best representative petrophysical values at the selected model porosities (0, 5, 10 and 15%). The results of analysis are found in Table 3.1. Values from Table 3.1 are used in building block porosity models and synthetic seismogram generation.

The results of the complex trace attribute analysis varied and examined separately in each well as geologic conditions changed. A common trait in all four wells is the 40Hz Ricker wavelet produced the best resolution to reveal changes in attribute character. However some useful information is derived from wells A-36, PAP-1, and M-16 at 20Hz. Occasionally, dependent on the Table Point Formation thinness, the 20Hz Ricker wavelet reflection character is dominated by the large amplitude associated with the Table Point-Goose Tickle Interface. The waveform energy from this dominant reflector obscures subtle waveform character within the reservoir units of the Upper Aguathuna Formation. 80Hz Ricker wavelet did not show distinguishing characteristics between the porosity models, indicative that most of the useful response information is revealed at lower frequencies. Instantaneous phase produces measureable attribute changes in the porosity modeled synthetics at the variable density scale, but did not prove useful in the empirical plots. Numerical instantaneous phase values at constant time provide no useful

information in the empirical plots. Instantaneous frequency and reflection strength are useful in both the empirical plots and variable density graphs. Instantaneous frequency correlated to the changes instantaneous phase in the plots by decreasing with increasing porosity. The decrease in instantaneous frequency correlated to the decreasing number of phase shift in the instantaneous phase analysis. In some cases, changes in attribute character are so subtle the empirical plots are better suited to display the results.

Well A-09 displays ambiguity between the 0% and 10% porosity modeled synthetics interpreted to be a petrophysical similarity between a 0% porous limestone and a 10% porous dolomite. The Goose Tickle- Table Point Interface reflector dominates the reflection amplitude information in the Upper Aguathuna Formation due to a thin succession of Table Point Formation in the well. Instantaneous phase displays subtle phase shift pattern changes at 40Hz with an overall decrease in phase shifts with increasing porosity. Instantaneous frequency at 40Hz displays significant attribute change differences between the porosity models in the middle of the Aguathuna Formation. Reflection strength increases overall with increasing porosity at 40Hz.

Well A-36 recorded useful information in the 20 and 40Hz Ricker wavelets. Both 20 and 40Hz Instantaneous phase and frequency analyses produce significant changes between the models in resolution high enough to derive useful information. Reflection strength produces very subtle changes of increasing reflection strength with increasing porosity, and only changes in the higher porosity models. Ambiguity exists in the 10% and 15% porosity in all attribute models, presumably from petrophysical statistical

similarity of dolomite at 10% and 15% porosities in this well. The attribute analysis suggests this well may be only useful in distinguishing zones of lower and higher porosities.

Well M-16 only contained statistically reliable modeling parameters up to 10% porosity. Both 20 and 40 Hz wavelets display mapable phase shift changes with increasing porosity with instantaneous phase. Instantaneous frequency is the strongest changing attribute analyzed, changing noticeably in the empirical and variable density plots. Instantaneous frequency, overall, decreases with increasing porosity along the models and is best displayed in the 20Hz variable density plot. Reflection strength attribute changes were also strong, increasing strength with increasing porosity.

The PAP-1 well displays the most change between each porosity modeled synthetic than any other well in the study. The behavior of the instantaneous phase analysis in the 20 and 40Hz wavelets was distinct between each porosity model. The number of phase shifts decrease with increasing porosity in the Aguathuna Formation. The instantaneous frequency attribute in the 20 to 40Hz wavelets decrease in strength with increasing porosity. Reflection strength decreases with increasing porosity in both 20 and 40Hz wavelets, unlike any other well reflection strength analysis.

Synthetic 2-D seismic models are generated in the absence of real 2-D seismic data. The synthetic 2-D seismic models are generated using petrophysical data from all wells in this study. The seismic models are built from velocity substitution models honouring the literature based reservoir architecture and Table Point Formation

thicknesses from the wells. Two different models of Table Point Formation representing thick and thin successions are constructed. Instantaneous phase, instantaneous frequency, and reflection strength are analyzed on the synthetic 2-D seismic models and compared to the results from chapter three.

The **thin** seismic line displays very clear distinction between zones of low (0-5%) and high (10-15%) in all of the attributes. Instantaneous phase decreases in the number of phase shift intervals with increasing porosity. This change is correlative to the A-09 and PAP-1 attribute analysis. Instantaneous frequency, again, displayed changing attribute character between zones of low and high porosity. The largest changes in instantaneous frequency did not lay within the reservoir zones. The PAP-1 well attributes are correlative to the changes in instantaneous frequency attribute, but the A-09 well only displayed minor similarity. Robust reflection strength changes in attribute character, increasing reflection strength with increasing porosity. Both A-09 and PAP-1, with thin successions of Table Point Formation, are correlative to the reflection strength changes in this seismic model. The largest contrast in reflections strength is between zones of lower and higher porosities, specifically between the 5% and 10% transition.

The **thick** seismic model displays more subtle changes in reservoir porosity zone attributes between the models than the **thin** model. The largest attribute change is observed in all three attributes between zones of low (0-5%) and high (10-15%) porosity in the reservoir porosity zones. Instantaneous phase lost resolution in the phase shift intervals from the **thin** seismic model. Only major phase shift intervals are revealed in

the lower 0 to 5% porosity zones and are of less detail than the previous seismic line. Phase shifts in the Aguathuna Formation are correlative to wells M-16 and A-36 where the Table Point Formation is thicker. Instantaneous frequency changes in this seismic do not show correlation with wells M-16 and A-36. Again, the largest attribute changes do not occur within the reservoir porosity zones. Reflection strength is a strong attribute in the **thick** model. It displayed subtle changes in each reservoir porosity zone, increasing reflection strength with increasing porosity. Wells M-16 and A-36 correlate to the reflection strength changes in the above seismic model.

A noise sensitivity analysis is conducted on both 2-D seismic line attributes analyses to determine the threshold of resolution in the complex trace attributes when noise is added. In the **thin** model, instantaneous phase response is resolvable at 1:1 signal to noise ratio. Reflection strength is recognizable at 2:1 signal to noise ratio. Instantaneous frequency is marginally recognizable at 2:1 signal to noise ratio, but mostly not coherent after the addition of noise. The **thick** model resolves attributes at lower signal to noise ratios than the **thin** seismic model. Instantaneous phase response is resolvable at 1:1 signal to noise ratio. Instantaneous frequency is marginally resolvable when noise is added at 2:1 signal to noise ratio. Reflection strength is recognizable to 1:1 signal to noise ratio. The results of the signal to noise ratio proves that complex trace attributes can maintain robustness and not be attenuated in the presence of noise.

This thesis has introduced a technique to add to the toolset available for preliminary reservoir delineation in carbonate reservoirs analogous to the Ordovician St.

George Groups of western Newfoundland. Its primary use is determining future well placement in areas with low well control and low number of seismic lines by revealing zones of porosity in the immediate vicinity of existing wells. This thesis has successfully demonstrated that the effects of porosity manifest in the complex trace attributes of 1-D synthetic seismograms and produce notable changes between differing porosity levels. Furthermore, this thesis proves that attribute changes associated with porosity can be observed across potential reservoir zones in synthetic 2-D seismic data.

5.2 Suggestions for Future Work

Optimally, this study would have utilized real 2-D seismic data on the Port au Port Peninsula. Therefore, the most significant recommendation for future work would be to use real seismic data instead of synthetically generated seismic lines from well data. The true applicability of this technique would be revealed with real data. A more realistic scale of the dimensionality of porosity zones could be revealed, rather than the arbitrarily sized porosity zones of the 2-D seismic models. Selecting high quality seismic data is also an important issue when choosing real seismic in this type of study.

The poor quality of the real seismic data examined in for potential use in this study was located in an incredibly structurally complex region of the Port au Port Peninsula. Consequently, amplitude information needed for complex trace analysis was not useful and was obscured. Regionally, there is another area with the same rock units of the Port au Port Peninsula that is also an area of oil and gas exploration. The Anticosti Basin is located directly west of the Port au Port Peninsula in the Gulf of St Lawrence.

The strata here is undeformed, flat lying, and contains exploration wells. Presumably, seismic data in this region would be apropos for use in this study and provide a source of real data. Although this study was intended for use in carbonates, its practical use in other lithology could be explored. This technique could be potentially implemented in siliclastic or argillaceous type reservoirs with features large enough to be imaged in seismic data.

References

- Azmy, K., D. Lavoie, I. Knight, and G. Chi, 2008, Dolomitization of the Lower Ordovician Aguathuna Formation carbonates, Port au Port Peninsula, western Newfoundland, Canada: implications for a hydrocarbon reservoir, *Canadian Journal of Earth Sciences*, vol. 45, no. 7, p. 795-813.
- Baker, D. Knight, I. (1993). The Catoche Dolomite Project, Anticosti basin Eastern Canada. Centre for Earth Resources Research Report St. John's Memorial University of Newfoundland: 174 p.
- Barnes, A. E., 2007, A tutorial on complex seismic trace analysis, *Geophysics*, vol. 72, no. 6, p. W33-W43.
- Bigelow, E., 2002, Introduction to Wireline Log Analysis, Baker Hughes, Houston, TX, 312 p.
- Boyce, W. D, 1996, Revised Ordovician trilobite biostratigraphy of the autochthon/parautochthon, western Newfoundland. Report of Activities - Newfoundland, Geological Survey Branch, Canada, Government of Newfoundland and Labrador, Geological Survey Branch : St. John's, NL, Canada, **1996**: 8-8.
- Boyce, W. D., 1997, Trilobite and conodont biostratigraphy of the St. George Group, Eddies Cove West area, western Newfoundland. Current Research Report, S.

- Stouge , Government of Newfoundland and Labrador. Geological Survey : St. John's, NL, Canada: 183-200 p.
- Boyce, W. D., Knight, I., Rohr, M., Williams, S. H., and Measures E. A., 2000. The upper St. George Group, western Port au Port Peninsula; lithostratigraphy, biostratigraphy, depositional environments and regional implications. Current Research Report. Government of Newfoundland and Labrador. Geological Survey : St. John's, NL, Canada: 101-125 p.
- Burden, E. T., 2004. Geology and evolution of the Humber Arm Allochthon, southwest Bay of Islands, Newfoundland; hydrocarbon prospects and challenges. Reservoir, vol. 31, no. 5: 5, p. 8-8.
- Calon, T., 2002. Stratigraphy and structure of sedimentary rocks in the Humber Arm Allochthon, southwestern Bay of Islands, Newfoundland. Current Research - Newfoundland. Geological Survey Branch, p. 35-45.
- Choquett, Pw and L. C. Pray, 1970. Geologic Nomenclature and Classification of Porosity in Sedimentary Carbonates. American Association of Petroleum Geologists Bulletin, vol. 54, no. 2, p. 207-&.
- Chow, N. and N. P. James, 1992. Synsedimentary Diagenesis of Cambrian Peritidal Carbonates - Evidence from Hardgrounds and Surface Paleokarst in the Port-Au-Port Group, Western Newfoundland, Bulletin of Canadian Petroleum Geology, vol. 40, no. 2, p. 115-127.

- Collins, J. A., 1975, Zinc deposits related to diagenesis and intrakarstic sedimentation in the lower Ordovician St. George Formation, western Newfoundland, *Bulletin of Canadian Petroleum Geology*, vol. 23, no. 2; 2, p. 393-427.
- Cooper, M., J. Weissenberger, I. Knight, D. Hostad, D. Gillespie, H. Williams, E. Burden, J. Porter-Chaudhry, D. Rae, and E. Clark, 2001, Basin evolution in western Newfoundland: New insights from hydrocarbon exploration, *AAPG Bulletin*, vol. 85, no. 3, p. 393-418.
- Cumming, I. M., 1968, St George-Table Head Disconformity and Zinc Mineralization Western Newfoundland, *Canadian Mining and Metallurgical Bulletin*, vol. 61, no. 674, p. 721-&.
- Davies, G. R., 2006, Structurally controlled hydrothermal dolomite reservoir facies: an overview, *AAPG Bulletin*, vol. 90, no. 11; 11, p. 1641-1690.
- Davies, G. R. and L. B. Smith Jr., 2007, Structurally controlled hydrothermal dolomite reservoir facies: An overview: Reply, *AAPG Bulletin*, vol. 91, no. 9, p. 1342-1344.
- Fetter, C. W, 2001, *Applied Hydrogeology* , Prentice Hall, Upper Saddle River, New Jersey. 120 p.

- Haywick, D. W., 1984, Dolomite within the St. George (Lower Ordovician), western Newfoundland . Memorial University of Newfoundland. St. John's, Nfld, **M.Sc.**: 281 p.
- Hallenburg, J., 1998, Standard methods of geophysical formation evaluation. CRC Press, Boca Raton, FL, 442 p.
- James, N. P., Klappa, C. F., 1980, Field trip guidebook; Trip 13, Cambro-Ordovician of West Newfoundland; sediments and faunas. Geologic Association. of Canada.
- Kallweit, R. S. and L. C. Wood, 1982, The Limits of Resolution of Zero-Phase Wavelets, Geophysics, vol. 47, no. 7, p. 1035-1046.
- Kerans, C., 1988, Karst-Controlled Reservoir Heterogeneity in Ellenburger Group Carbonates of West Texas, Aapg Bulletin-American Association of Petroleum Geologists, vol. 72, no. 10, p. 1160-1183.
- Kindle, C. H. and Whitting, Hb, 1965, New Cambrian and Ordovician Fossil Localities in Western Newfoundland, Geological Society of America Bulletin, vol. 76, no. 6, p. 683-&.
- Knight, I., 1977, The Cambro- Ordovician platformal rocks of the Northern Peninsula, Newfoundland. D. o. M. a. E.-. Mineral Development Division. St.John's: 1-27.

- Knight, I. and N. P. James, 1987, The Stratigraphy of the Lower Ordovician St-George Group, Western Newfoundland - the Interaction between Eustasy and Tectonics, *Canadian Journal of Earth Sciences*, vol. 24, no. 10, p. 1927-1951.
- Knight, I., 1989, The St. George Unconformity, Ordovician, Northern Appalachians: effects of lithosphere dynamics on the Sauk-Tippecanoe sequence boundary, *Atlantic Geology*, vol. 25, no. 3: 3, p. 214-214.
- Knight, I., N. P. James, and T. E. Lane, 1991, The Ordovician St-George Unconformity, Northern Appalachians - the Relationship of Plate Convergence at the St-Lawrence Promontory to the Sauk Tippecanoe Sequence Boundary, *Geological Society of America Bulletin*, vol. 103, no. 9, p. 1200-1225.
- Knight, I., Azmy, K., Greene, M., Lavoie, D., 2007, "Lithostratigraphic setting of diagenetic, isotopic, and geochemistry studies of Ibexian and Whiterockian carbonates of the St. George and Table Head groups in western Newfoundland." Newfoundland and Labrador Department of Natural Resources, **Geological Survey Report 07-1** 55-84.
- Lane, T. E., 1990, Dolomitization, brecciation and zinc mineralization and their paragenetic, stratigraphic and structural relationships in the Upper St. George Group (Ordovician) at Daniel's Harbour, western Newfoundland., Memorial University of Newfoundland, St. John's, Nfld. 496 p.

- Lavoie, D., 2005, Hydrothermal dolomite reservoirs in Eastern Canada; a promising newly recognized play in Paleozoic carbonates, Abstracts: Annual Meeting - American Association of Petroleum Geologists, vol. 14, p. A79-A79.
- Lavoie, D., 2006, Hydrocarbons in the Paleozoic basins of Eastern Canada; significant newly recognized potential, *Atlantic Geology*, vol. 42, no. 2-3; 2-3, p. 194-194.
- Levesque, R. J., 1978, Stratigraphy and sedimentology of Middle Cambrian to Lower Ordovician shallow water carbonate rocks, western Newfoundland, Canada.
- Logan, W. E. (1863). Geology of Canada. Montreal Dawson Brothers.
- Pratt, B. R., 1986, The St George Group (Lower Ordovician) of western Newfoundland; tidal flat island model for carbonate sedimentation in shallow epeiric seas, *Sedimentology*, vol. 33, no. 3; 3, p. 313-343.
- Rider, M. H. .1991, *The geological interpretation of well logs- Rev. Ed.*, Caithness, UK Whittles Publishing. 120 p.
- Sheehan, P. M. and D. R. J. Schiefelbein, 1984, The Trace Fossil *Thalassinoides* from the Upper Ordovician of the Eastern Great Basin: Deep Burrowing in the Early Paleozoic, *Journal of Paleontology*, vol. 58, no. 2, Trace Fossils and Paleoenvironments: Marine Carbonate, Marginal Marine Terrigenous and Continental Terrigenous Settings, p. pp. 440-447.

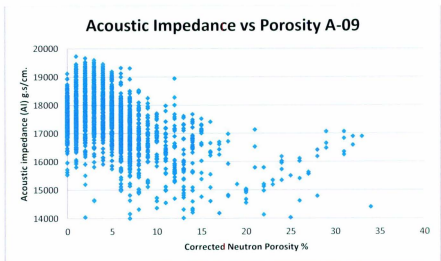
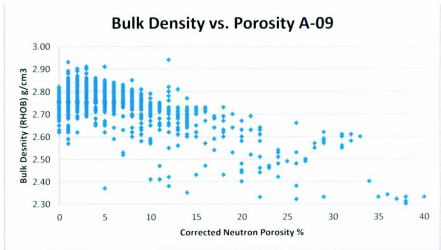
- Sheriff, R. E., 1988, Processing and interpretation of seismic reflection data; an historical precis, *Geophysics: The Leading Edge of Exploration*, vol. 7, no. 1; 1, p. 40-42.
- Sheriff, R. E. and Geldart, L. P., 1995, *Exploration Seismology*. New York, Cambridge University Press. 628 p.
- Smith, L. B., Jr.[editor], 2006, Structurally controlled hydrothermal alteration of carbonate reservoirs, *AAPG Bulletin*, vol. 90, no. 11; 11, p. 1635-1861.
- Stenzel, S. R., 1990, Carbonate platform to foreland basin: revised stratigraphy of the Table Head Group (Middle Ordovician), western Newfoundland, *Canadian Journal of Earth Sciences = Revue Canadienne des Sciences de la Terre*, vol. 27, no. 1; 1, p. 14-26.
- Stockmal, G. S., 2004, Basement-involved inversion at the Appalachian structural front, western Newfoundland; an interpretation of seismic reflection data with implications for petroleum prospectivity, *Bulletin of Canadian Petroleum Geology*, vol. 52, no. 3; 3, p. 215-233.
- Waldron, J. W. F., 1991, Mid-Paleozoic thrusting at the Appalachian deformation front: Port au Port Peninsula, western Newfoundland, *Canadian Journal of Earth Sciences = Revue Canadienne des Sciences de la Terre*, vol. 28, no. 12; 12, p. 1992-2002.

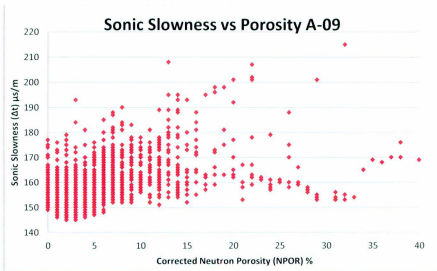
- Waldron, J. W. F., 1993, Basin development and inversion at the Appalachian structural front, Port au Port Peninsula, western Newfoundland Appalachians, *Canadian Journal of Earth Sciences = Revue Canadienne des Sciences de la Terre*, vol. 30, no. 9; 9, p. 1759-1772.
- Waldron, J. W. F., 1998, Evolution of the Appalachian Laurentian margin: Lithoprobe results in western Newfoundland, *Canadian Journal of Earth Sciences = Revue Canadienne des Sciences de la Terre*, vol. 35, no. 11; 11, p. 1271-1287.
- Waldron, J. W. F., 2008, Taconian foreland basins in the Gulf of St. Lawrence region, *Abstracts with Programs - Geological Society of America*, vol. 40, no. 2; 2, p. 29-29.
- White, R., 1991, Properties of instantaneous seismic attributes, *Geophysics: The Leading Edge of Exploration*, vol. 10, no. 7; 7, p. 26-32.
- Williams, H., 1979, Appalachian Orogen in Canada, *Canadian Journal of Earth Sciences = Revue Canadienne des Sciences de la Terre*, vol. 16, no. 3; 3, p. 792-807.
- Williams, H., 1974, *The ancient continental margin of eastern North America*, United States, Springer-Verlag : New York, United States, 781 p.
- Williams, H., 1987, Definition of the Iapetus rift-drift transition in western Newfoundland, *Geology [Boulder]*, vol. 15, no. 11; 11, p. 1044-10

Appendix A: Petrophysical X-Y Cross Plots.

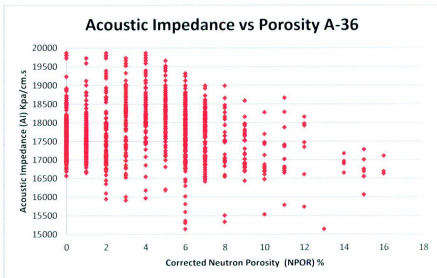
Listed in this appendix is the compilation of all remaining X-Y petrophysical cross plots for wells: St. George's Bay A-36, Long Point M-16, Long Range A-09, and Port Au Port One PAP-1. Bulk density (RHOB), acoustic impedance (AI), and sonic interval transit time (Δt) are compared to matrix corrected neutron porosity (NPOR) and examined for a correlative relationship.

Well Long Range A-09:

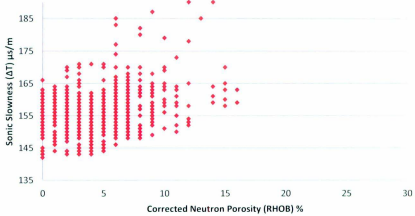




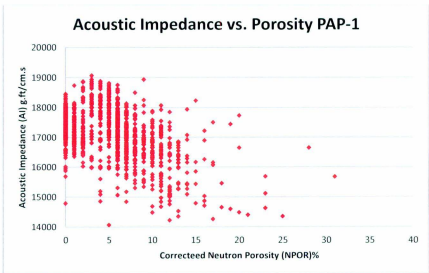
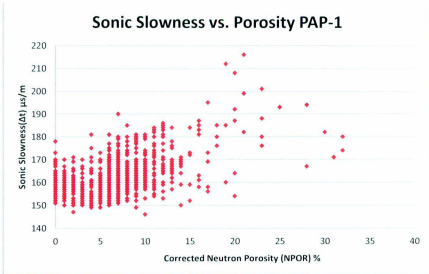
Well St. George's Bay A-36:

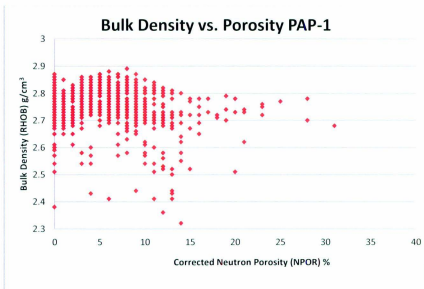


Sonic Slowness vs. Porosity A-36

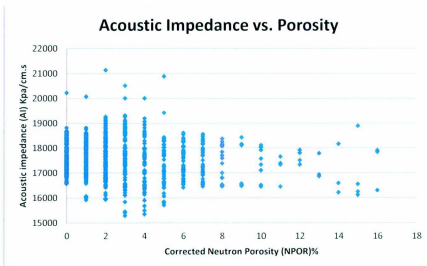


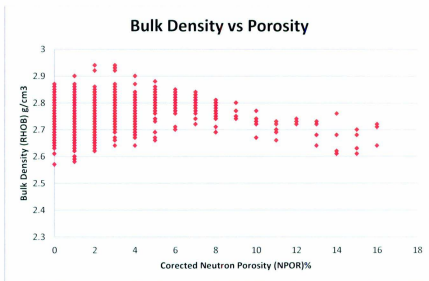
Well Port Au Port (PAP-1):





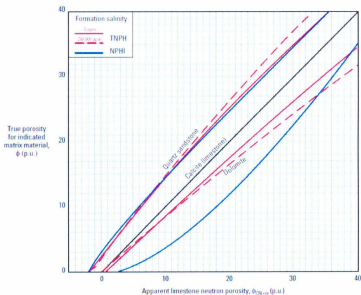
Well Long Point M-16:





Appendix B: Neutron Porosity Matrix Correction Curve

The following diagram displays graphical representation of the matrix correction equation used for dolomite from a limestone matrix in this study.

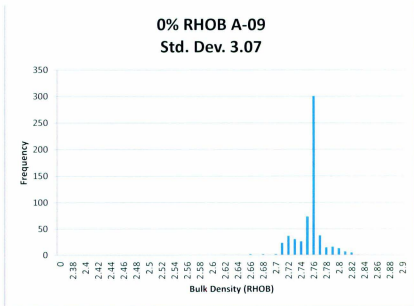


Mark of Schlumberger
© Schlumberger

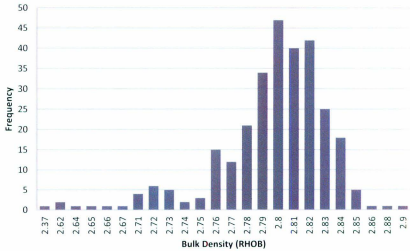
Appendix C:

Frequency distribution analyses of petrophysical properties occurring at 0-15% porosity

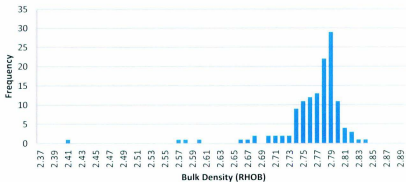
The following histograms display results from the frequency analysis petrophysical properties at certain porosities in wells A-09, A-36, M-16, and PAP-1 . Bulk density (RHOB) is in g/cm^3 and sonic interval transit time (DT) is in $\mu\text{s/m}$.



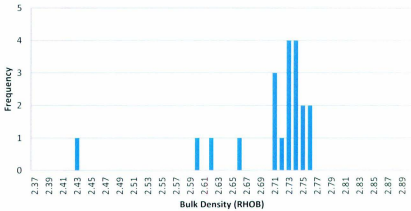
5%RHOB A-09
STDV= 0.049



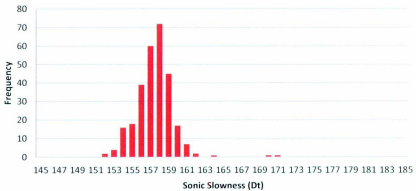
10%RHOB A-09
stdev= 0.0508



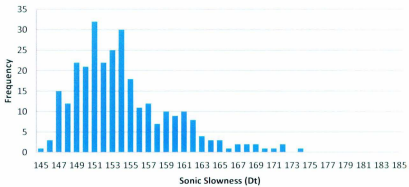
15% RHOB A-09
STDEV:0.074



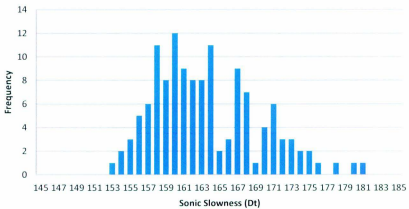
0%DT A-09
STDEV: 2.12



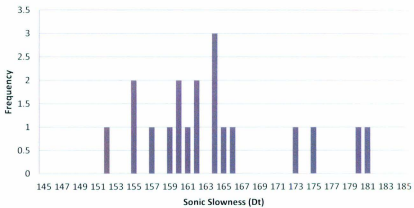
5%DT A-09
STDEV: 5.41



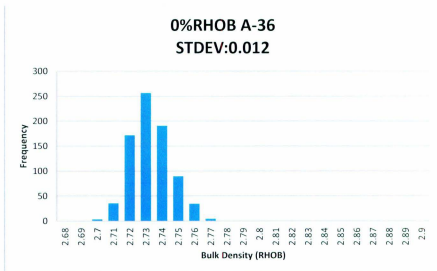
10%DT A-09
STDEV: 6.55



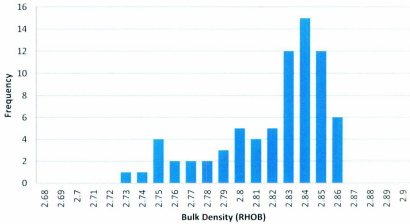
15%DT A-09
STDEV: 10.21



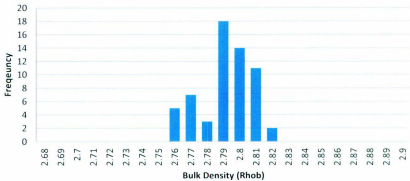
For A-36 well:



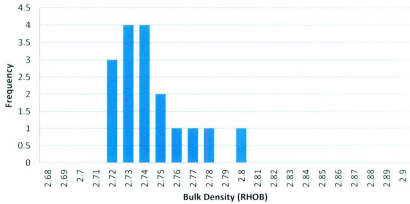
5%RHOB A-36
STDEV: 0.033



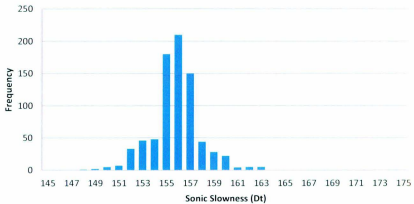
10% RHOB A-36
STDEV: 0.015



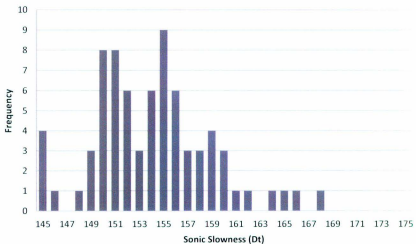
15% RHOB A-36
STDEV:0.022



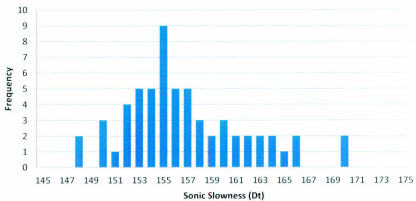
0%DT A-36
STDEV:2.03



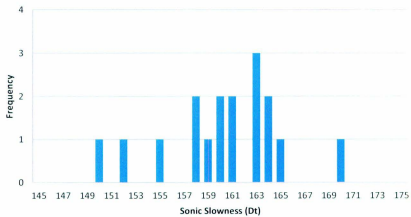
5%DT A-36
STDEV: 4.87



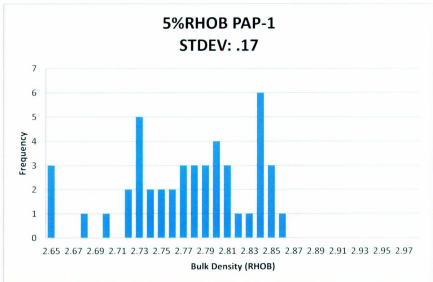
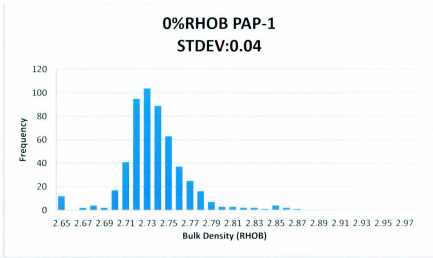
10%DT A-36
STDEV: 4.97



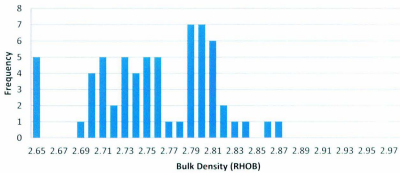
15%DT A-36
STDEV:4.88



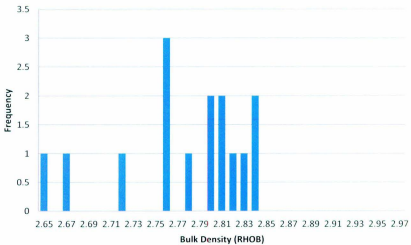
For the PAP-1 well.



10%RHOB PAP-1
STDEV:0.06

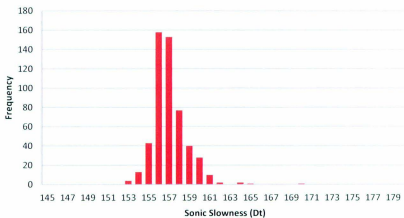


15%RHOB PAP-1
STDEV:0.08



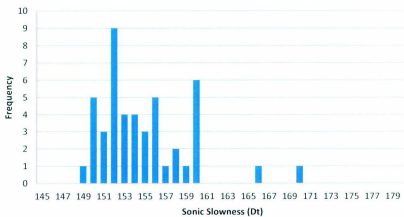
0%DT PAP-1

STDEV: 1.7

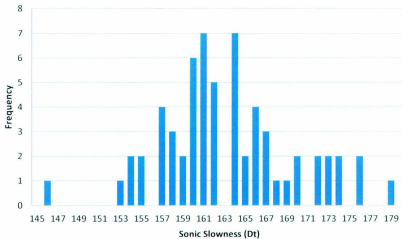


5%DT PAP-1

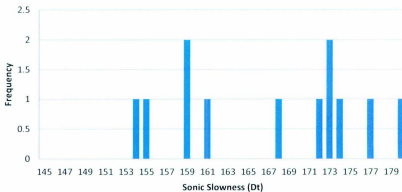
STDEV: 4.33



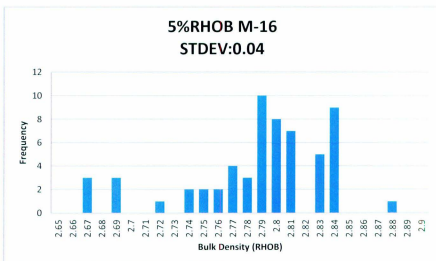
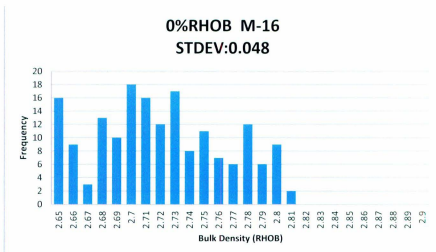
10%DT PAP-1
STDEV:7.41



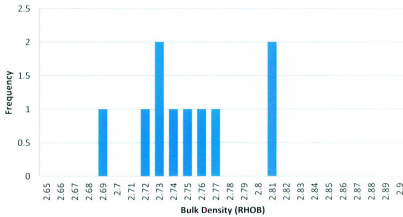
15%DT PAP-1
STDEV: 10.4



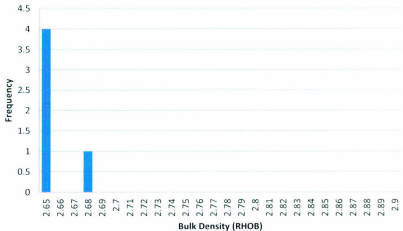
For well M-16:



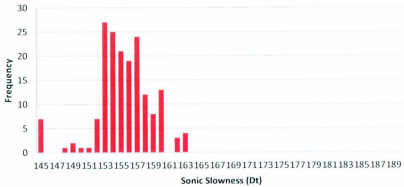
10% RHOB M-16
STDEV:0.038



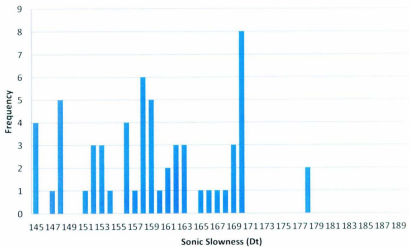
15% RHOB M-16
STDEV:0.03



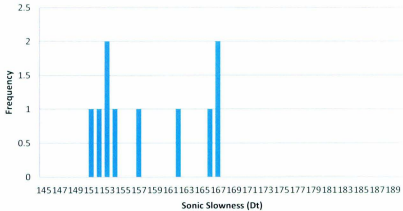
0%DT M-16
STDEV:6.21



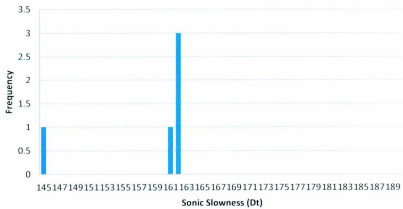
5%DT M-16
STDEV:19.5



10%DT M-16
STDEV:6.6

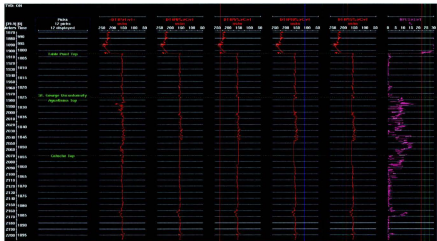


15%DT M-16
STDEV: 28.2

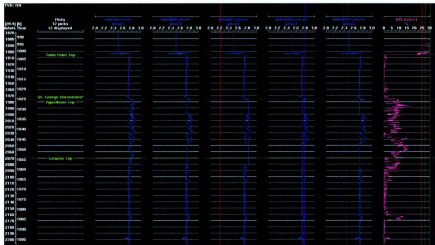


Appendix D: Block Porosity Models

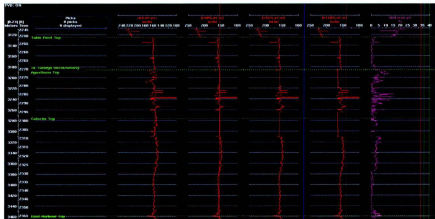
Diagrams displaying the implementation of block porosity models on the bulk density (blue) and sonic velocity (red) block porosity models are in the regions of straight lines in the well curves. Neutron Porosity shown in purple.



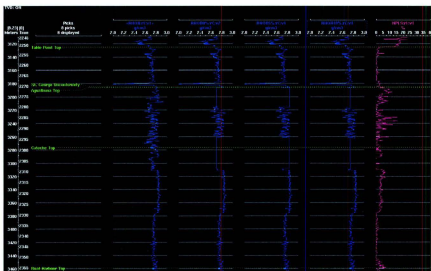
Well A-36 Sonic slowness curve block porosity model, 0-15% porosity models. (Red) Neutron Porosity (purple)



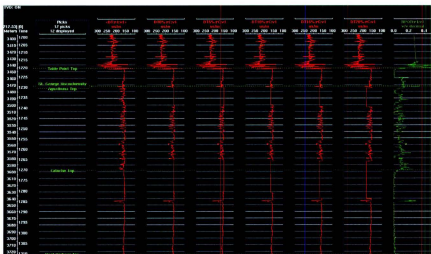
Well A-36 Bulk Density curve block porosity model, 0-15% porosity models (Blue) Neutron Porosity (purple)



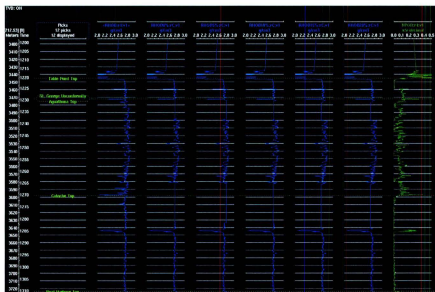
Well M-16 Sonic Slowness curve block porosity model, 0-10% porosity models (Red) Neutron Porosity (purple)



Well M-16 Bulk Density curve block porosity model. 0-10% porosity models (Blue) Neutron Porosity (purple)



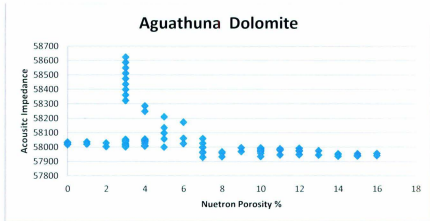
Well PAP-1 Sonic Slowness curve block porosity model. 0-20% porosity models (Red) Neutron Porosity (green)



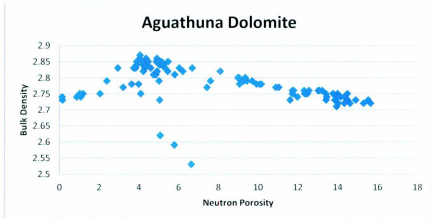
Well PAP-1 Bulk Density curve block porosity model. 0-20% porosity models (Blue) Neutron Porosity (green)

Appendix E: Lithologic Cross plots

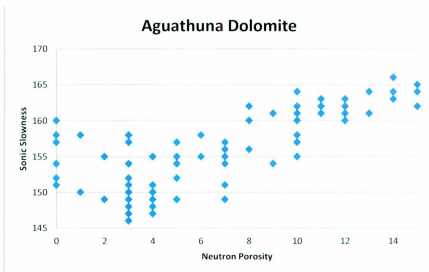
Graphs showing petrophysical properties from intervals of know lithology in the well logs.



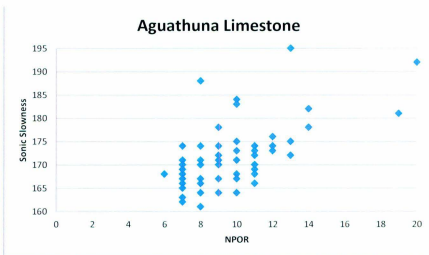
Acoustic Impedance. A-09 Depth 3310m-3325m. Dolomite, Aguathuna formation

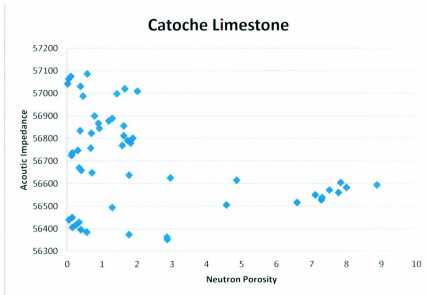


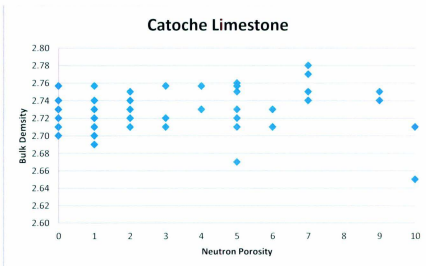
Bulk Density. Depth 3310m-3325m. Dolomite A-09, Aguathuna dolomite



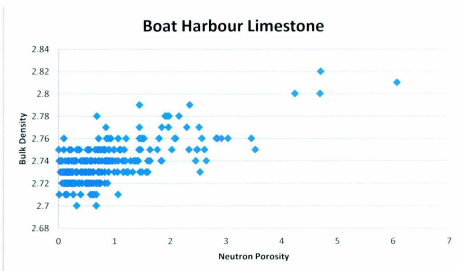
Sonic Slowness - 3310- 3325m, A-09 Aguathuna Dolomite



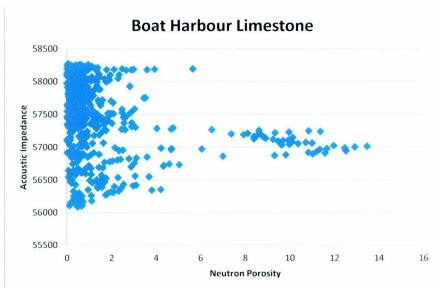




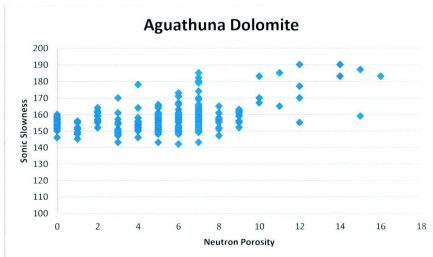
Bulk Density, Depth 3465-3475m A-09 Catoche limestone



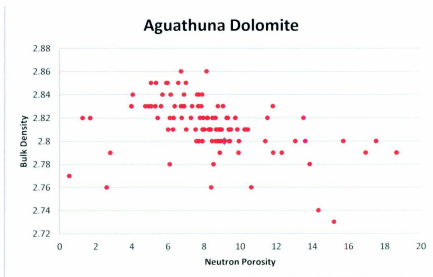
Bulk Density, A-36, Depth 2103-2230 Boat Harbour limestone with intermittent dolomitic



Acoustic Impedance: A-36, Depth 2103-2230, Boat Harbour limestone with intermittent dolominitic



A-36 Sonic Slowness Depth 1976- 2020m Aguathuna Formation dolomite



A-36 Bulk Density Depth 1976-2020m Aguathuna Formation dolomite

